AD NUMBER

AD457511

NEW LIMITATION CHANGE

TO

Approved for public release, distribution unlimited

FROM

Distribution authorized to U.S. Gov't. agencies and their contractors; Administrative/Operational Use; DEC 1964. Other requests shall be referred to Air Force Flight Dynamics Laboratory, Attn: RTD, Wright-Patterson AFB, OH 45433.

AUTHORITY

AAFFDL ltr, 21 Oct 1974

DRAG CHARACTERISTICS OF SEVERAL TWO-BODY SYSTEMS AT TRANSONIC AND SUPERSONIC SPEEDS

TECHNICAL DOCUMENTARY REPORT No. RTD-TDR-63-4226

DECEMBER 1964

AF FLIGHT DYNAMICS LABORATORY
RESEARCH AND TECHNOLOGY DIVISION
AIR FORCE SYSTEMS COMMAND
WRIGHT-PATTERSON AIR FORCE BASE, OHIO

Project No. 6065, Task No. 606503

(Prepared under Contract No. AF 33(657)-11184 by the Department of Aeronautics and Engineering Mechanics, University of Minnesota, Minneapolis, Minnesota; Helmut G. Heinrich and R. Sheldon Hess, Authors)

NOTICES

When Government drawings, specifications, or other data are used for any purpose other than in connection with a definitely related Government procurement operation, the United States Government thereby incurs no responsibility nor any obligation whatsoever; and the fact that the Government may have formulated, furnished, or in any way supplied the said drawings, specifications, or other data, is not to be regarded by implication or otherwise as in any manner licensing the holder or any other person or corporation, or conveying any rights or permission to manufacture, use, or sell any patented invention that may in any way be related thereto.

Qualified users may obtain copies of this report from Defense Documentation Center.

Foreign announcement and dissemination of this report is not authorized.

DDC release to CFSTI is not authorized. The distribution of this report is limited because the report contains technology identifiable with items on the strategic embargo lists excluded from export or re-export under U. S. Export Control Act of 1949 (63 Stat. 7) as amended (50 U.S.C.App. 2020.2031) as implemented by AFR 400-10.

Copies of this report should not be returned to the Research and Technology Division unless return is required by security considerations, contractual obligations, or notice on a specific document.

300 - February 1965 - 448-27-613

FOREWORD

This report was prepared by the staff of the Department of Aeronautics and Engineering Mechanics of the University of Minnesota in compliance with United States Air Force Contract No. AF 33(657)-11184, Project No. 6065 and Task No. 606503, "Theoretical Parachute Investigations."

The work being accomplished under these contracts is sponsored jointly by QM Research and Engineering Command, Department of the Army; Bureau of Aeronautics and Bureau of Ordnance, Department of the Navy; and Air Force Systems Command, Department of the Air Force, and is directed by a Tri-Service Steering Committee concerned with Aerodynamic Retardation. Contract administration has been conducted by the Research and Technology Division (AFSC), and Messrs. Rudi J. Berndt and James H. DeWeese of the Retardation and Recovery Branch, AF Flight Dynamics Laboratory, have been project engineers.

Participants in the experimentation and data reduction include Messrs. Gunars Stumbris, J. G. Ballinger, J. W. Parks, R. C. Horn, and G. H. Thornberg, staff members of Rosemount Aeronautical Laboratories, and a number of students of aero-space engineering of the University of Minnesota.

ABSTRACT

The drag coefficients as well as the stagnation and base pressures of systems using an ogive cylinder or skirted hemisphere as primary body and a flat plate, 45° half-angle cone, sphere, and hollow hemisphere as secondary body have been measured at transonic and supersonic speeds.

The Mach number range was from 0.85 to 1.25 and 4.35. Secondary body size and body separation distance were selected parameters. This is the fourth report in a series of studies dealing with the free stream drag and wake phenomena of bodies of revolution (see Refs 2, 3 and 4).

With a few exceptions in the transonic range, the system drag was less than the sum of the free stream drag of the fore and aft bodies.

This technical documentary report has been reviewed and is approved.

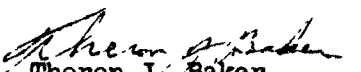

Theron J. Baker
Vehicle Equipment Division
AF Flight Dynamics Laboratory

TABLE OF CONTENTS

ILLUSTRATIONS

ILLUSTRATIONS (cont.)

ILLUSTRATIONS (cont.)

ILLUSTRATIONS (cont.)

ILLUSTRATIONS (cont.)

ILLUSTRATIONS (cont.)

ILLUSTRATIONS (cont.)

LIST OF SYMBOLS

$C_D = \frac{\text{Drag}}{q_\infty S}$		drag coefficient
$C_{D_t} = \frac{\text{System drag}}{q_\infty S_1}$		system drag coefficient
C_{D_∞}	-	drag coefficient in the free stream
$C_p = \frac{p - p_\infty}{q_\infty}$		pressure coefficient
$C_{p_b} = \frac{p_b - p_\infty}{q_\infty}$		body base pressure coefficient
$C_{p_s} = \frac{p_s - p_\infty}{q_\infty}$		body stagnation pressure coefficient
D	-	maximum primary body diameter
d	-	maximum secondary body diameter
M_∞	-	free stream Mach number
p	-	local pressure
p_b	-	base pressure
p_s	-	stagnation pressure
p_∞	-	free stream static pressure
q_∞	-	free stream dynamic pressure
Re	-	Reynolds number (based on D)
$S_1 = \frac{\pi D^2}{4}$		maximum frontal area of primary body
$S_2 = \frac{\pi d^2}{4}$		maximum frontal area of secondary body
X	-	distance downstream from primary body base
$\eta = \frac{C_{D_t}}{C_{D_{1_\infty}} + C_{D_{2_\infty}} \frac{S_2}{S_1}}$		system drag efficiency

Subscripts:

1	-	primary body
2	-	secondary body
∞	-	free stream

1. INTRODUCTION

The deceleration or stabilization of a body moving through the air at high speed is often accomplished by deploying a second body downstream from this body to increase the aerodynamic drag on the system. To predict the performance of such a system, it is necessary to know the drag characteristics of the two bodies when operating in combination. Obviously, the drag device, or secondary body, will perform differently when in the wake of another body than in the free stream. In particular, one would expect it to have less drag in the wake than in the free stream.

It is not enough, however, to consider only the effect of the wake on the secondary body, since its presence may alter the drag characteristics of the primary body (by increasing the primary body base pressure, for instance). This would be particularly true when the drag device is positioned relatively close to the primary body. Thus, it appears that one should perhaps consider the two bodies as a system when the distance separating the two bodies is not large.

Information on the behavior of such two-body systems is limited, particularly at high speeds. Therefore, an experimental study of the drag characteristics of some two-body systems at transonic speeds and at $M_\infty = 4.35$ has been conducted and the results are reported here.

Manuscript released by the authors December 1963 for publication as an RTD Technical Documentary Report.

2. MODELS, FACILITIES AND INSTRUMENTATION

2.1 Models

The two wake producing or primary bodies, an ogive cylinder and a hemisphere-cylinder-cone combination called a skirted hemisphere, are shown in Fig 1. The representative decelerators or secondary bodies used were a circular flat plate, a cone with a 45° half-angle, a sphere and a hollow hemisphere. Two sets of these bodies were constructed, one with a diameter equal to that of the primary body and one with twice that diameter. The smaller bodies were positioned at 2, 4, 6 and 8 primary body diameters downstream from the primary body, while the larger ones were positioned at 2, 4 and 8 diameters downstream. Positioning of the hollow hemisphere varied slightly from these values.

A rod of the proper length was permanently attached to the nose of the secondary bodies, as shown for the larger bodies in Fig 2. The end of the rod was threaded for affixing the primary bodies, which were thus interchangeable. The assembled systems with the large cone as secondary body are shown in Fig 3.

Pressure taps for measuring primary and secondary body base pressures and secondary body stagnation pressure were located as shown in Fig 4.

2.2 Wind Tunnels

The tests were conducted at the wind tunnel facilities of Rosemount Aeronautical Laboratories. Transonic tests were performed in the 12" x 16" continuous flow, induction type of transonic wind tunnel, and supersonic tests were conducted in the 6" x 9" continuous flow supersonic wind tunnel. Details concerning these facilities are presented in Ref 1.

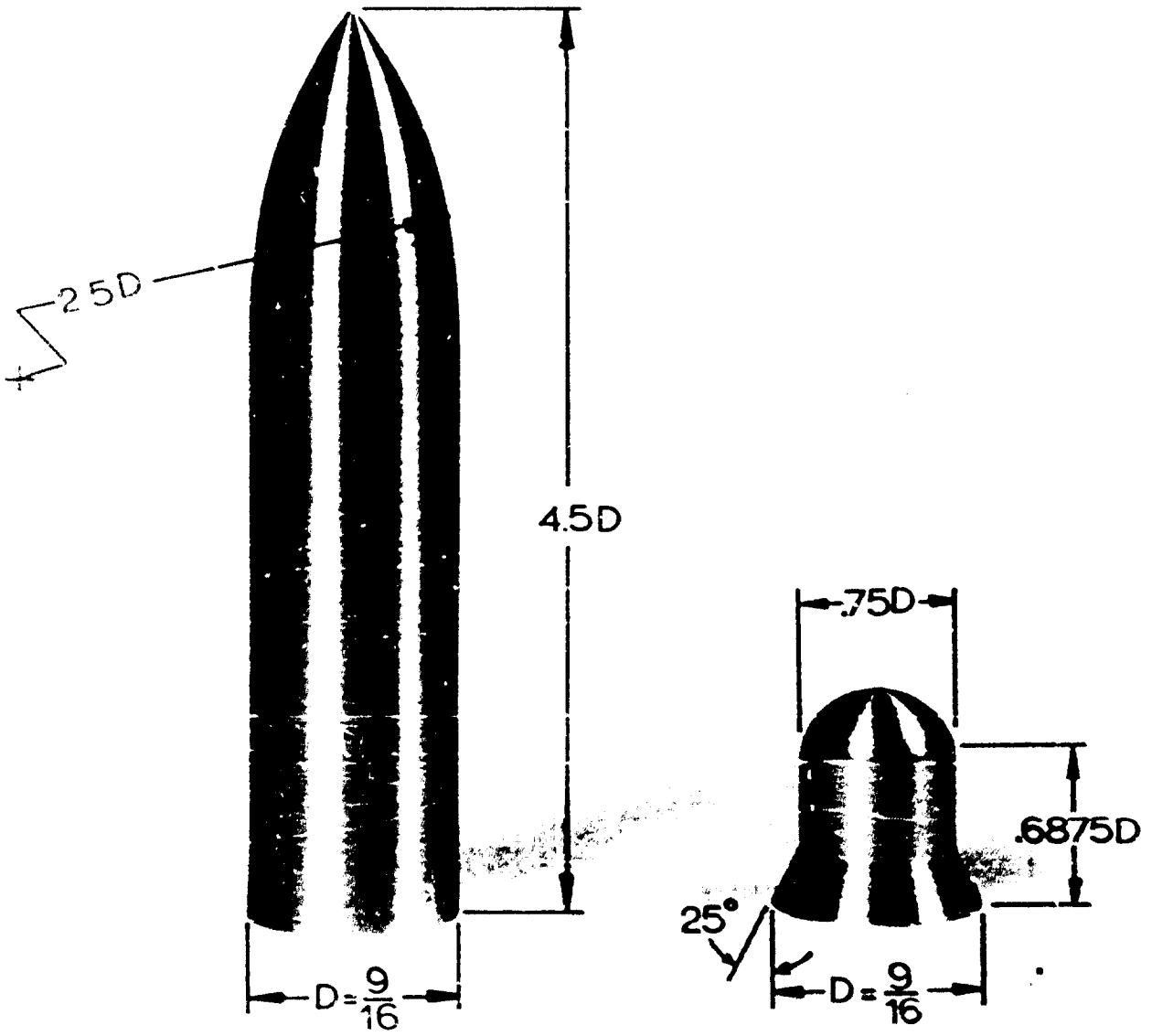

OGIVE CYLINDER SKIRTED HEMISPHERE

FIG 1. PRIMARY BODIES

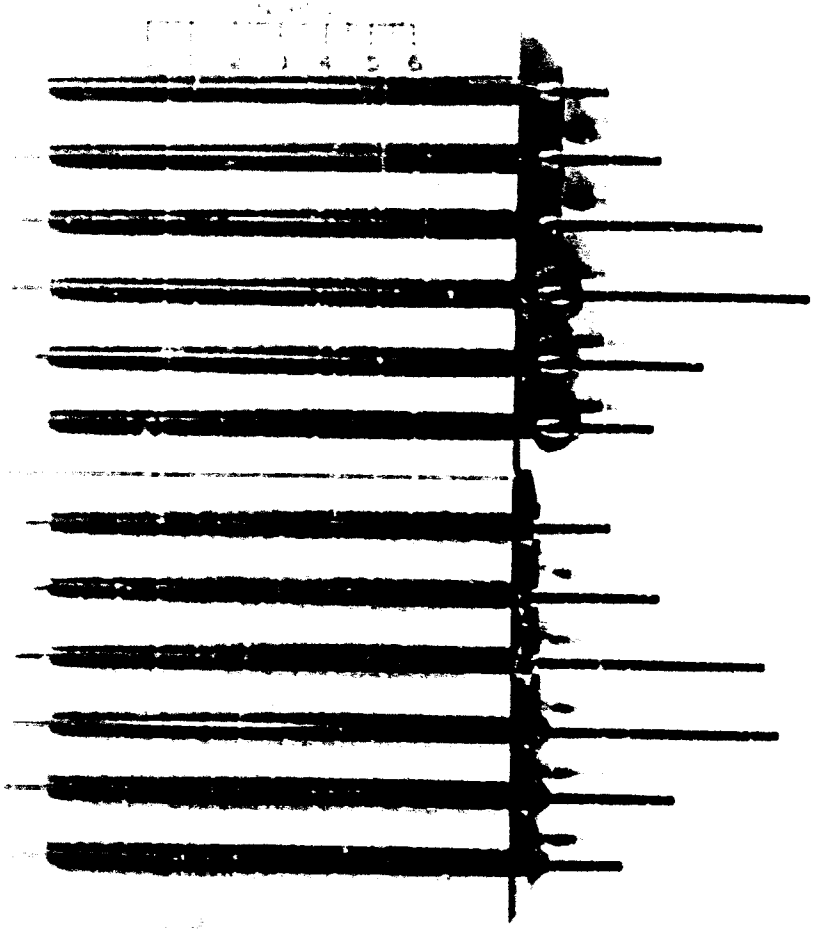

FIG 2 SECONDARY BODIES (45° HALF ANGLE CONE, CIRCULAR FLAT PLATE, SPHERE, AND HOLLOW HEMISPHERE)

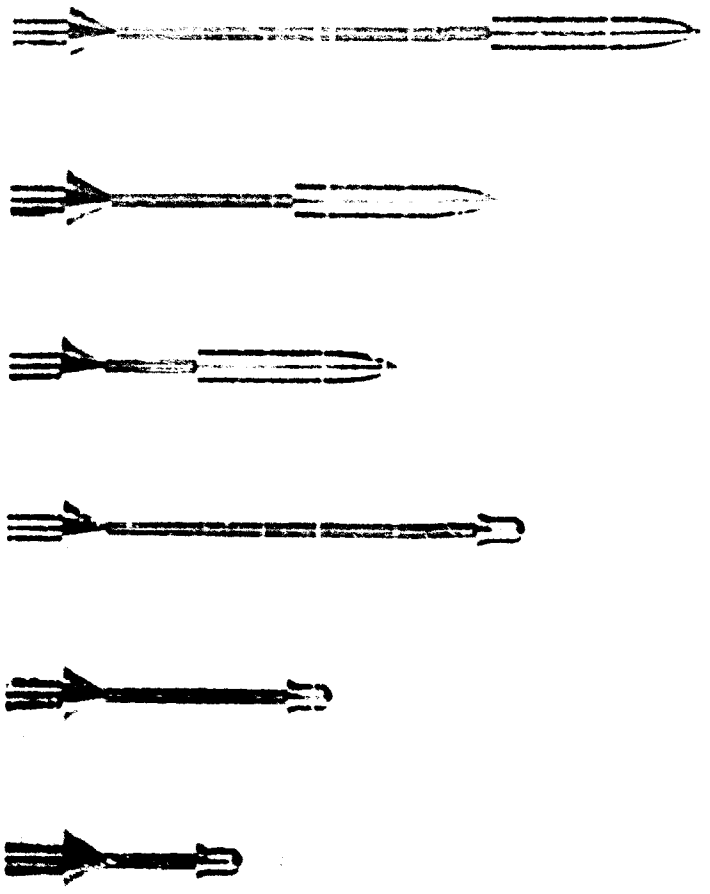

FIG 3 45° HALF-ANGLE CONE IN COMBINATION WITH BOTH PRIMARY BODIES FOR VARIOUS X/D POSITIONS

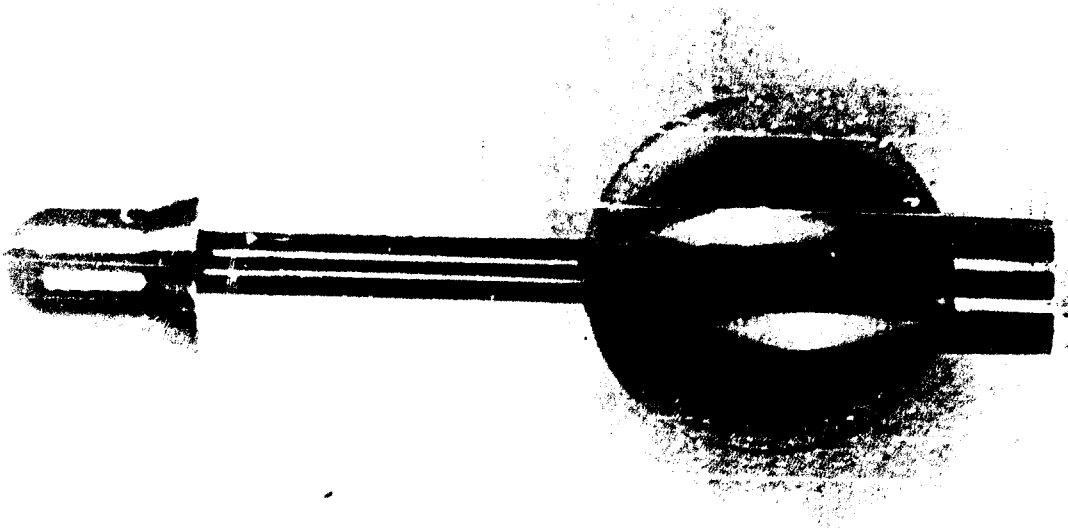

PHOTOGRAPH SHOWING LOCATION OF BASE AND STAGNATION PRESSURE

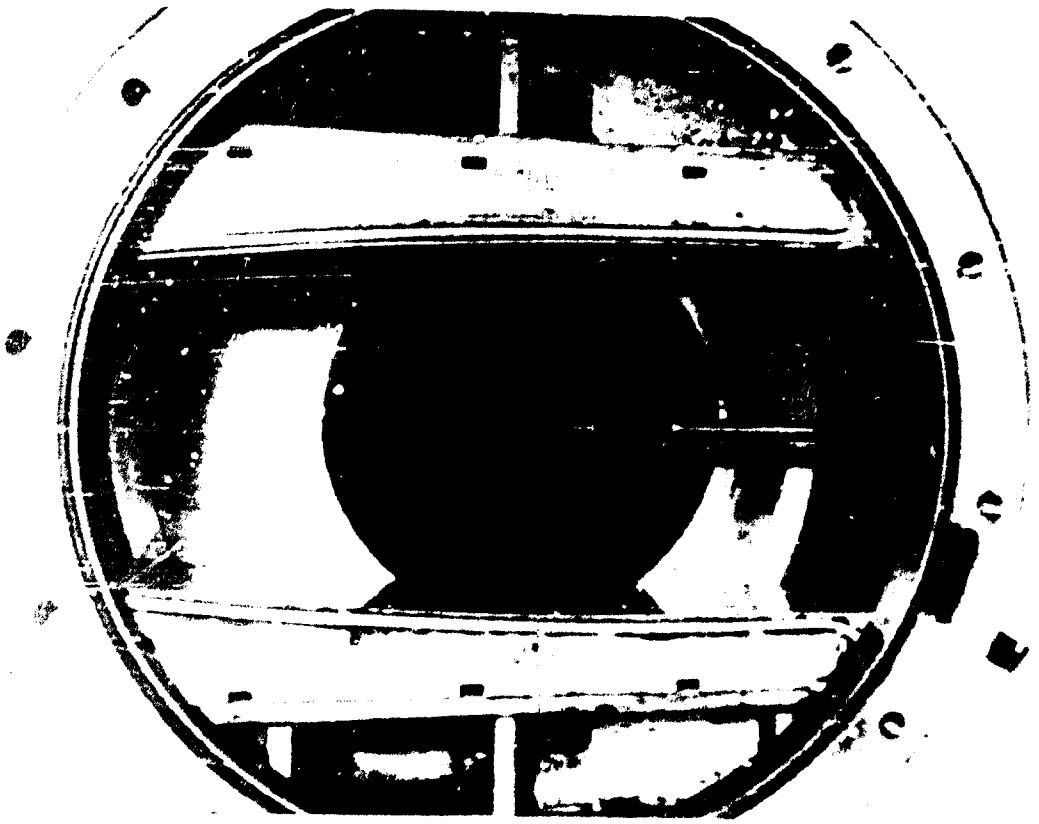

A typical model installation in the supersonic tunnel is shown in Fig 5.

2.3 Drag Balance

The drag balance used to measure the drag of the system is a mechanical-electrical device with its force sensing unit mounted co-axially with the models. The drag force on the two-body system is transmitted by its support sting to flexible steel diaphragms inside the sensing unit. Deflection of these diaphragms is sensed by the motion of the core of a Schaevitz Linear Variable Differential Transformer (LVDT), resulting in an electrical output from the transformer proportional to the drag on the system. The signal from the LVDT is transmitted through a control unit to a Brown Variable Span Recorder, which gives a permanent record of the drag values. A more detailed description of the balance is presented in Appendix III.

2.4 Flow Visualization

Conventional shadowgraph and Schlieren systems were used for transonic and supersonic tests, respectively, to observe and record flow characteristics about the bodies.

2.5 Pressure Measurements

In addition to the body base and stagnation pressures mentioned above, the balance internal pressure was measured for sting corrections. The pressure taps were connected by plastic tubing to mercury or merriam fluid (sp. g. = 1.05) manometer boards, which were photographed during each test to provide a permanent pressure recording.

3. RESULTS

The drag coefficients of the systems using the skirted hemisphere as primary body were measured at free stream Mach numbers of about 0.85, 0.95, 1.05, 1.20 and 4.35. For the systems using the ogive cylinder as primary body, the drag coefficients in the transonic range were obtained from the results of Ref 2, with direct measurements made only at $M_\infty = 4.35$. All drag coefficients are based on the primary body frontal area, which was the same for all systems.

The results of these investigations are presented in this section. Base and stagnation pressure coefficient for the systems with the skirted hemisphere are included in Appendix I, while photographs which indicate characteristic or particularly interesting flow patterns are presented in Appendix II.

As shown in Fig 3, in most cases a thin rod was arranged between the primary and secondary bodies in order to assure proper body alignments. This arrangement with center rod was chosen primarily because of its simplicity. In a few cases a centerline wire was used and a number of experiments were also made without a connecting member between the two bodies. In spite of the fact that one may suspect that the presence of a rod or a centerline wire influences the results of the measurements, merely the conventional sting correction has been made in order to account for the presence of the rod or the wire.

With the two bodies positioned relatively close to each other, the flow region between them is practically identical to the one of the turbulent wake, and one may expect that in these cases the influence of the rod or the centerline wire is indeed negligible. When the secondary body is arranged farther downstream, and particularly in a higher velocity flow

field, the flow pattern about the secondary body may be altered to a certain extent through the centerline wire or the rod. However, the results obtained with the various test arrangements, including those without connecting members, do not provide differences distinctive enough to allow definite statements concerning the effect of the connecting members.

From the practical viewpoint, the neglect of the rod or wire effects also appears permissible since all trailing aerodynamic decelerators do require some means of suspension between the primary body and the trailing decelerator. Therefore, the results obtained in the described fashion appear to be acceptable for practical performance calculations.

3.1 Drag Coefficients at Transonic Speeds With Skirted Hemisphere as Primary Body

The drag coefficients of the systems using the skirted hemisphere as primary body at transonic speeds are presented in Figs 6 through 13. The Reynolds numbers for these tests varied from 3.1×10^5 to 3.3×10^5. The lower reference curve in each of these figures gives the free stream drag coefficient of the primary body, while the upper curve gives the sum of the free stream drag coefficients of the primary and secondary bodies (both based on the primary body projected area). These reference curves were obtained from Ref 3.

Considering first the results for the systems with the flat plate (Figs 6 and 7), we note that the drag of the system is considerably less than the sum of the free stream drags of the two bodies. With the smaller secondary body, the system drag with the plate close to the primary body is only slightly larger than the free stream drag of the primary body alone. As the body separation distance is increased, the drag increases, except in going from $X/D = 6$ to $X/D = 8$.

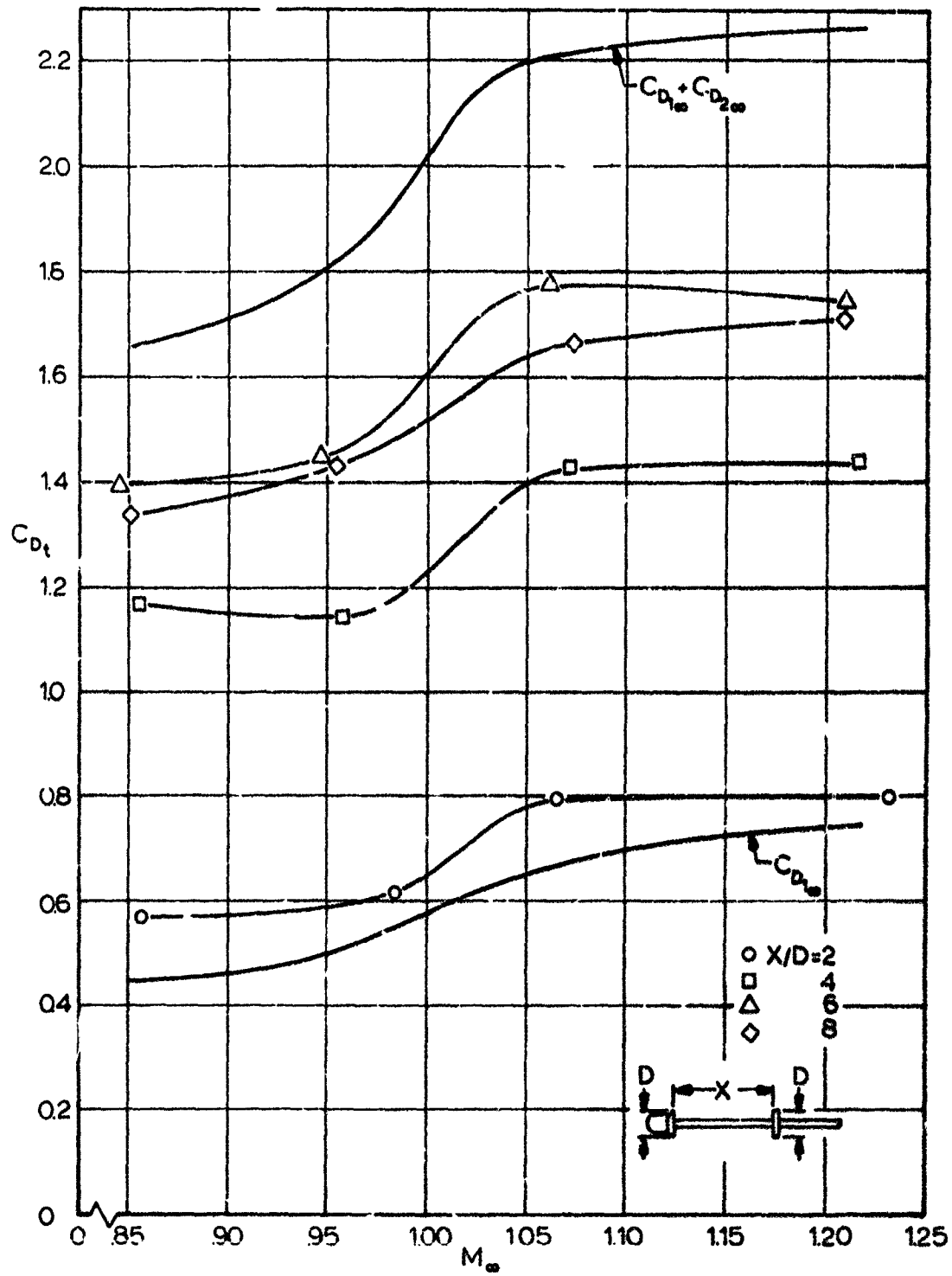

FIG 6. SYSTEM DRAG COEFFICIENT FOR SKIRTED HEMISPHERE AND FLAT PLATE WITH d/D=1 AT TRANSONIC SPEEDS.

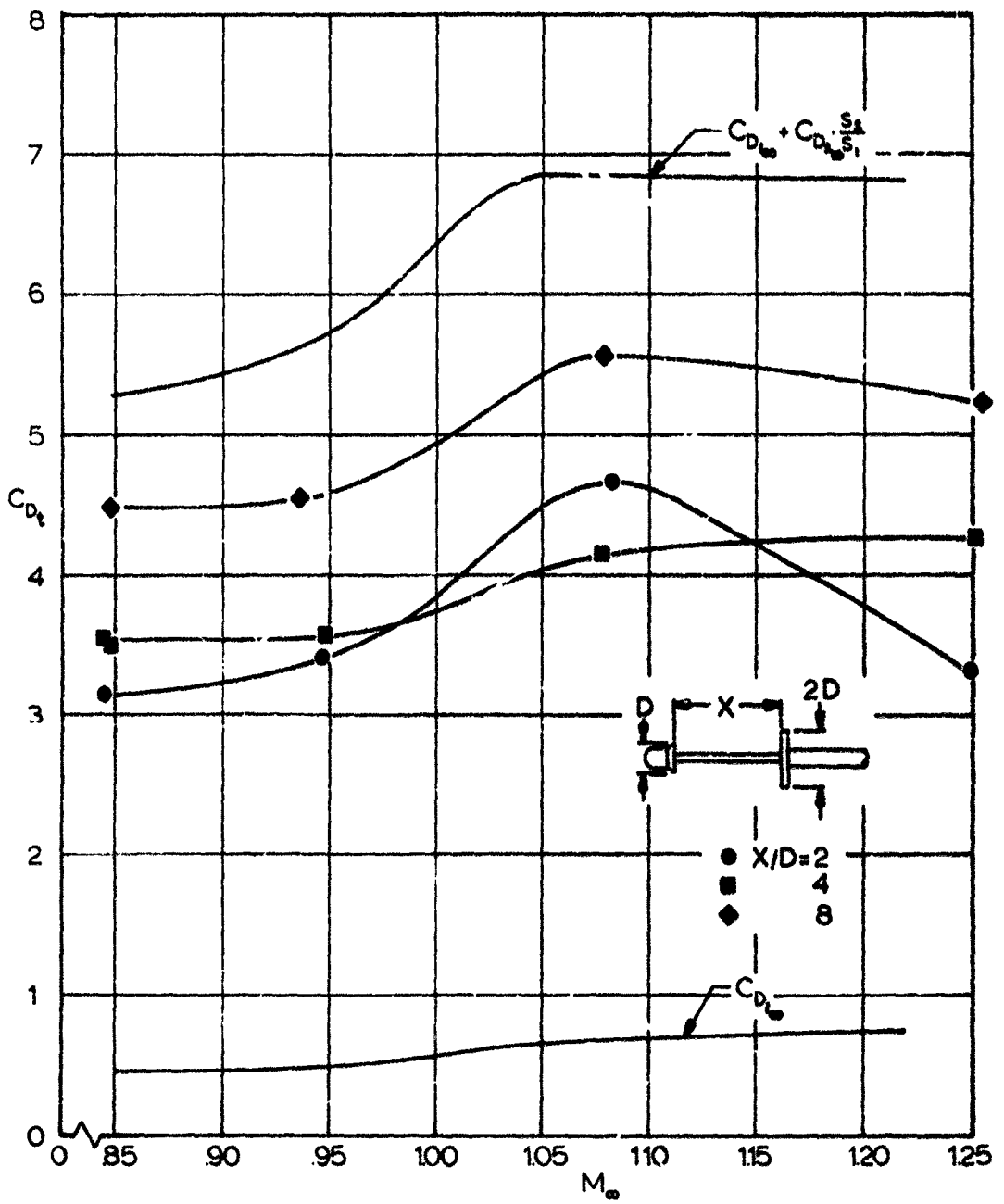

FIG 7. SYSTEM DRAG COEFFICIENT FOR SKIRTED HEMISPHERE AND FLAT PLATE WITH d/D = 2 AT TRANSONIC SPEEDS.

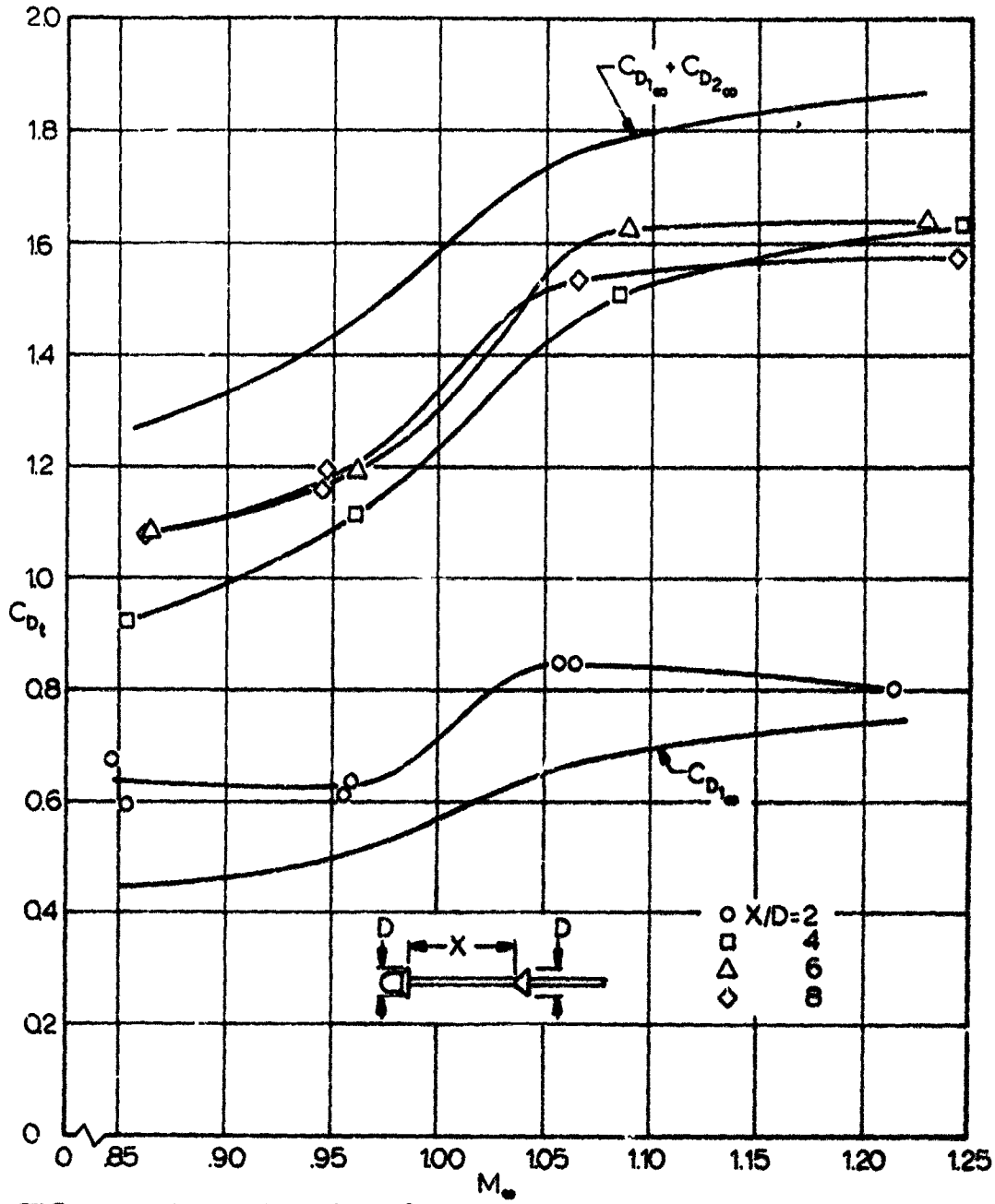

FIG 8. SYSTEM DRAG COEFFICIENT FOR SKIRTED HEMISPHERE AND 45° HALF-ANGLE CONE WITH d/D=1 AT TRANSONIC SPEEDS.

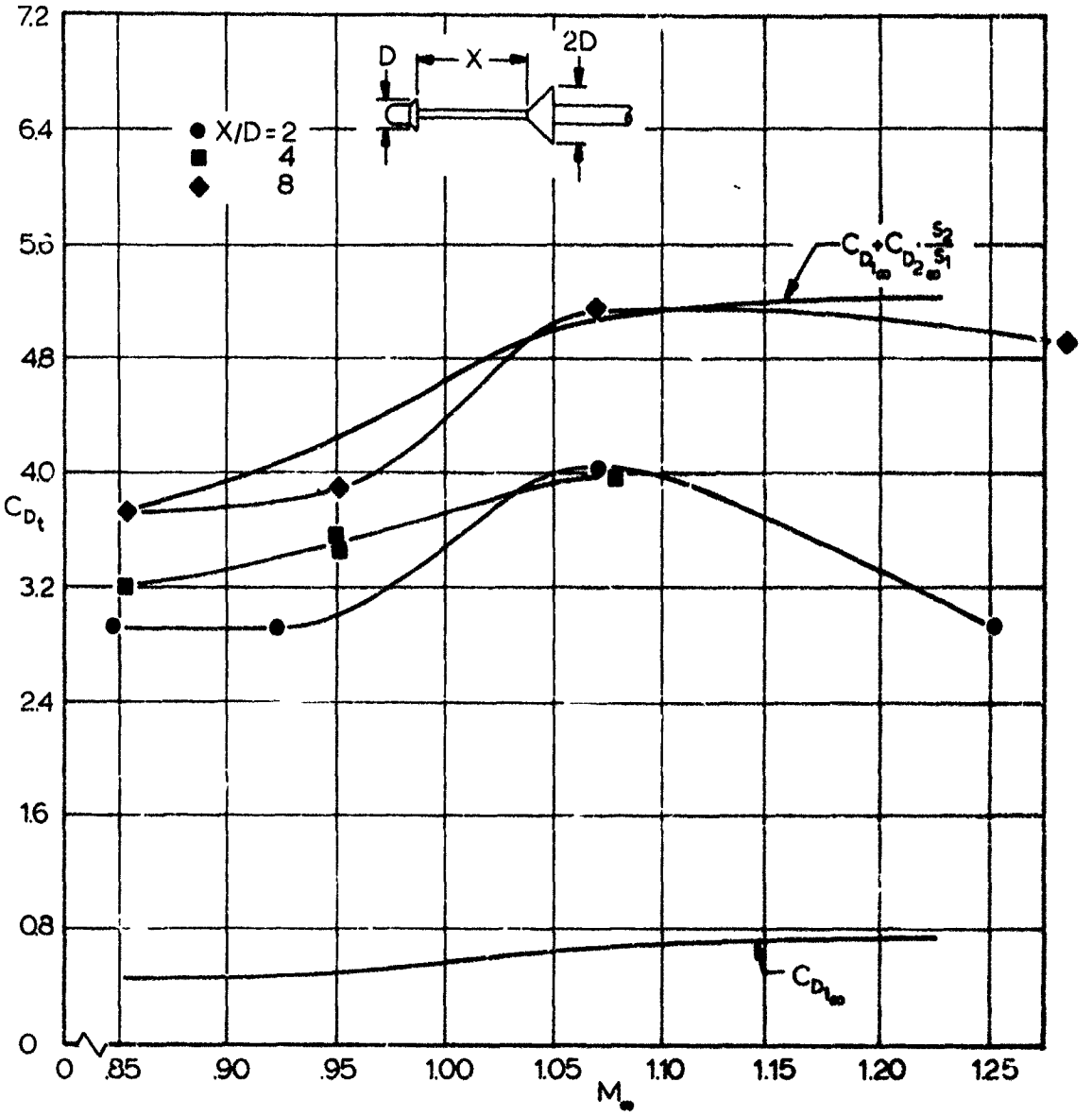

FIG 9. SYSTEM DRAG COEFFICIENT FOR SKIRTED HEMISPHERE AND 45° HALF-ANGLE CONE WITH d/D=2 AT TRANSONIC SPEEDS.

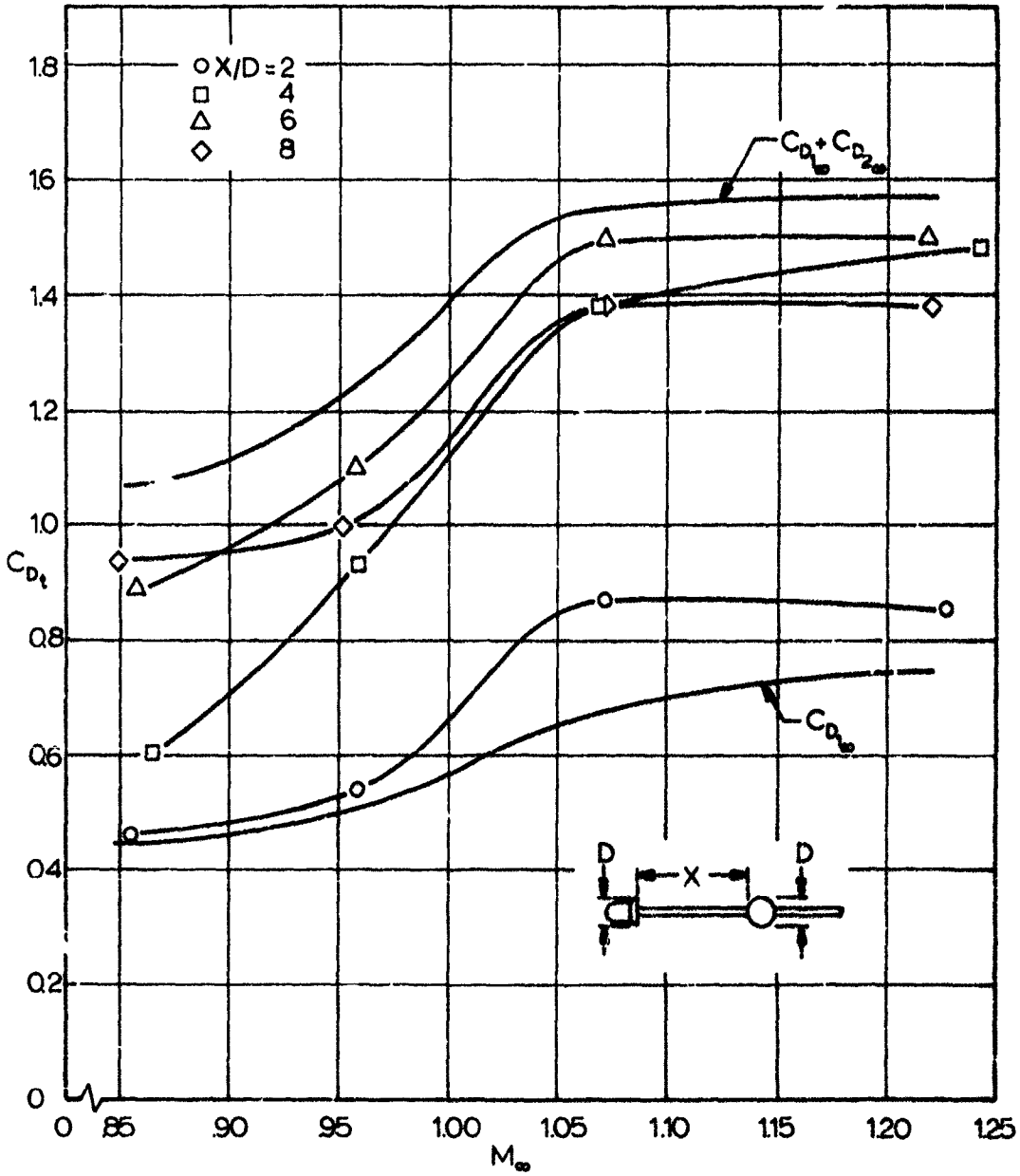

FIG 10. SYSTEM DRAG COEFFICIENT FOR SKIRTED HEMISPHERE AND SPHERE WITH d/D = 1 AT TRANSONIC SPEEDS.

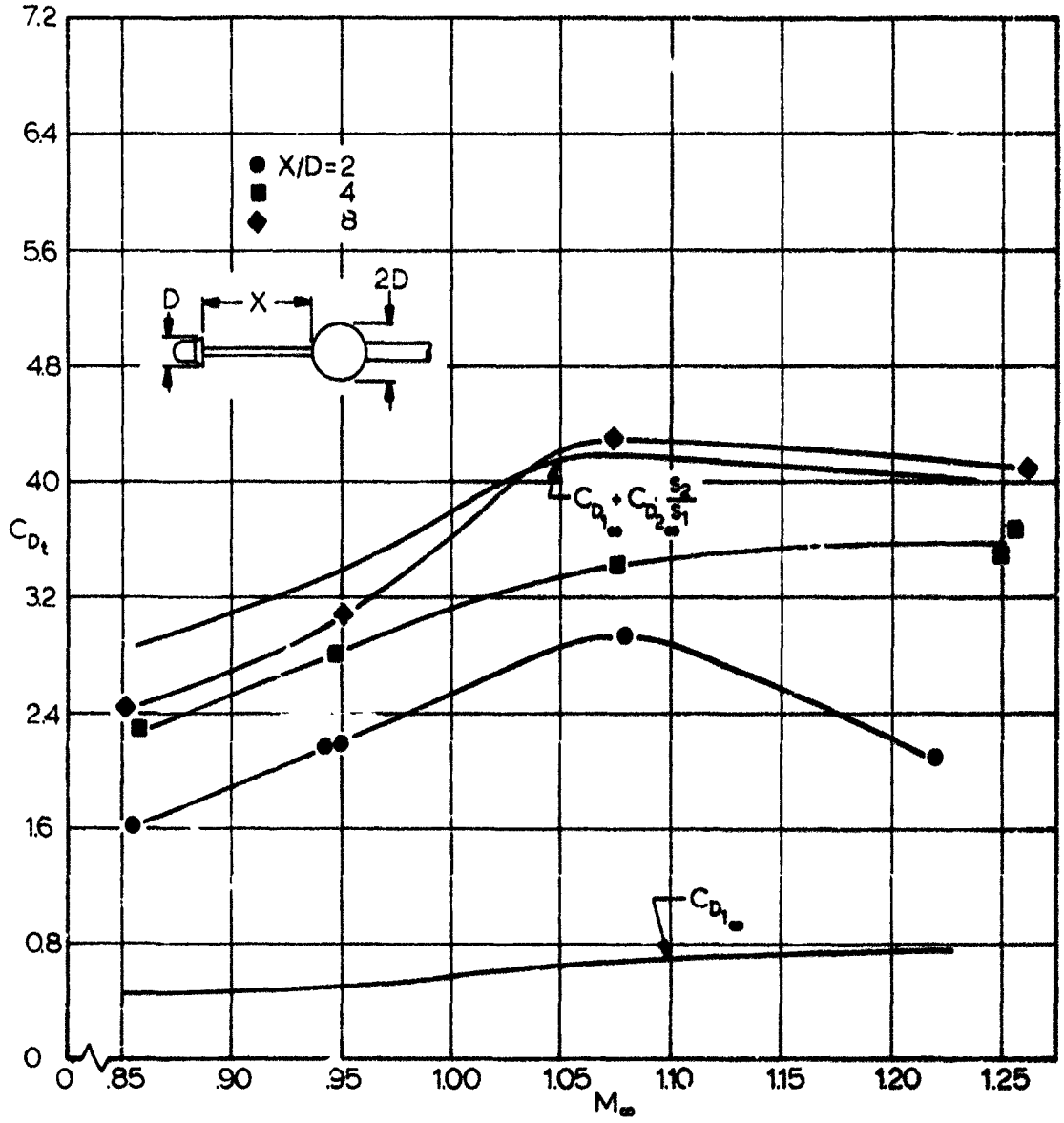

FIG 11. SYSTEM DRAG COEFFICIENT FOR SKIRTED HEMISPHERE AND SPHERE WITH d/D=2 AT TRANSONIC SPEEDS.

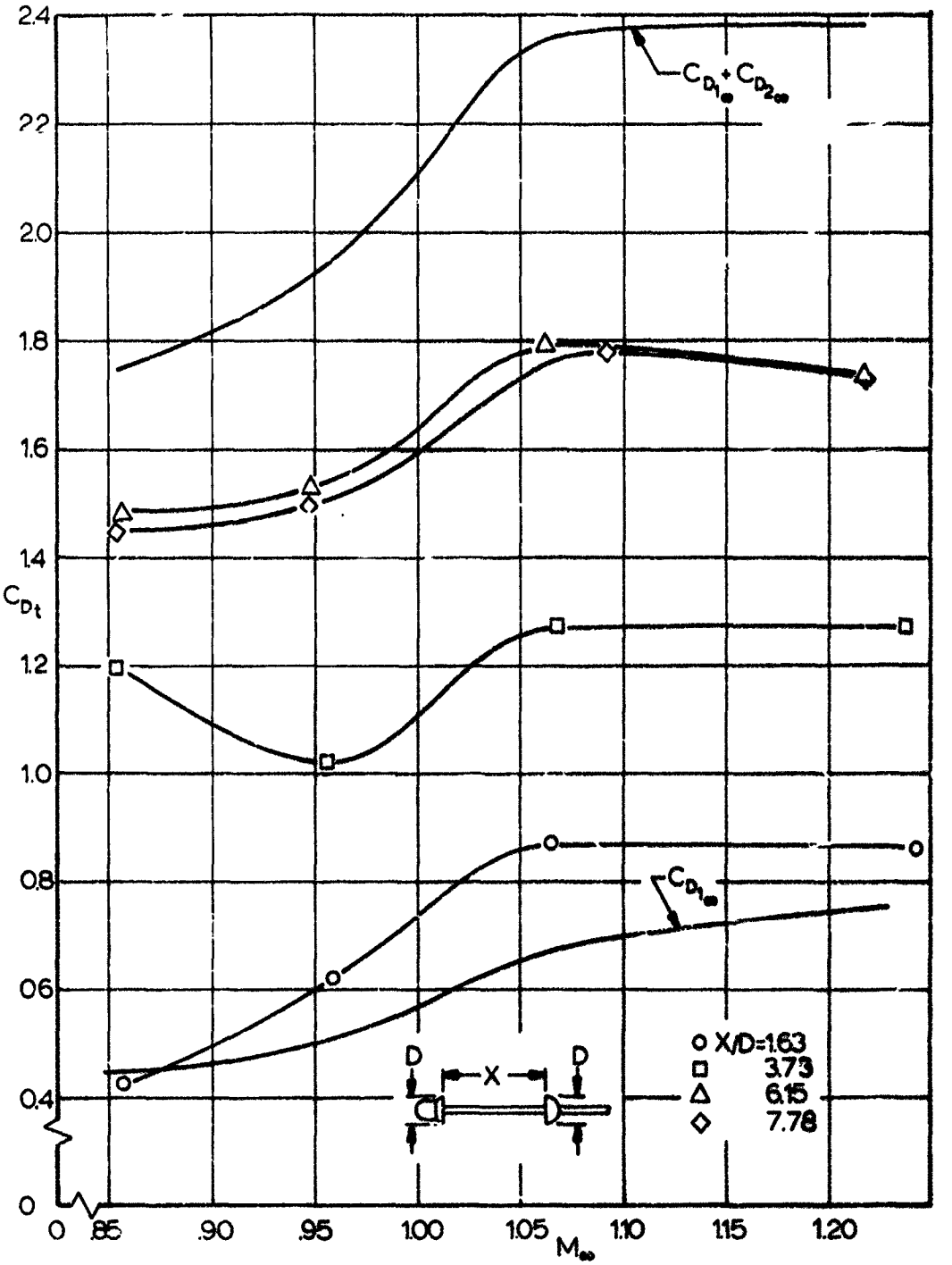

FIG 12. SYSTEM DRAG COEFFICIENT FOR SKIRTED HEMISPHERE AND HOLLOW HEMISPHERE WITH d/D=1 AT TRANSONIC SPEEDS.

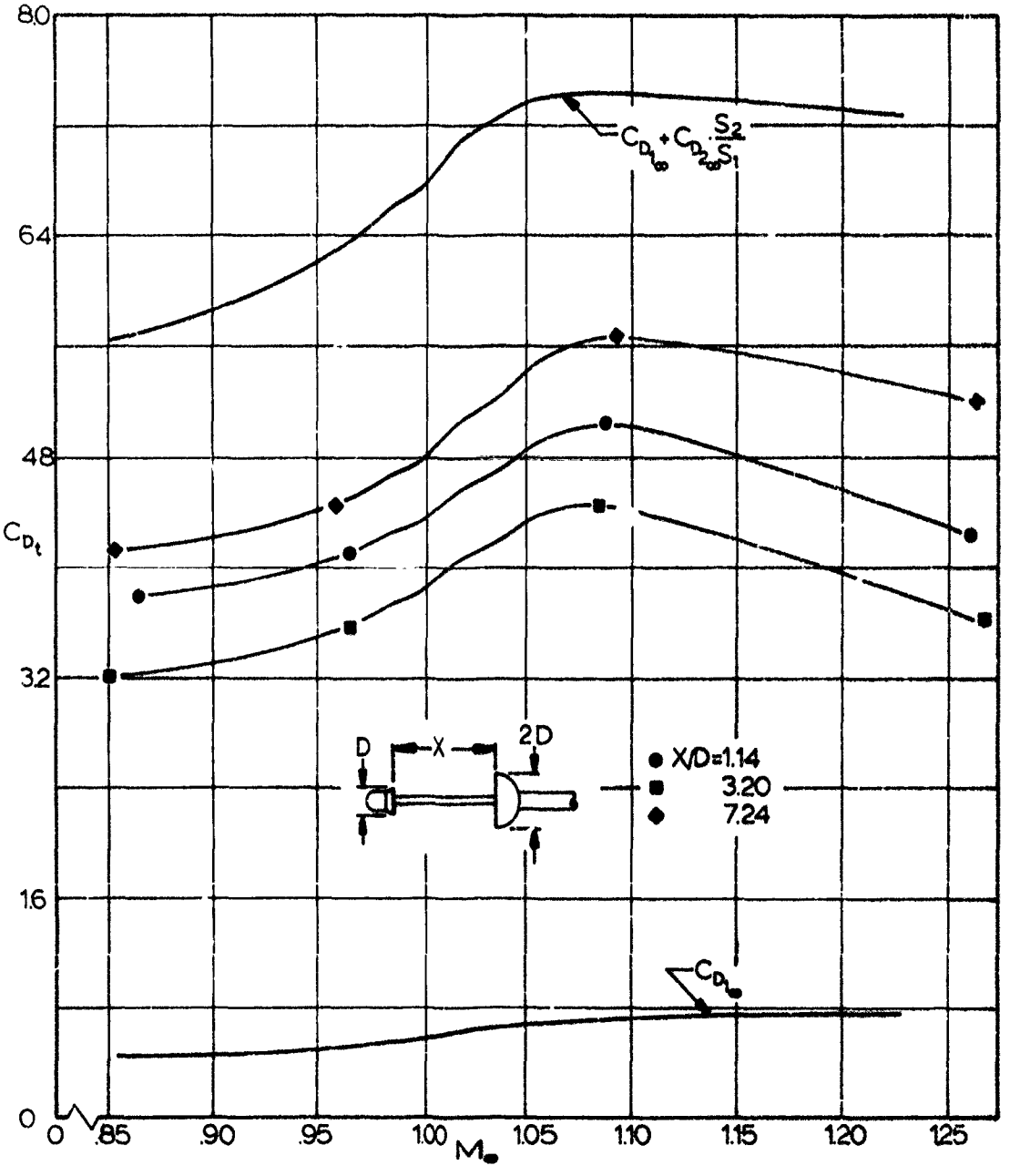

FIG 13. SYSTEM DRAG COEFFICIENT FOR SKIRTED HEMISPHERE AND HOLLOW HEMISPHERE WITH d/D = 2 AT TRANSONIC SPEEDS.

This unexpected decrease, which occurs also for the systems with the other secondary bodies (Figs 8, 10 and 12), has not been explained. It is not due to experimental error, since the pressure measurements show the same trends. See Figs 34 and 35 for an example. Whether it is caused by some wind tunnel interference phenomenon or by the particular suspension system used or is actually characteristic of such two-body systems has not been established.

With the larger plate as secondary body the change in drag with separation distance is not so great. It is interesting to note that the measurements at $M_\infty = 1.05$ indicate more drag with the secondary body at X/D = 2 than at 4. This occurs for d/D = 2 at this Mach number for both the plate and cone, while it occurs at all transonic Mach numbers for the hollow hemisphere. Figure 35 indicates that a higher pressure exists on the front of the plate at X/D = 2 than at 4, and Fig 36 indicates lower base pressure, substantiating this result. It is probably caused by interactions between the primary body wake and the secondary body.

The results for the systems with the 45° half-angle cone as secondary body, given in Figs 8 and 9, show the same general trends, however with a closer approach to the upper reference curve. The drag of the system with the large cone at X/D = 8 is approximately equal to the sum of the free stream drags of the two bodies.

The systems with the sphere and hollow hemisphere (Figs 10 through 13) also behave in the same general manner, with the trends for the system with the sphere being more like those of the cone and those for the system with the hollow hemisphere more like the flat plate.

These results are also plotted as drag efficiency, $\eta = C_{D_t}/(C_{D_{1\infty}} + C_{D_{2\infty}}\frac{S_2}{S_1})$, versus X/D in Figs 14 through 17. The systems with d/D = 1 show a smooth increase in drag with increasing body separation distance (except from X/D = 6 to

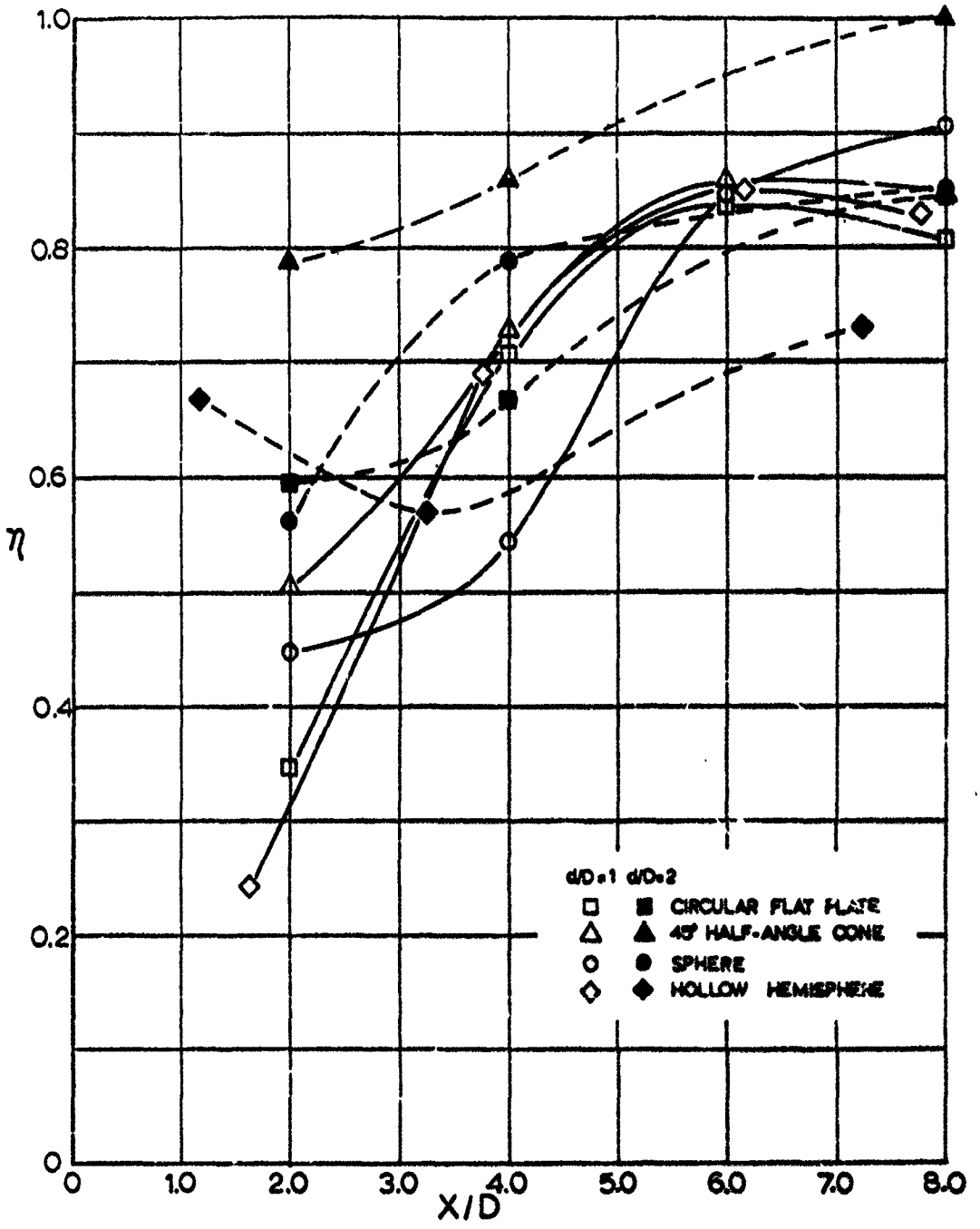

FIG 14. SYSTEM DRAG EFFICIENCY OF SKIRTED HEMISPHERE AND VARIOUS SECONDARY BODIES AT $M_\infty = 0.85$.

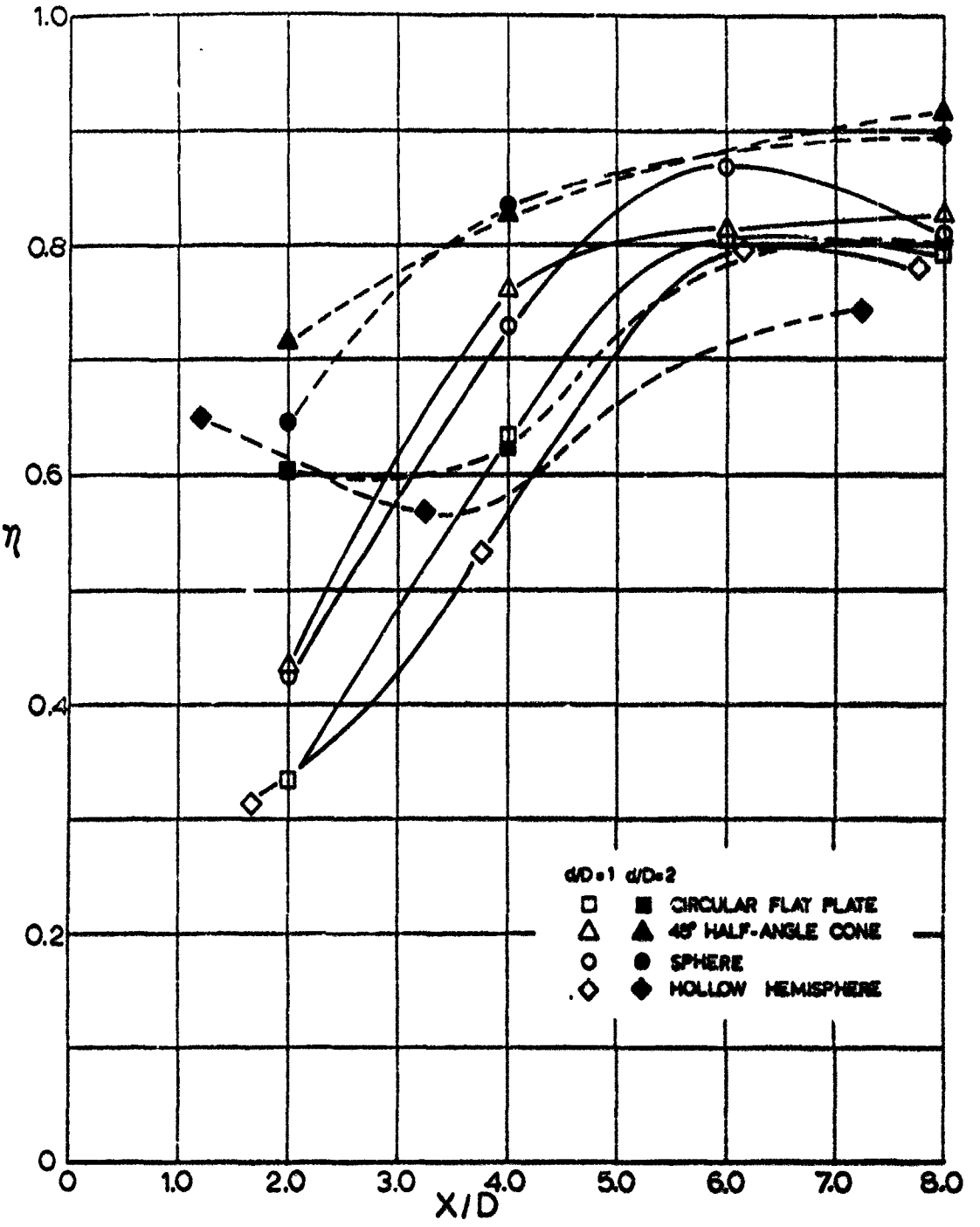

FIG 15. SYSTEM DRAG EFFICIENCY OF SKIRTED HEMISPHERE AND VARIOUS SECONDARY BODIES AT $M_\infty = 0.95$.

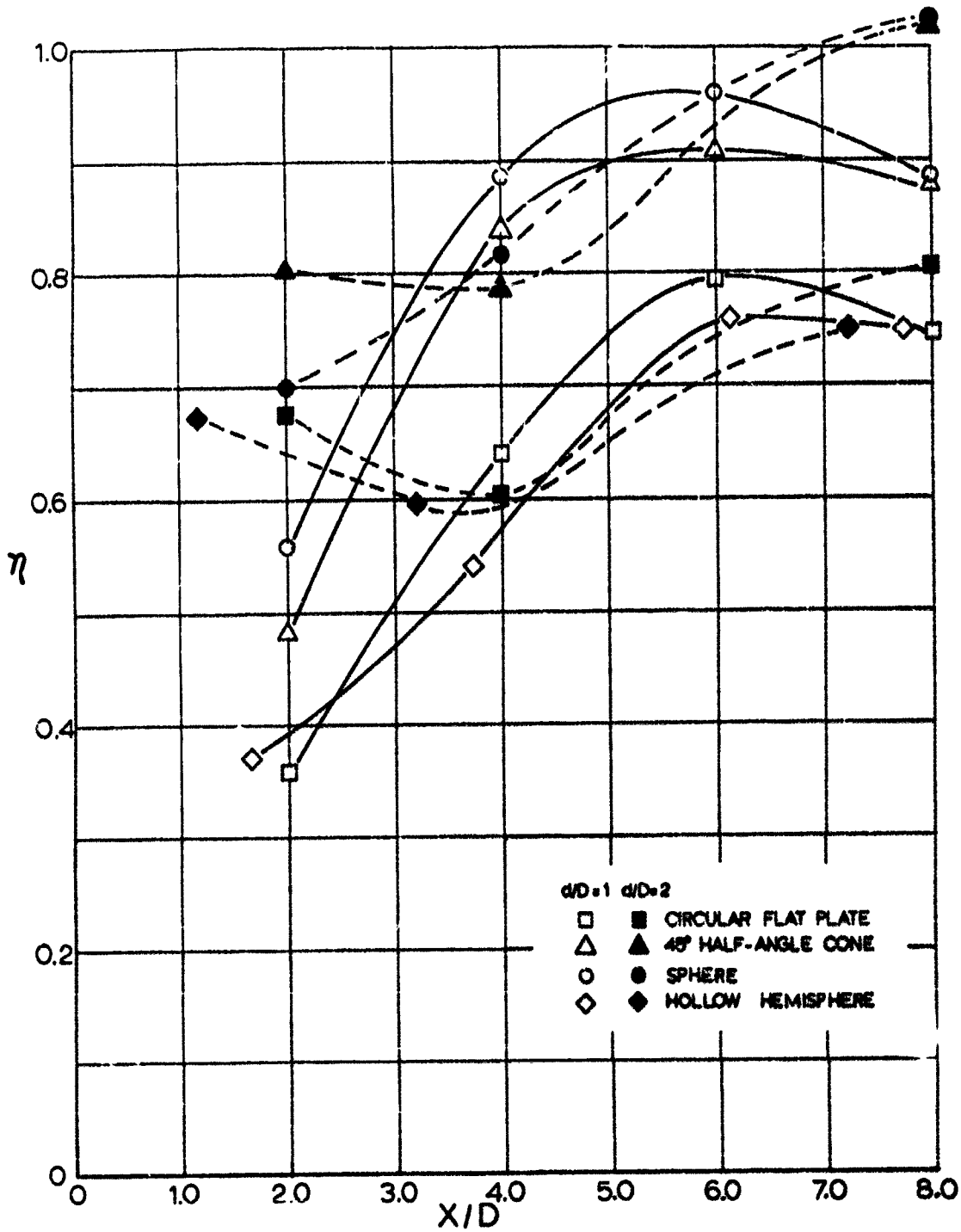

FIG 16. SYSTEM DRAG EFFICIENCY OF SKIRTED HEMISPHERE AND VARIOUS SECONDARY BODIES AT $M_\infty = 1.07$.

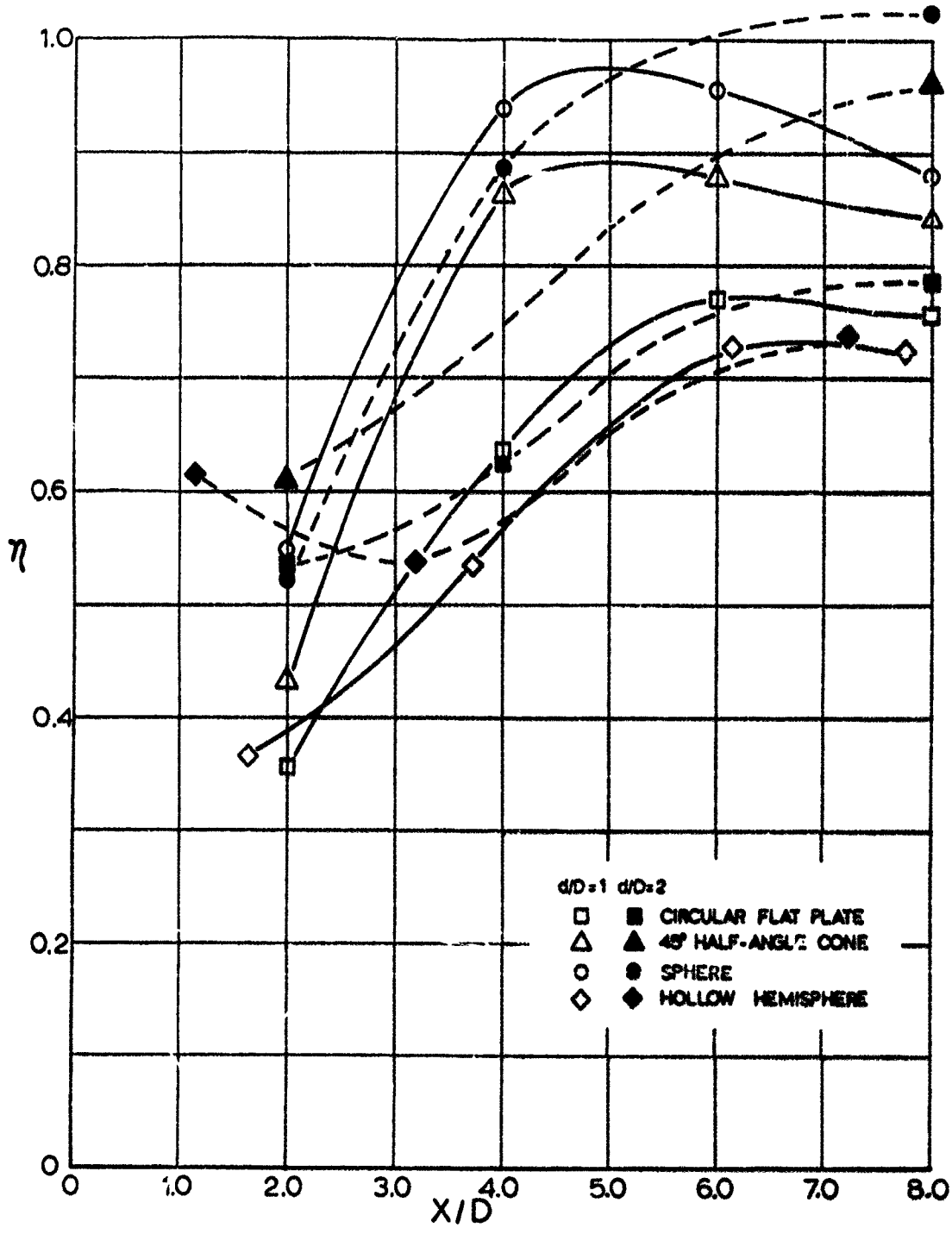

FIG 17. SYSTEM DRAG EFFICIENCY OF SKIRTED HEMISPHERE AND VARIOUS SECONDARY BODIES AT $M_\infty = 1.22$.

8, as noted previously), while those with d/D = 2 tend to dip at about X/D = 4. At the lowest Mach number (0.85) all of the systems with d/D = 1 have about the same drag efficiency; at higher Mach numbers the curves spread, however, with the spread increasing with increasing Mach number.

The systems with the sphere and 45° half-angle cone are generally more efficient than those with the plate and hollow hemisphere. It is also interesting to note that the systems with the flat plate and hollow hemisphere as secondary body have about the same drag efficiency at d/D = 1 as at d/D = 2 for X/D ≥ 4, particularly at the higher Mach numbers.

3.2 Drag Coefficients at Transonic Speeds with Ogive Cylinder as Primary Body

Reference 2 presents the drag coefficients of a flat plate, 45° half-angle cone, and sphere in the wake of a cylindrical body at transonic speeds. Included are measurements of the base and surface pressure on the cylinder. With the assumption that the wake of the cylindrical body used in these tests is the same as that of an ogive cylinder and that the presence of a downstream body would not alter the pressure on the nose of the ogive cylinder (which is indicated to be true in Appendix IV of Ref 2), these test results were used to calculate the system drag of the ogive cylinder in combination with the flat plate, 45° half-angle cone, and sphere. The system drag was thus calculated by

$$C_{D_t} = \frac{S_2}{S_1} C_{D_2} \text{ (from Ref 2)} + C_{D_1} \text{ (from Ref 3)} - (C_{p_{b_1}} - C_{p^*_{b_1}}),$$

where $C_{p_{b_1}}$ is the base pressure coefficient of the cylinder with the secondary body present and $C_{p^*_{b_1}}$ is the base pressure

coefficient of the cylinder without a secondary body. Values for $C_{p_{b_1}}$ and $C^*_{p_{b_1}}$ were obtained from Ref 2.

The results of the calculations are presented in Figs 18 through 23. The trends indicated are very similar to those observed through direct measurements for the systems with the skirted hemisphere as primary body. The drag of the systems with the smaller secondary bodies at X/D = 2 is not as close to the lower reference curve, however.

It is interesting to note that for $M_\infty > 1$ the ogive cylinder - flat plate system with d/D = 2 has more drag with the plate at X/D = 2 than at 4, just as the skirted hemisphere - flat plate system did at $M_\infty = 1.08$.

These results are also plotted as drag efficiency versus X/D in Figs 24 through 27. The same general trends are indicated for the ogive cylinder primary body systems as for those with the skirted hemisphere as primary body, except that the curves for d/D = 1 are not as steep from X/D = 2 to X/D = 4.

3.3 Drag Coefficients at $M_\infty = 4.35$

The drag coefficients of the various systems at $M_\infty = 4.35$ are presented in Figs 28 through 31. The Reynolds number for these tests was about 3.0×10^5, except where noted differently. Free stream reference values given are from Ref 3.

There is some similarity between these curves and those at transonic speeds, but the drag coefficient values are generally much farther below the upper reference values. For the systems with the skirted hemisphere as primary body and d/D = 1 (Fig 28). C_{D_t} at X/D = 2 is about equal to the drag coefficient of the skirted hemisphere alone. It increases as X/D increases to 4, but then drops of remains about the same with further increase to X/D = 8.

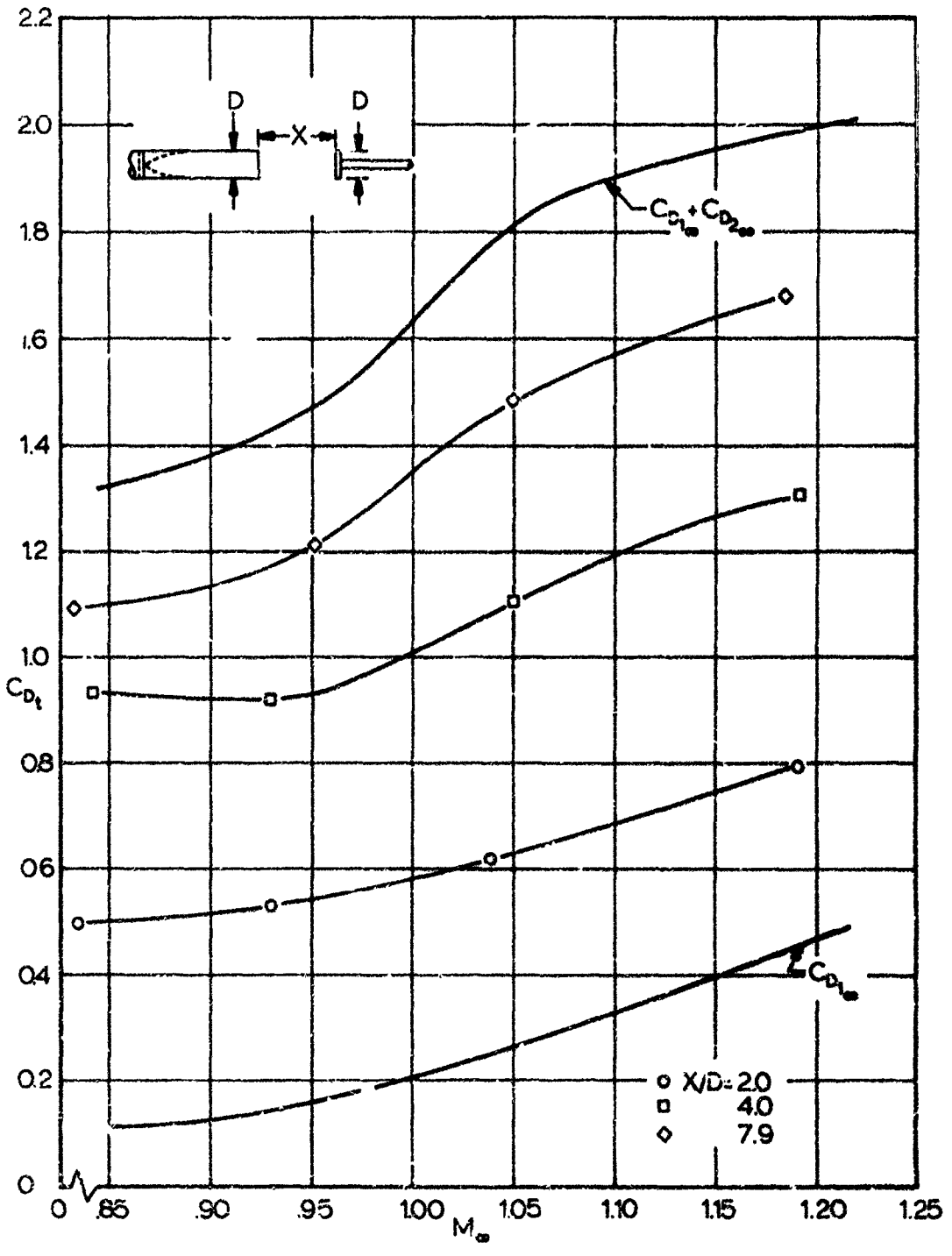

FIG 18. SYSTEM DRAG COEFFICIENT FOR OGIVE CYLINDER AND FLAT PLATE WITH d/D=1 AT TRANSONIC SPEEDS. (CALCULATED FROM RESULTS OF REF 2)

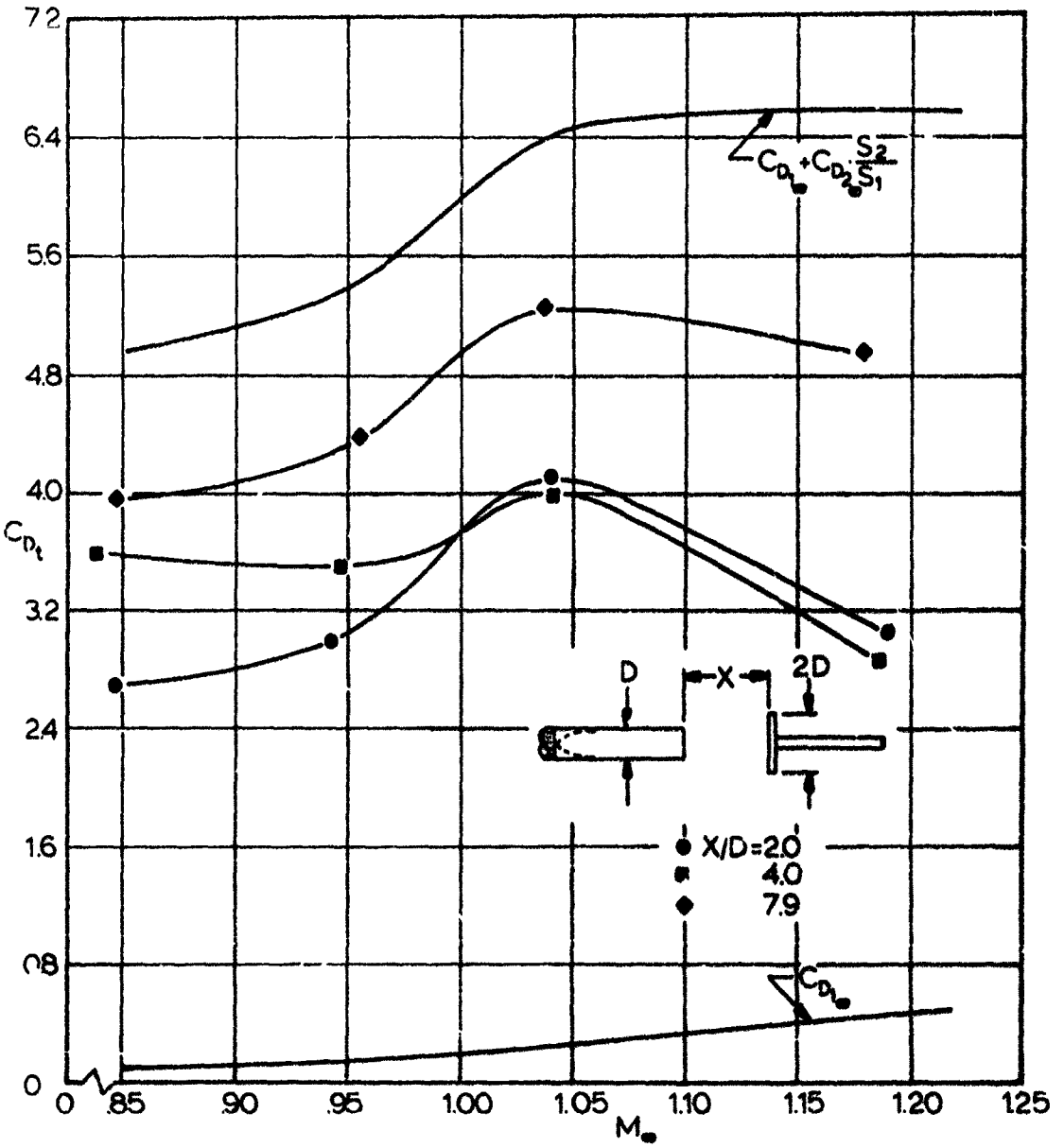

FIG 19. SYSTEM DRAG COEFFICIENT FOR OGIVE CYLINDER AND FLAT PLATE WITH d/D=2 AT TRANSONIC SPEEDS. (CALCULATED FROM RESULTS OF REF. 2)

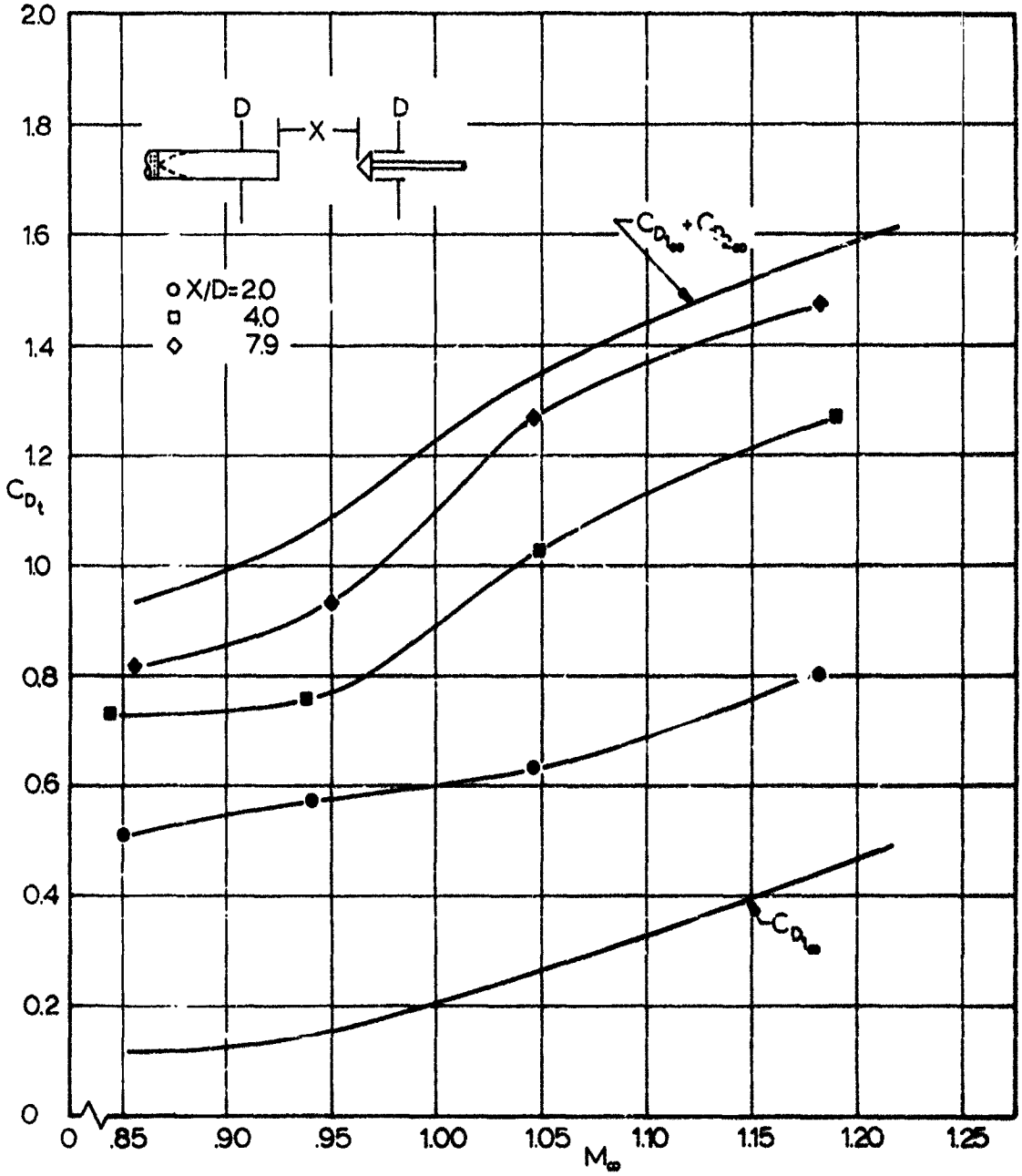

FIG 20. SYSTEM DRAG COEFFICIENT FOR OGIVE CYLINDER AND 45° HALF-ANGLE CONE WITH d/D=1 AT TRANSONIC SPEEDS. (CALCULATED FROM RESULTS OF REF. 2)

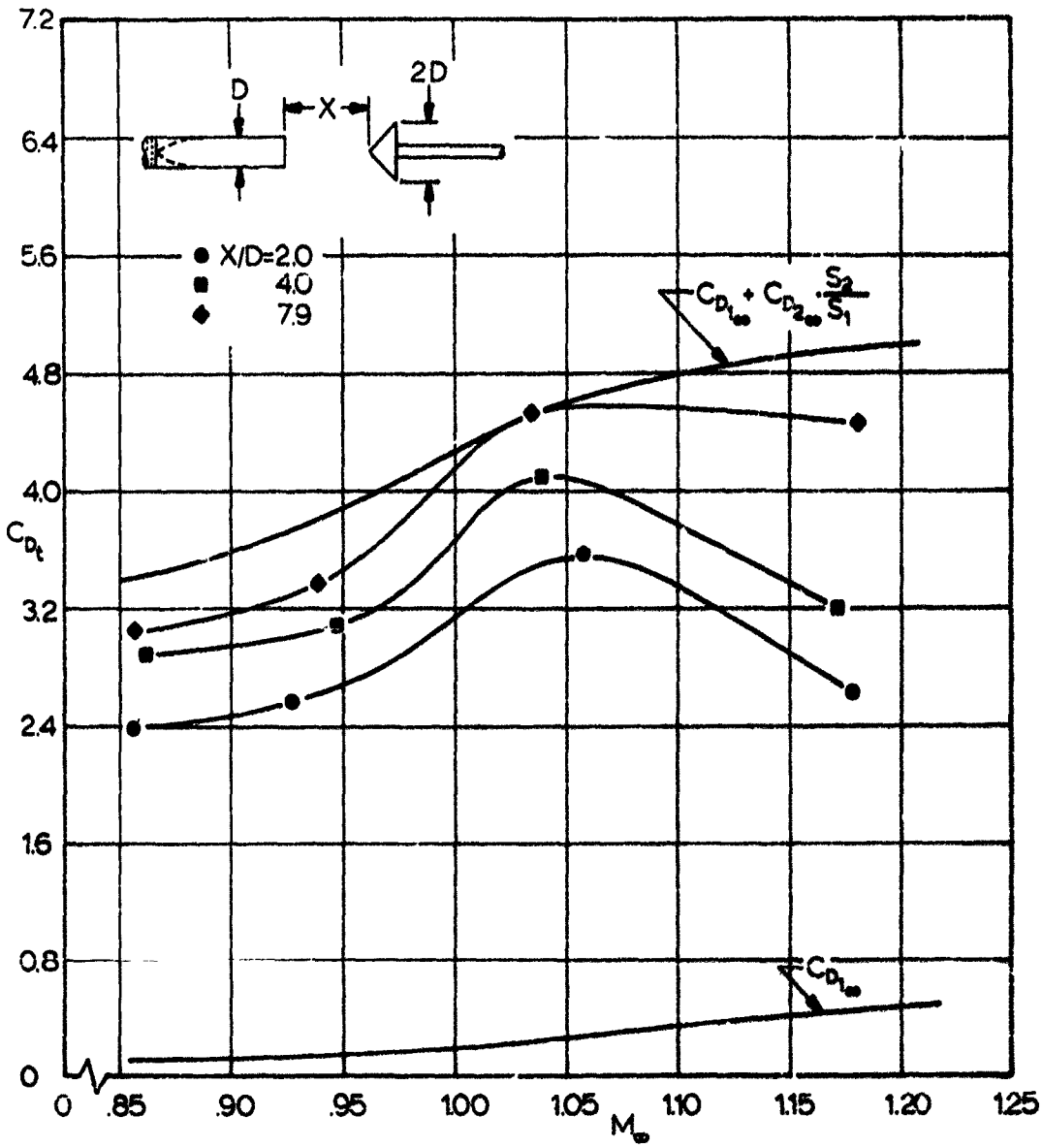

FIG 21. SYSTEM DRAG COEFFICIENT FOR OGIVE CYLINDER AND 45° HALF-ANGLE CONE WITH d/D=2 AT TRANSONIC SPEEDS. (CALCULATED FROM RESULTS OF REF. 2)

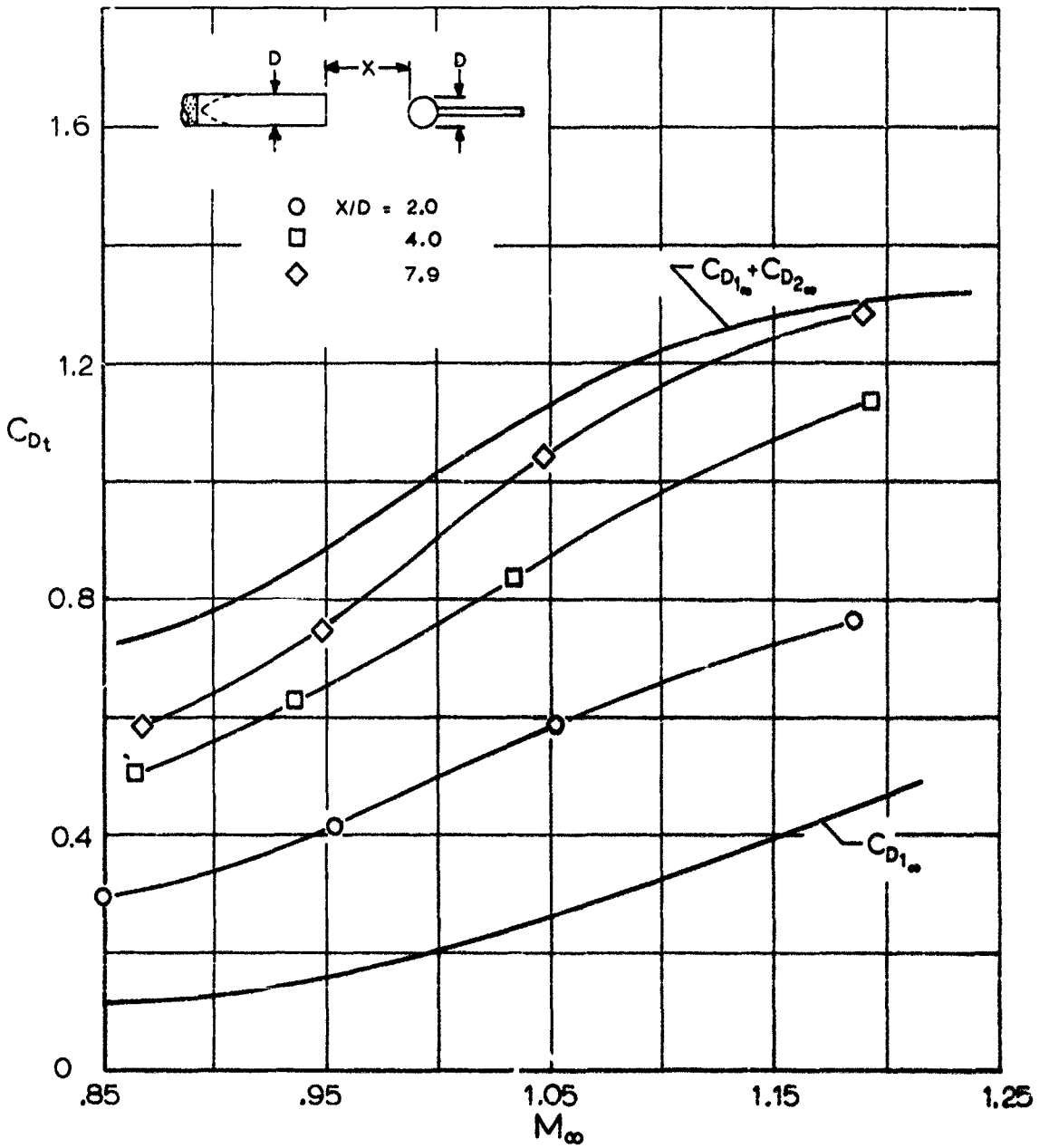

FIG 22. SYSTEM DRAG COEFFICIENT FOR OGIVE CYLINDER AND SPHERE WITH d/D = 1 AT TRANSONIC SPEEDS. (CALCULATED FROM RESULTS OF REF 2)

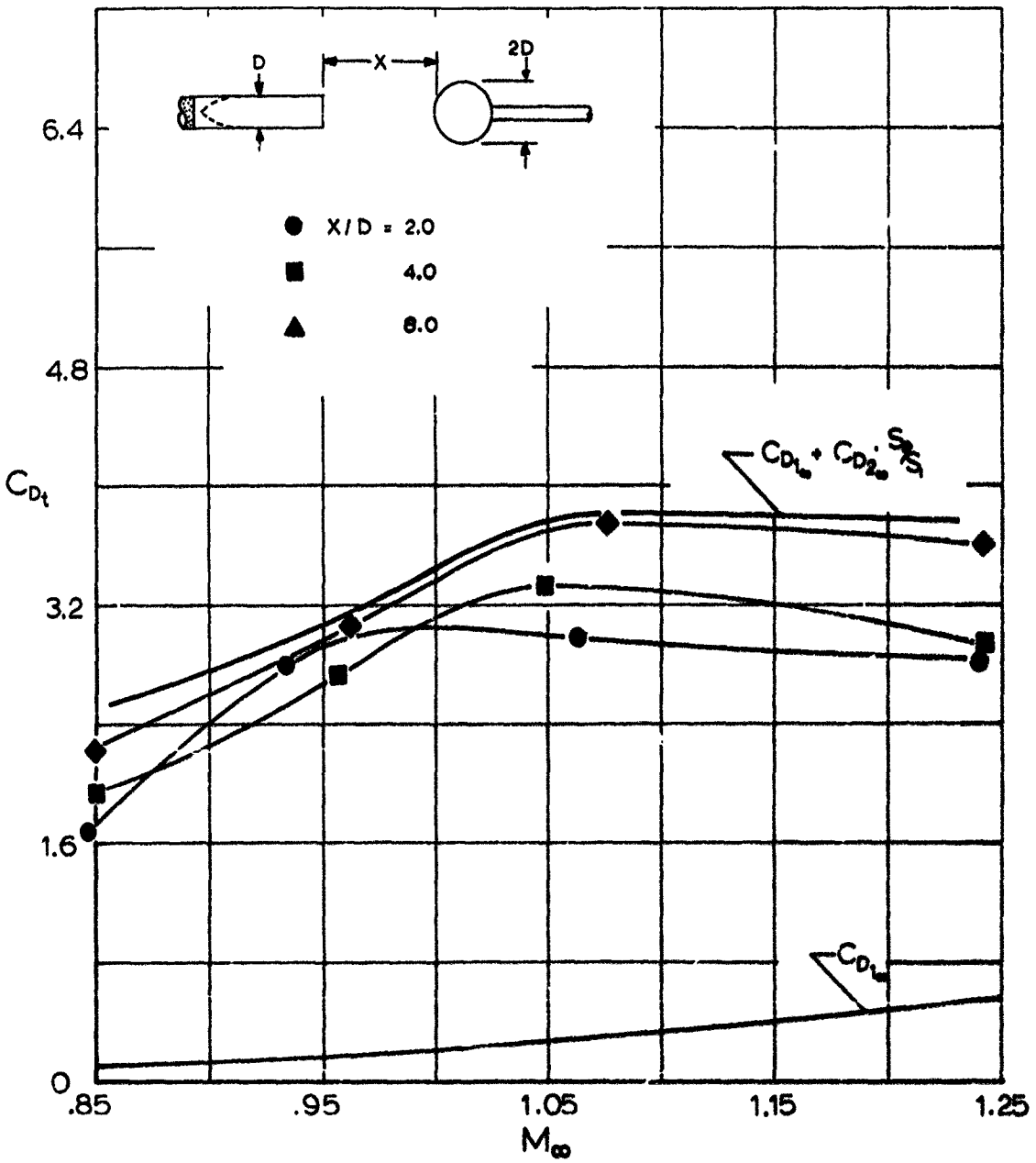

FIG 23. SYSTEM DRAG COEFFICIENT FOR OGIVE CYLINDER AND SPHERE WITH d/D = 2 AT AT TRANSONIC SPEEDS. (CALCULATED FROM RESULTS OF REF 2)

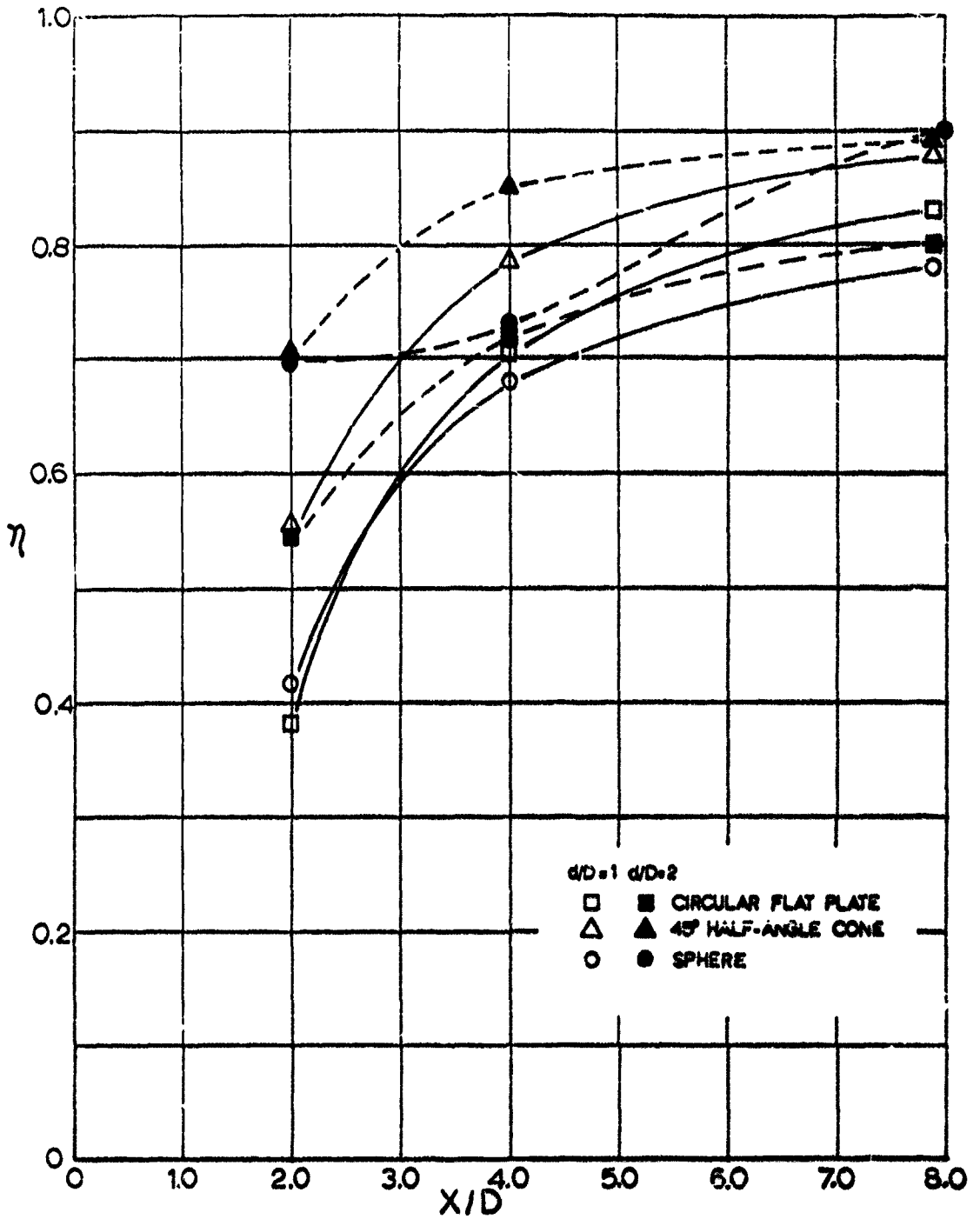

FIG 24. SYSTEM DRAG EFFICIENCY OF OGIVE CYLINDER AND VARIOUS SECONDARY BODIES AT $M_\infty = 0.85$.

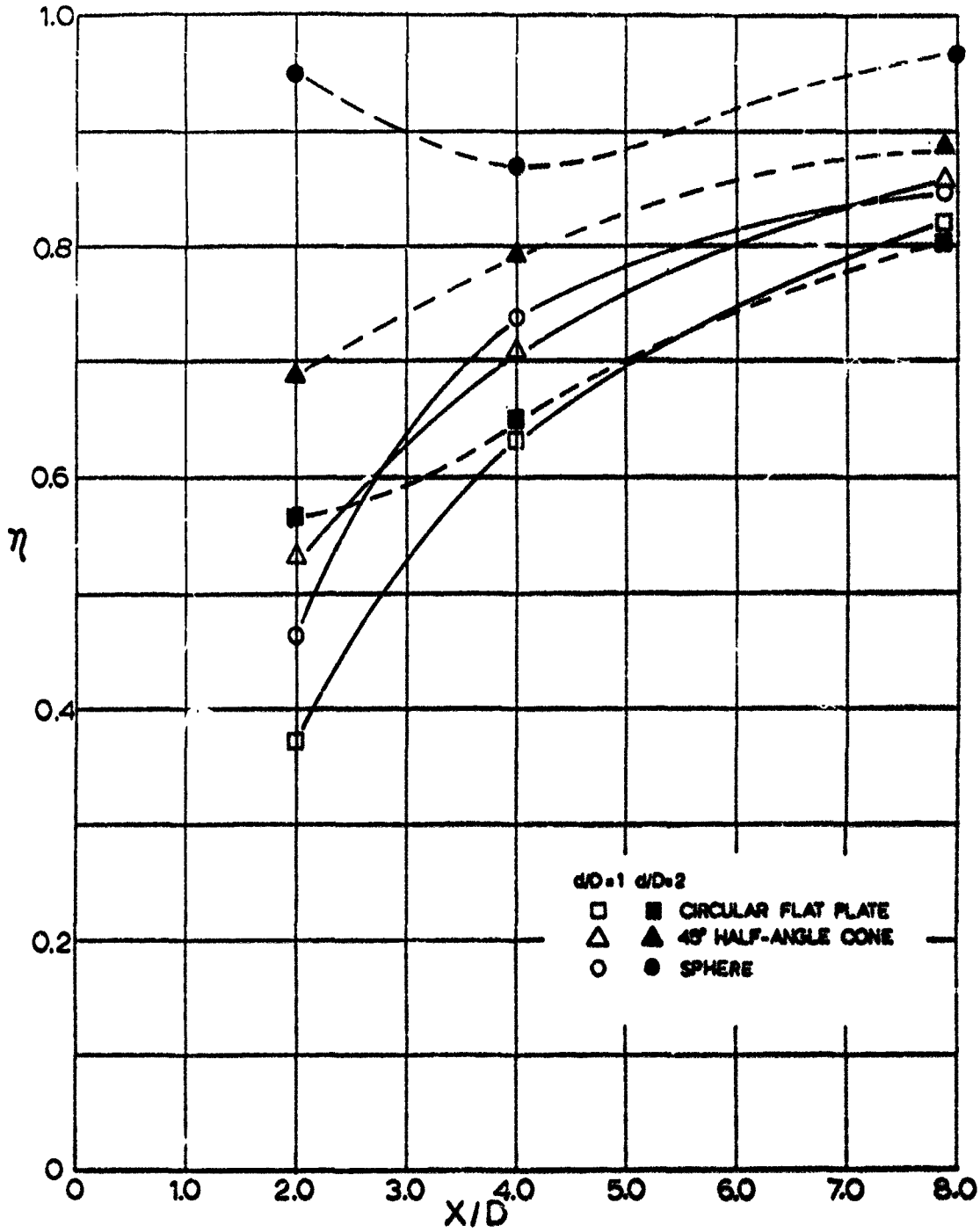

FIG 25.SYSTEM DRAG EFFICIENCY OF OGIVE CYLINDER AND VARIOUS SECONDARY BODIES AT $M_\infty = 0.95$.

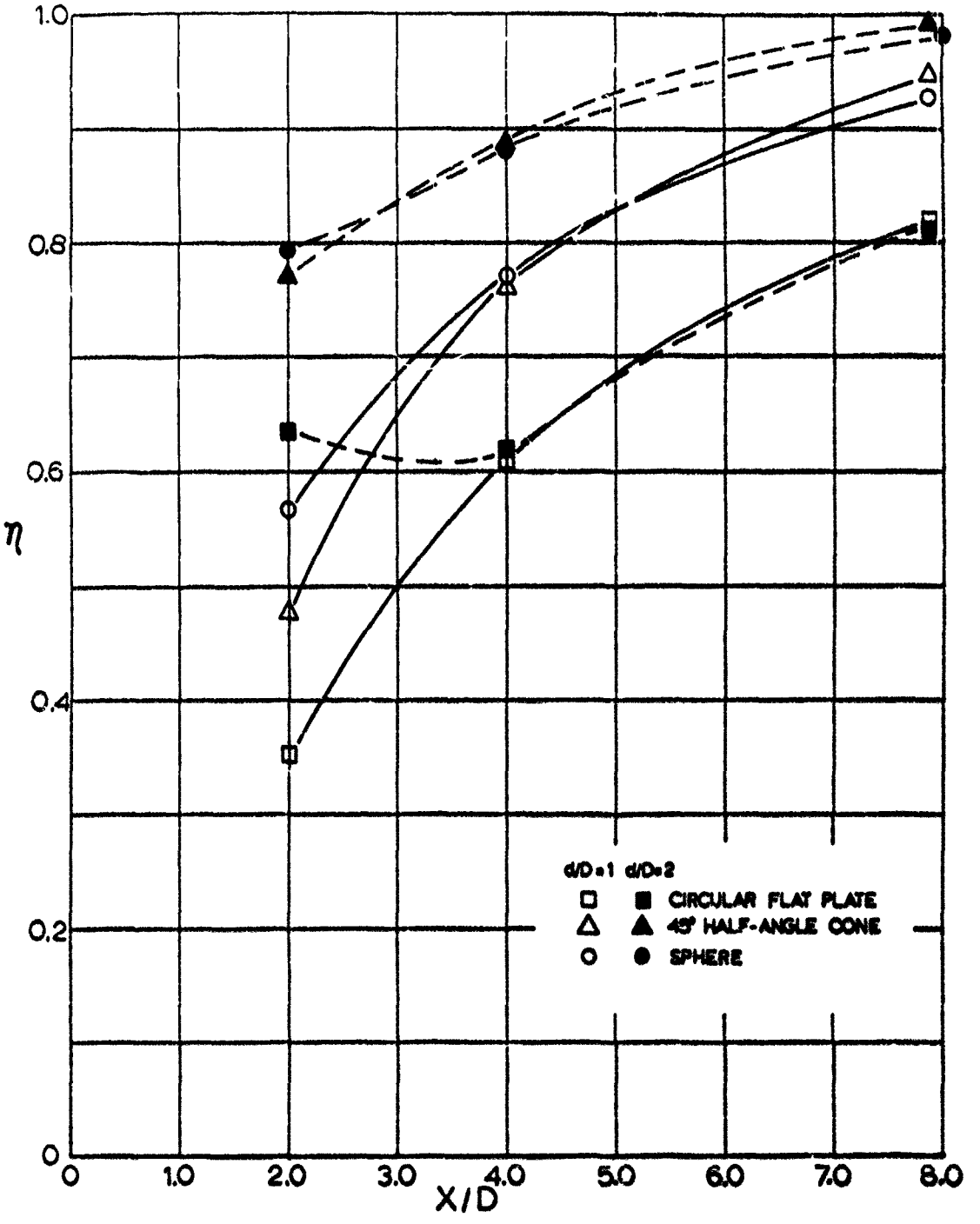

FIG 26. SYSTEM DRAG EFFICIENCY OF OGIVE CYLINDER AND VARIOUS SECONDARY BODIES AT $M_\infty = 1.05$.

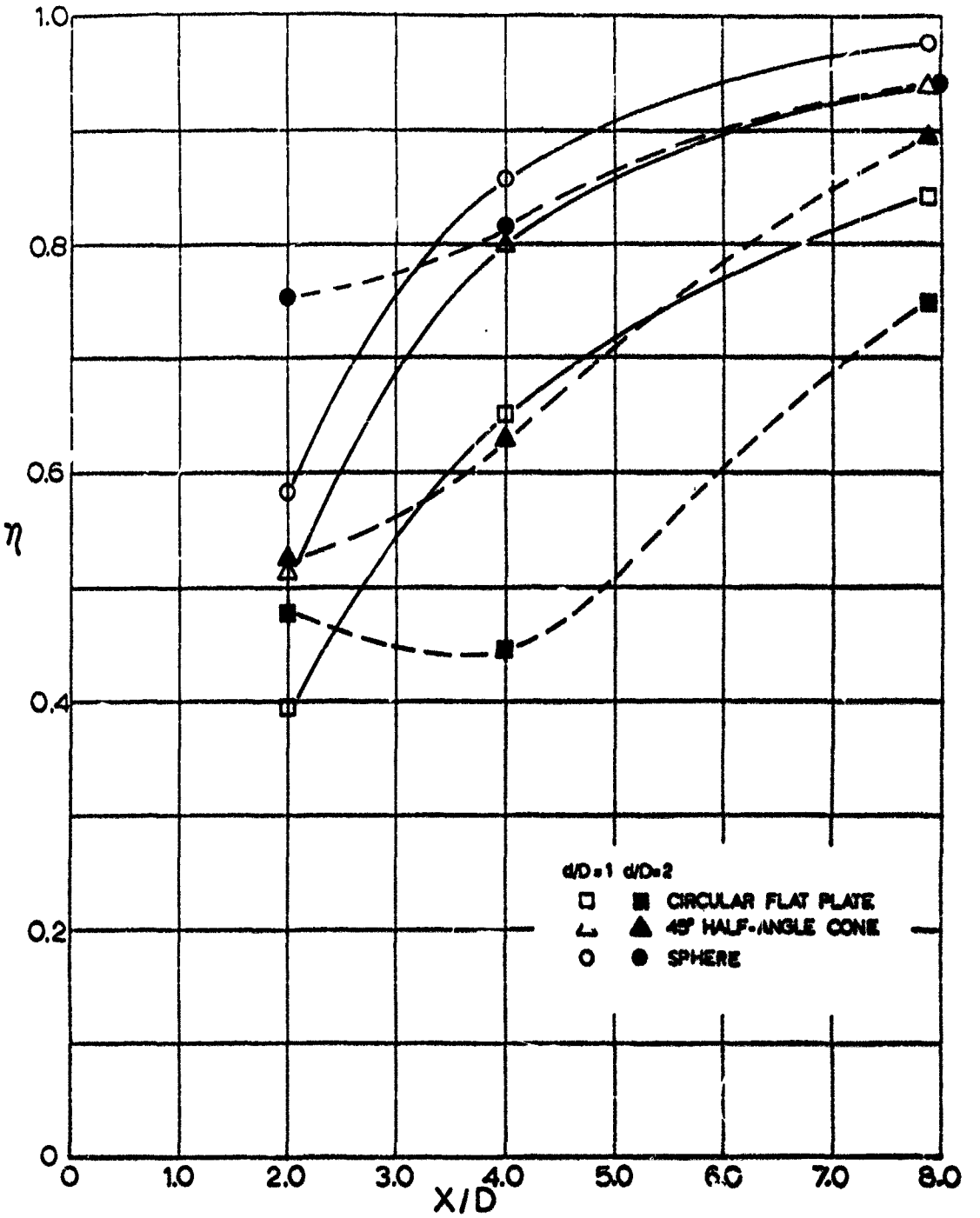

FIG 27. SYSTEM DRAG EFFICIENCY OF OGIVE CYLINDER AND VARIOUS SECONDARY BODIES AT $M_\infty = 1.18$.

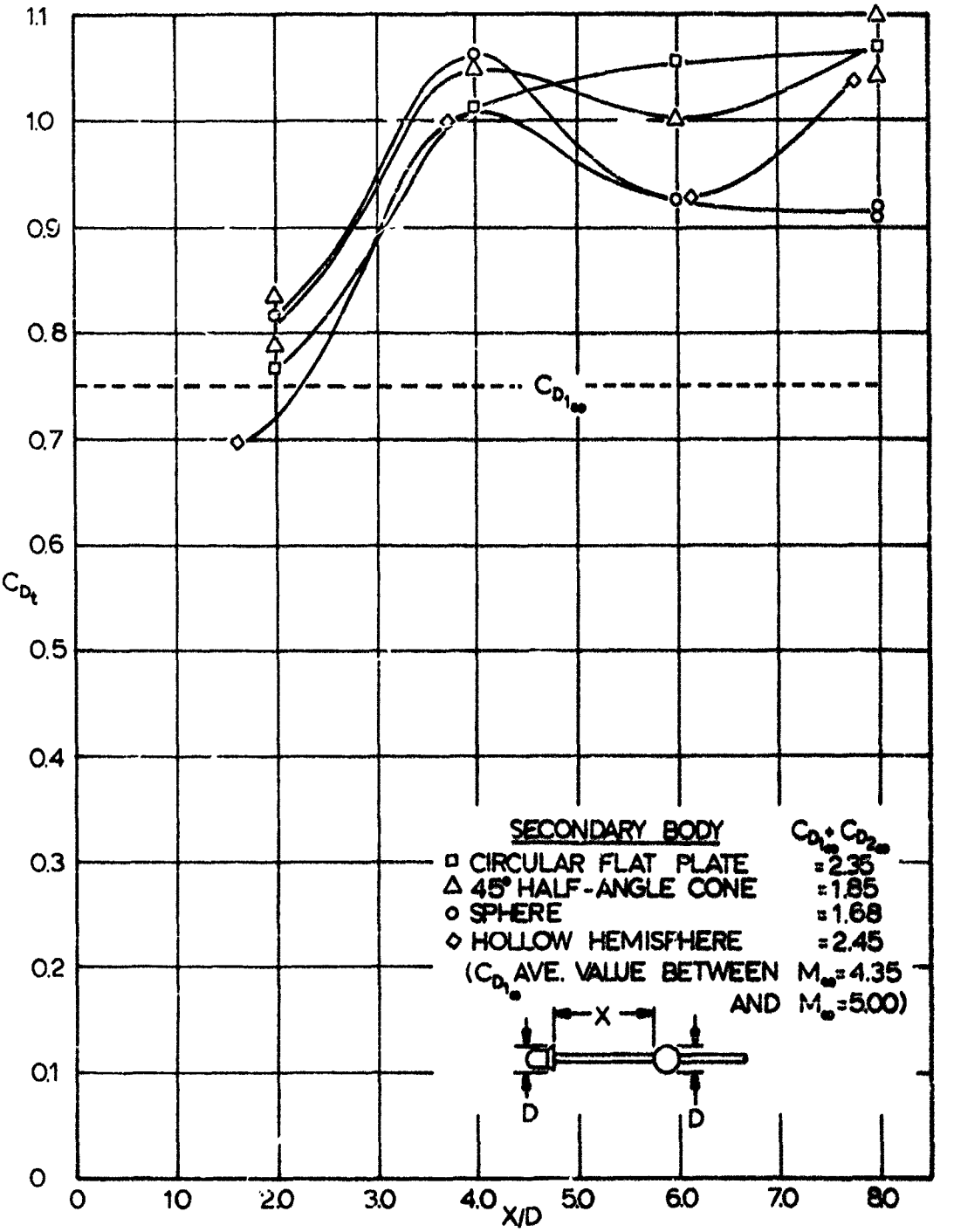

FIG 28. SYSTEM DRAG COEFFICIENT FOR SKIRTED HEMISPHERE AND VARIOUS SECONDARY BODIES WITH d/D=1 AT M_∞= 4.35.

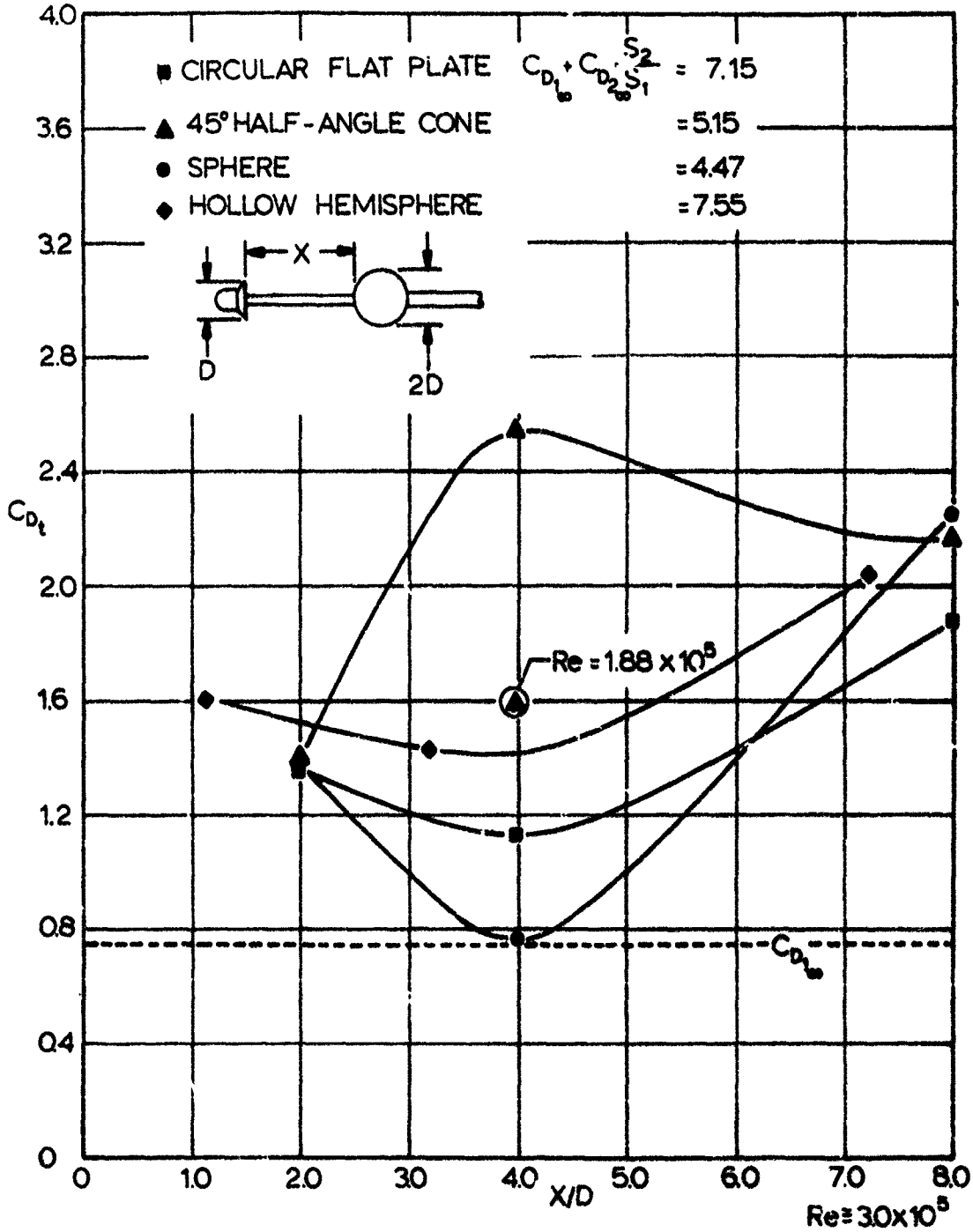

FIG 29. SYSTEM DRAG COEFFICIENT FOR SKIRTED HEMISPHERE AND VARIOUS SECONDARY BODIES WITH d/D=2 AT M_∞ = 4.35.

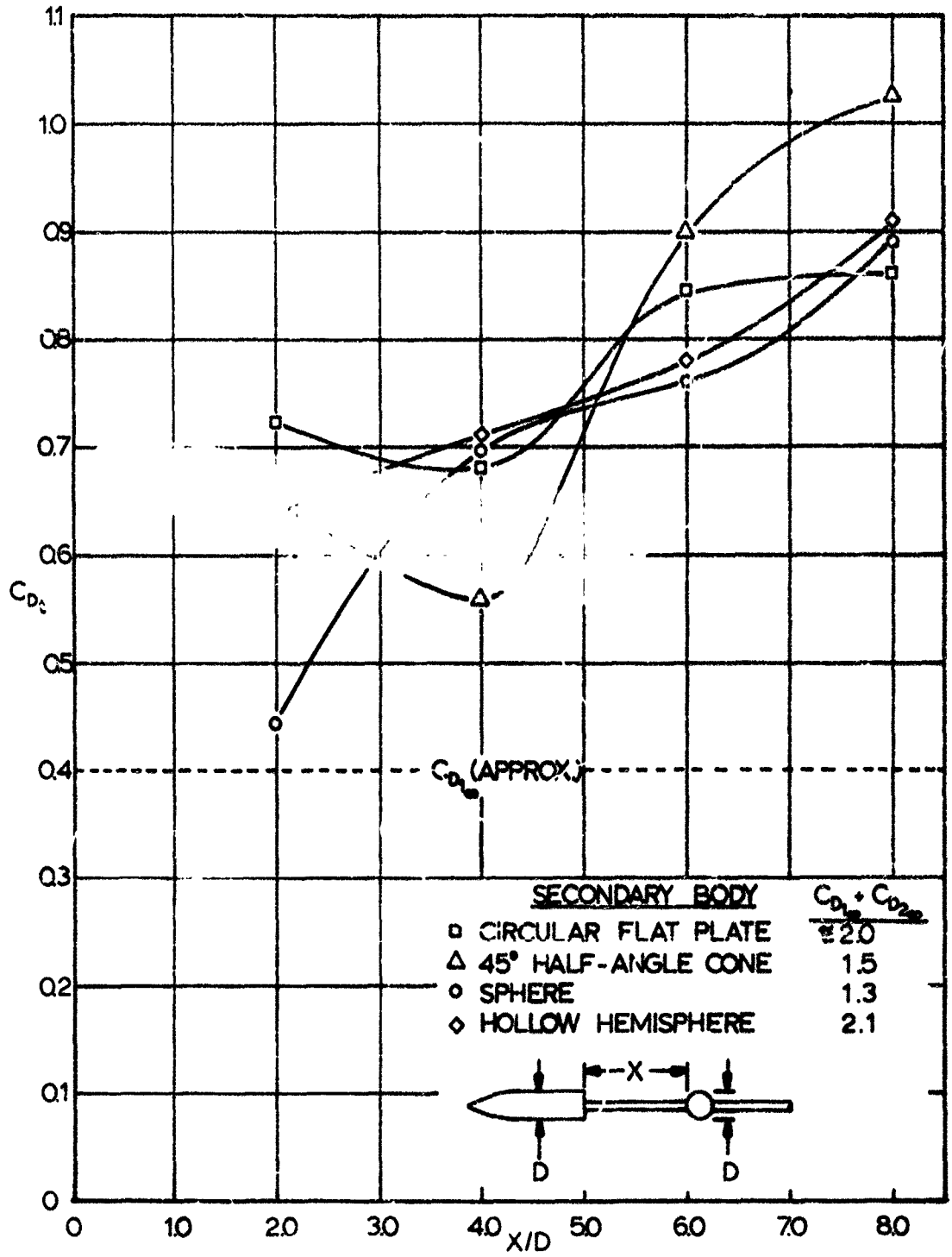

FIG 30. SYSTEM DRAG COEFFICIENT FOR OGIVE CYLINDER AND VARIOUS SECONDARY BODIES WITH d/D=1 AT M_∞= 4.35.

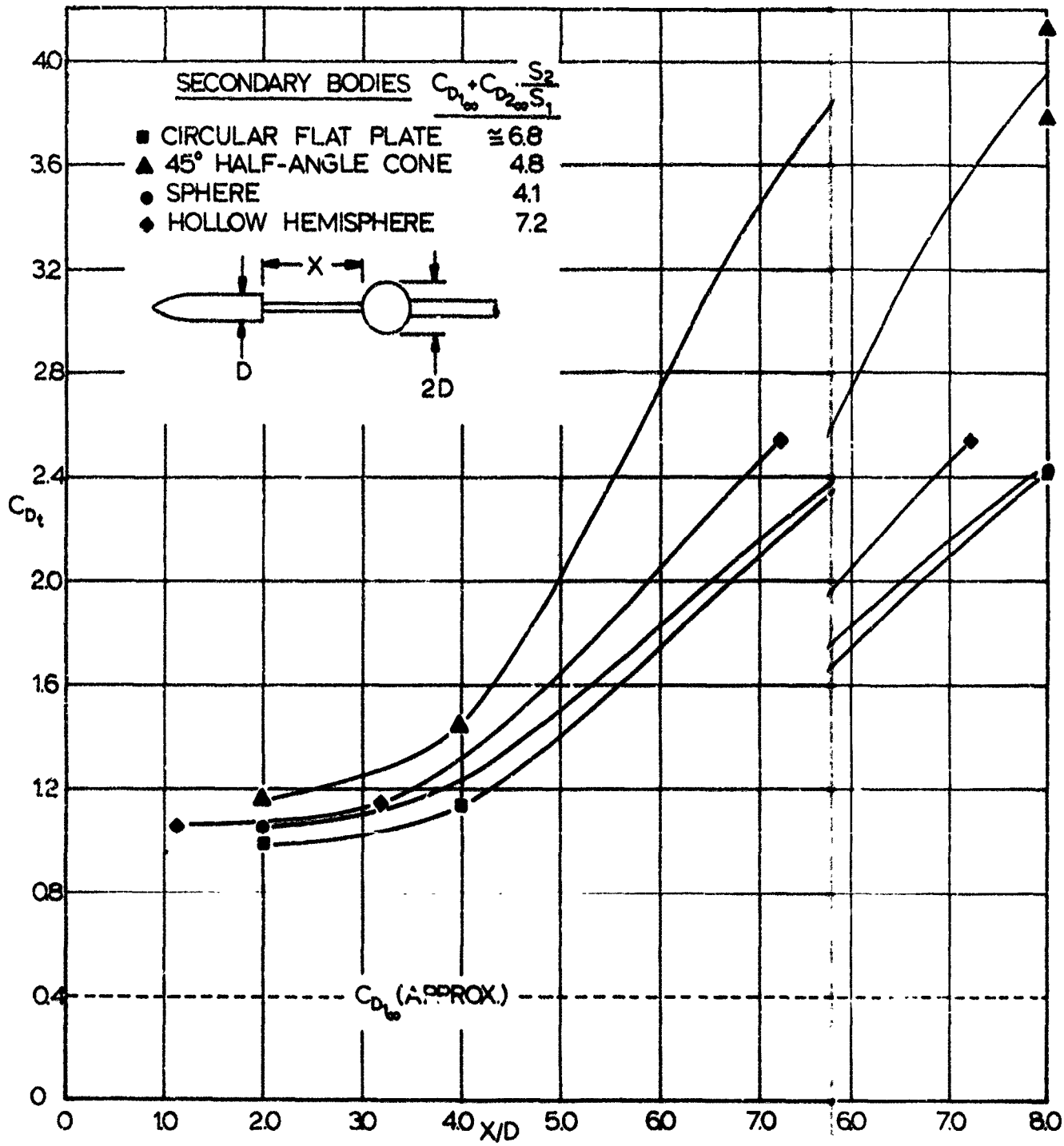

FIG 31. SYSTEM DRAG COEFFICIENT FOR OGIVE OR OGIVE CYLINDER AND VARIOUS SECONDARY BODIES WITBODIES WITH d/D = 2 AT M_∞ = 4.35.

With the larger secondary bodies (Fig 29), except for the conc, C_{D_t} decreases from X/D = 2 to X/D = 4 and then begins a gradual increase. A lower value for the cone at X/D = 4 (flagged symbol) was obtained by lowering the wind tunnel stagnation pressure by about half. Pressure coefficient changes on the bodies (Fig 47) substantiate the lower value. This indicates the possibility of strong Reynolds number effects. This phenomenon was not studied any further because it was beyond the scope of this investigation.

The systems with the ogive cylinder as primary body (Figs 30 and 31) indicate a more regular increase of drag with increasing body separation distance, but as in Figs 28 and 29 the type of secondary body does not seem to be particularly significant, except for the large cone. The system with the cone shows a drag coefficient at X/D = 8 of better than 80% of the free stream reference value, while with the other bodies it is around 50% and less. The Schlieren photograph of this test (Fig 66c) shows a strong, steady secondary body shock.

It should be noted here that the Schlieren photographs in Appendix II indicate that unsteady flow phenomena about the secondary body accompany many of the supersonic tests, particularly those with the large flat plate and hollow hemisphere. The drag values presented represent the average of a continuous recording taken over a short period of time.

It is interesting to note that with the larger secondary bodies the systems with the more streamlined primary body have the greater drag at X/D = 8, indicating that the reduction in secondary body drag due to the larger wake of the skirted hemisphere more than offsets the greater drag of this body.

These results are also presented as drag efficiency versus body separation distance in Figs 32 and 33. Generally,

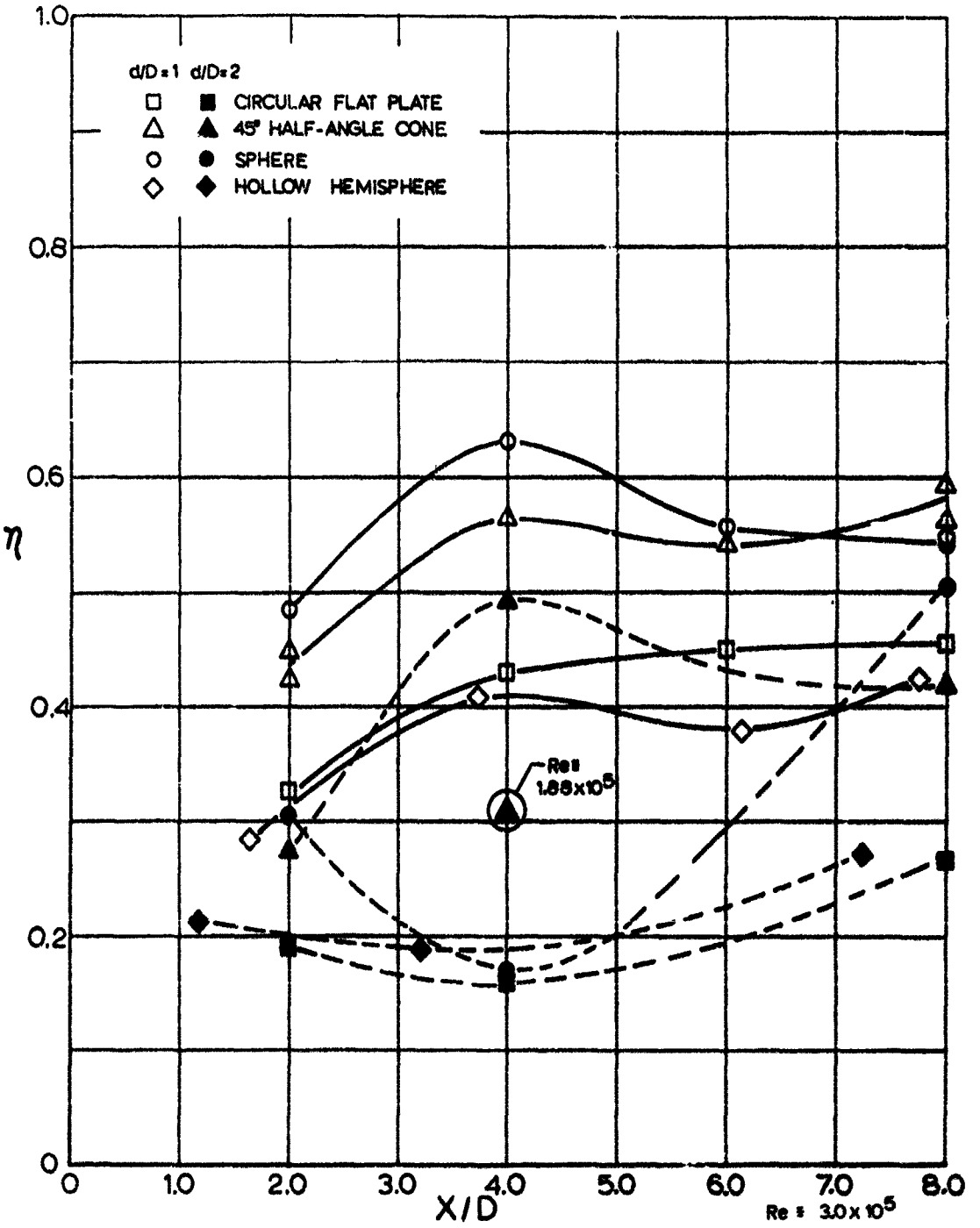

FIG 32. SYSTEM DRAG EFFICIENCY OF SKIRTED HEMISPHERE AND VARIOUS SECONDARY BODIES AT $M_\infty = 4.35$.

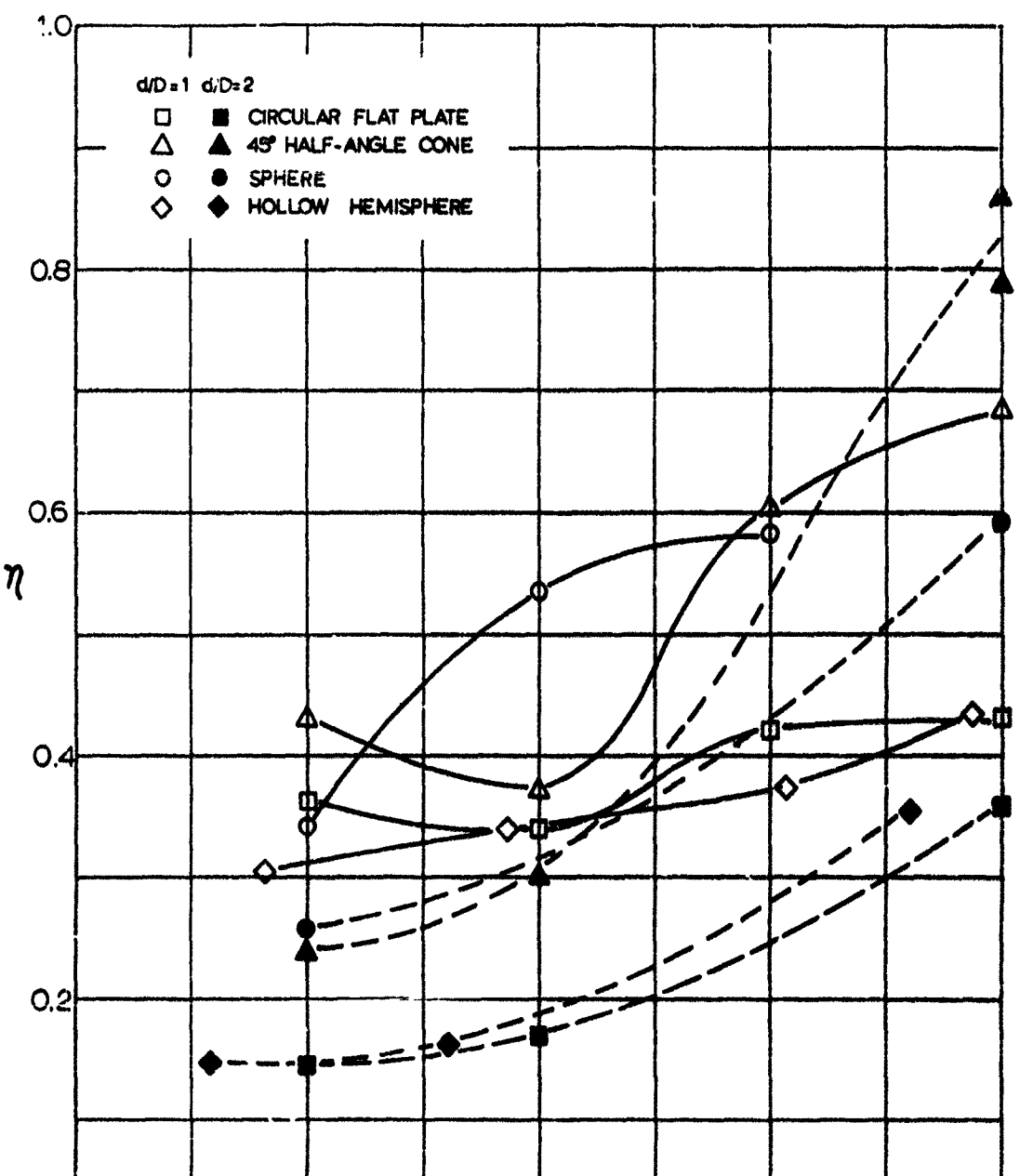

FIG 33. SYSTEM DRAG EFFICIENCY OF OGIVE CYLINDER AND VARIOUS SECONDARY BODIES AT $M_\infty = 4.35$.

the systems with d/D = 1 have greater efficiency than those with d/D = 2 in the X/D range of these tests. This may be understood in view of the fact that the drag of the primary body, which is only slightly altered by the presence of the secondary body, is a large percentage of the system drag.

Also, as in transonic flow, the systems with the flat plate and hollow hemisphere have quite similar efficiencies at $M_\infty = 4.35$. The same is true with the sphere and 45° half-angle cone.

4. CONCLUSIONS

Within the scope of this study, a strong interaction between the drag of the forebody and the secondary body was noticed. With a few exceptions in the transonic range, the drag of the system was less than the sum of the drag of the two bodies in the free stream. In the exceptional cases the drag of the system was about equal to the sum of the drag components.

The relative size and location of the secondary body, as well as the free stream Mach number, are the governing parameters. In an isolated case involving the 45° half-angle cone as secondary body, an appreciable Reynolds number influence was detected. (A further summary of other but related wake phenomena is given in Ref 5.)

APPENDIX I

PRESSURE COEFFICIENTS

As support for the drag measurements and also to indicate the pressure levels to which similar decelerators may be subjected, the primary body base pressure and secondary body stagnation and base pressure coefficients have been determined. Those for the systems with the skirted hemisphere as primary body at transonic speeds are given in Figs 34 through 45. For the tests at supersonic speed the pressures are presented in Figs 46 through 53.

Similar data for the ogive cylinder as forebody are presented in Ref 2.

Since the trends here are generally the same as those for the drag coefficients, a detailed discussion of these results is not presented. However, a few interesting points may be made.

The base pressure of the secondary bodies varies very little with X/D at both transonic and supersonic speeds. At $M_\infty = 4.35$ the primary body base pressure also is little affected by X/D changes, particularly with d/D = 1. Thus, it appears that most of the reduction in system drag at supersonic speeds is due to reduced pressures on the front side of the secondary body.

Figures 46 through 53 indicate that at $M_\infty = 4.35$ the primary body base pressure and secondary body stagnation pressure are generally about the same when the bodies are close together, indicating the presence of a more or less completely separated region between them.

In a review of the following graphs, a certain allowance should be made for experimental errors.

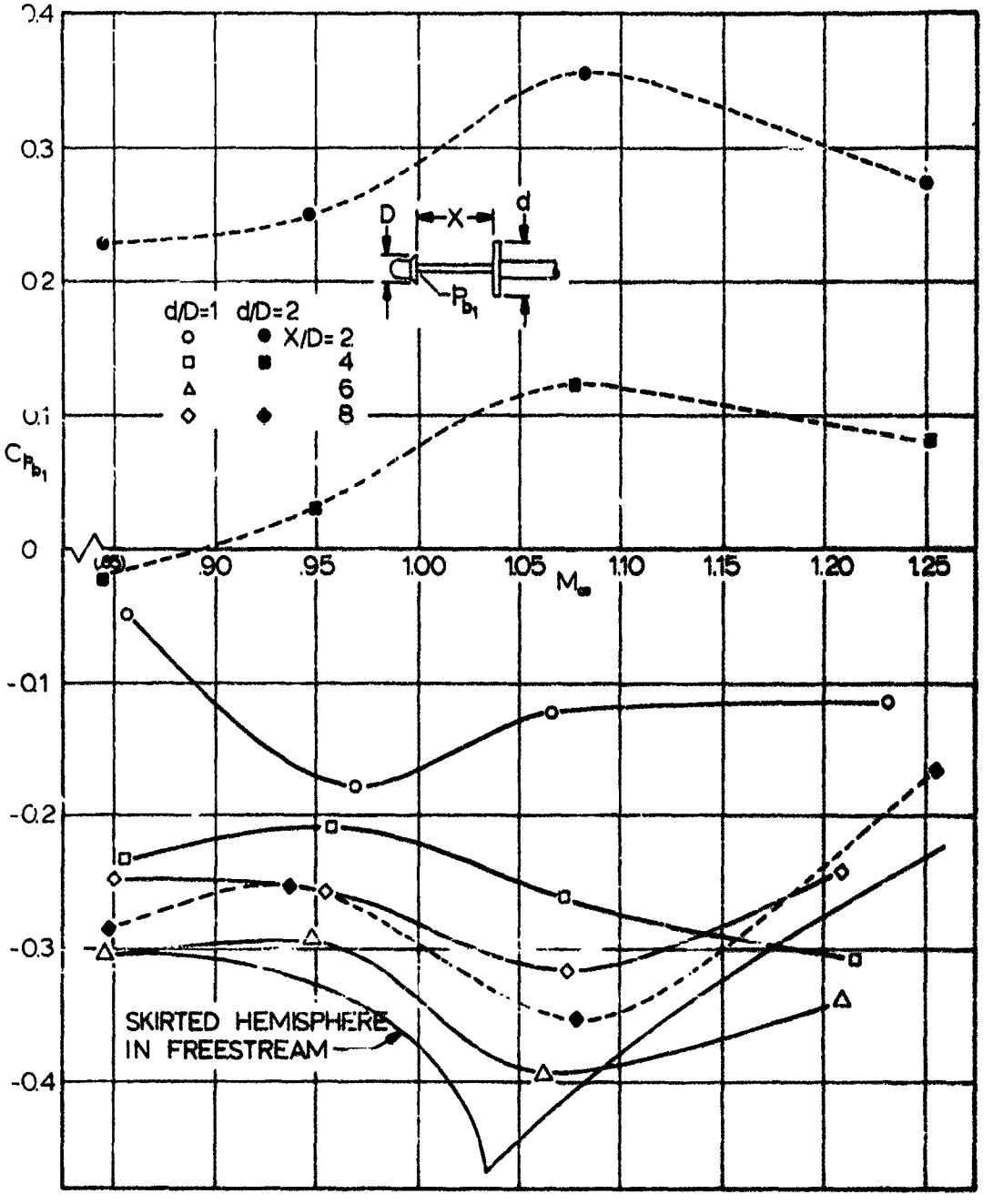

FIG 34. BASE PRESSURE COEFFICIENT OF SKIRTED HEMISPHERE WITH FLAT PLATE IN WAKE AT TRANSONIC SPEEDS.

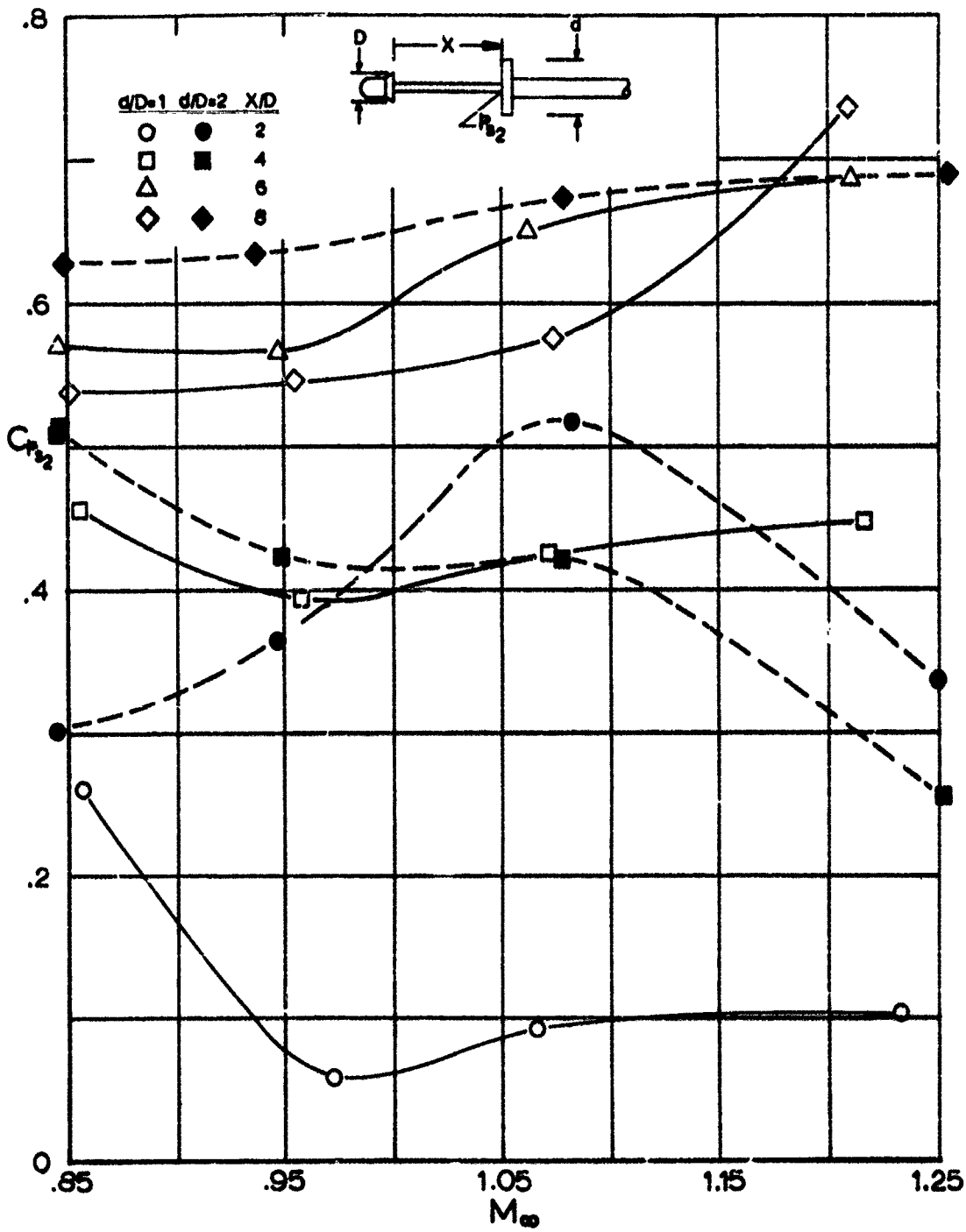

FIG 35. STAGNATION PRESSURE COEFFICIENT OF FLAT PLATE IN WAKE OF SKIRTED HEMISPHERE AT TRANSONIC SPEEDS.

THIS
PAGE
IS
MISSING
IN
ORIGINAL
DOCUMENT

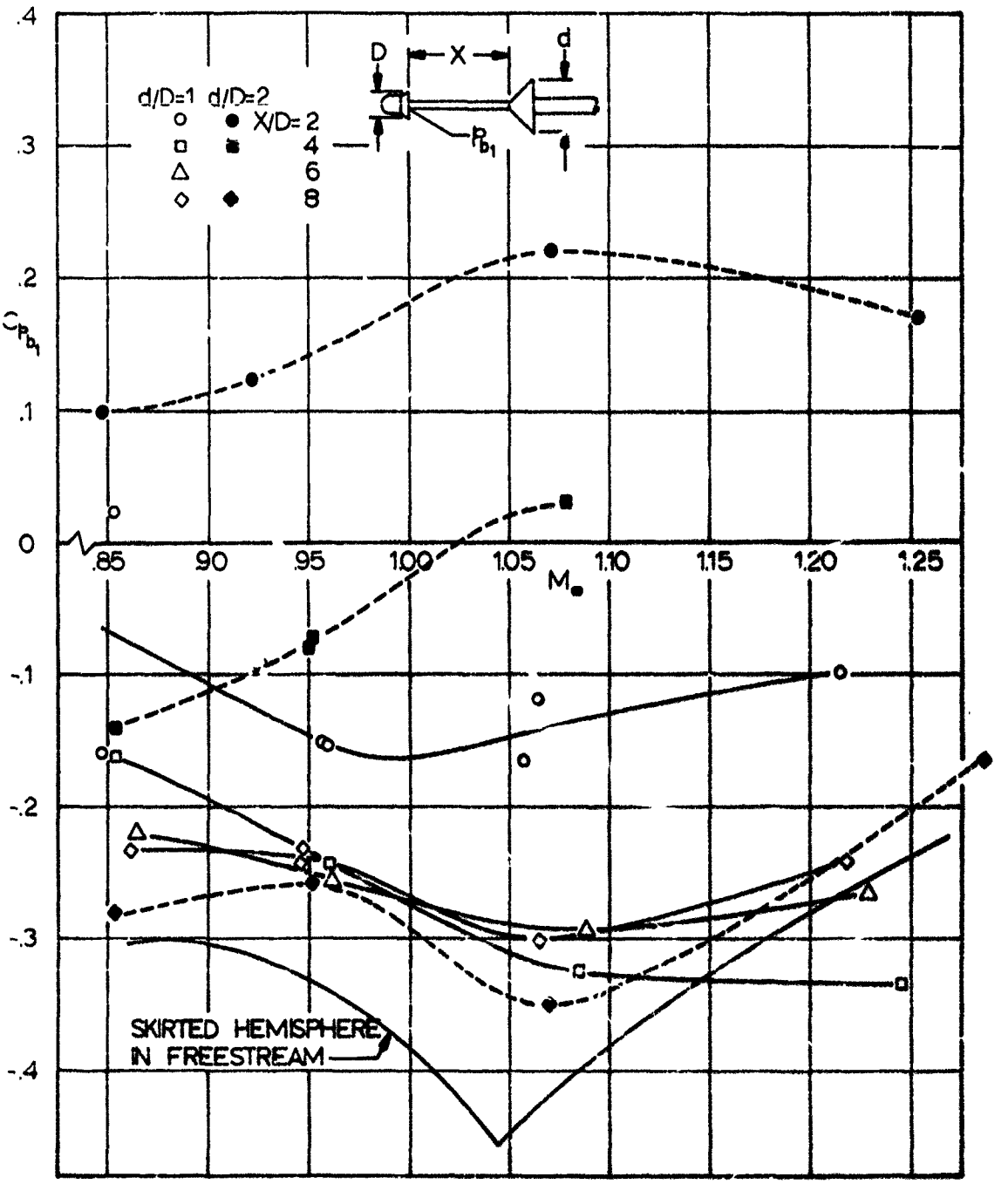

FIG 37. BASE PRESSURE COEFFICIENT OF SKIRTED HEMISPHERE WITH 45° HALF-ANGLE CONE IN WAKE AT TRANSONIC SPEEDS.

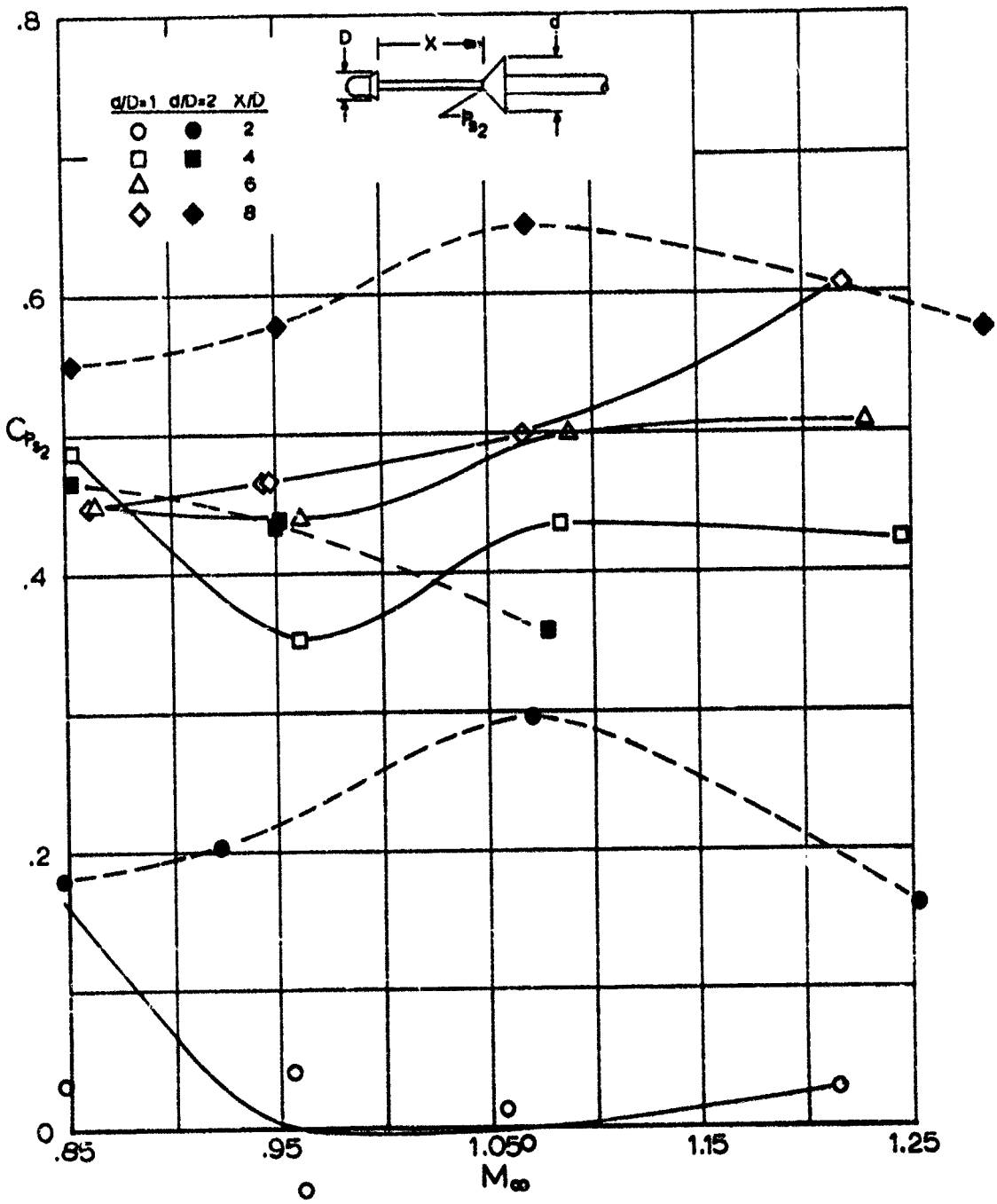

FIG 38. STAGNATION PRESSURE COEFFICIENT OF 45° HALF-ANGLE CONE IN WAKE OF SKIRTED HEMISPHERE AT TRANSONIC SPEEDS.

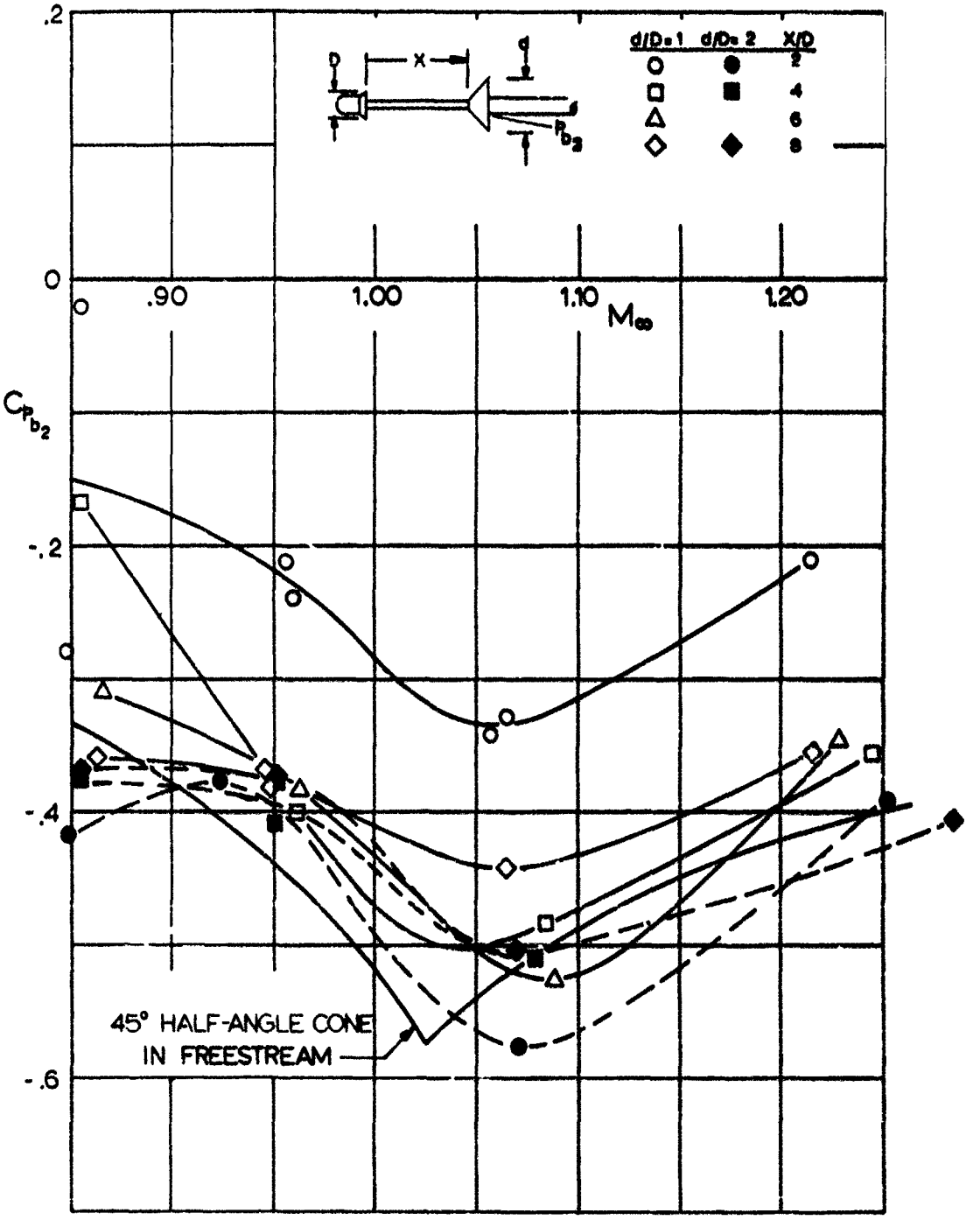

FIG 39. BASE PRESSURE COEFFICIENT OF 45° HALF-ANGLE CONE IN WAKE OF SKIRTED HEMISPHERE AT TRANSONIC SPEEDS.

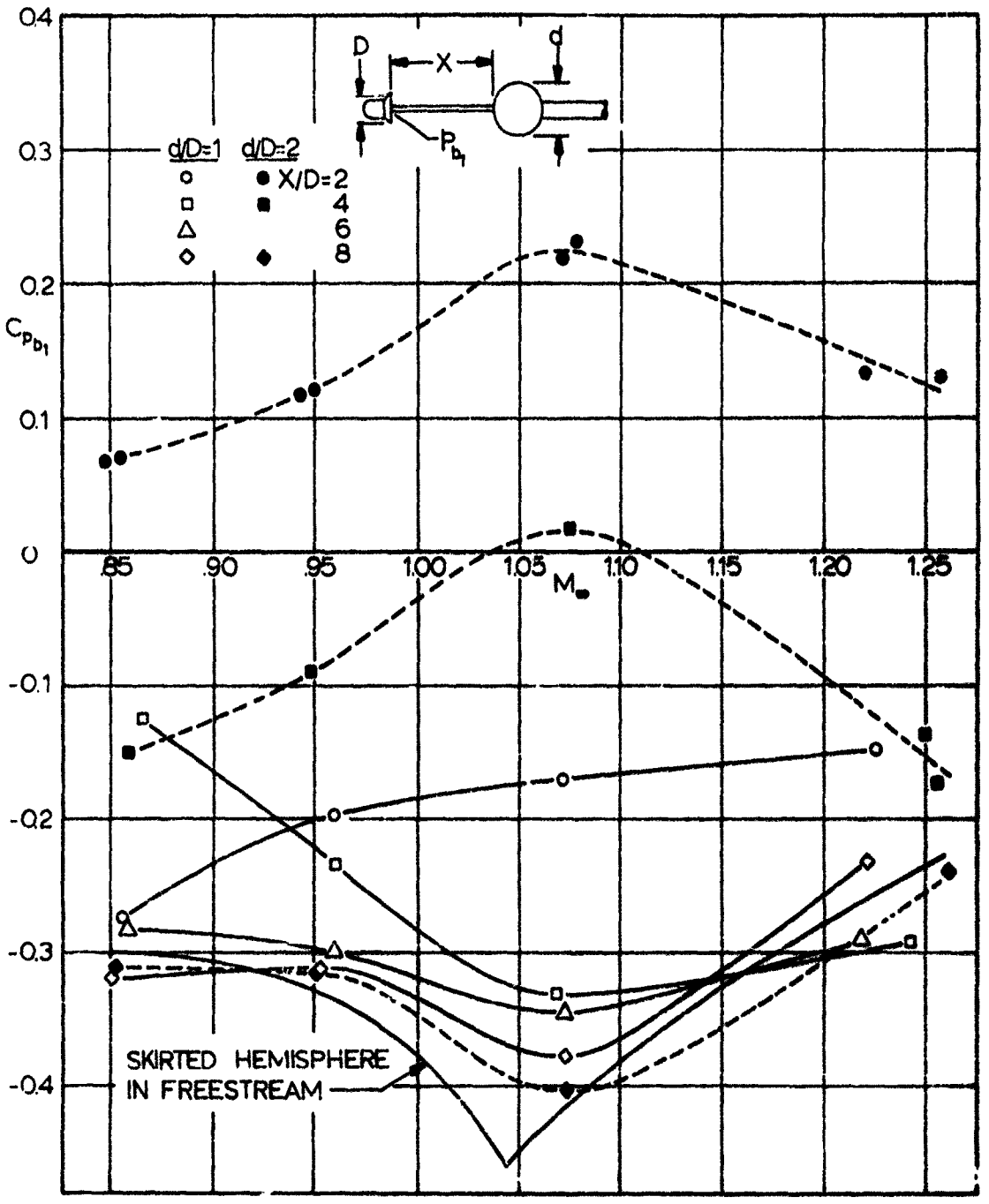

FIG 40. BASE PRESSURE COEFFICIENT OF SKIRTED HEMISPHERE WITH SPHERE IN WAKE AT TRANSONIC SPEEDS.

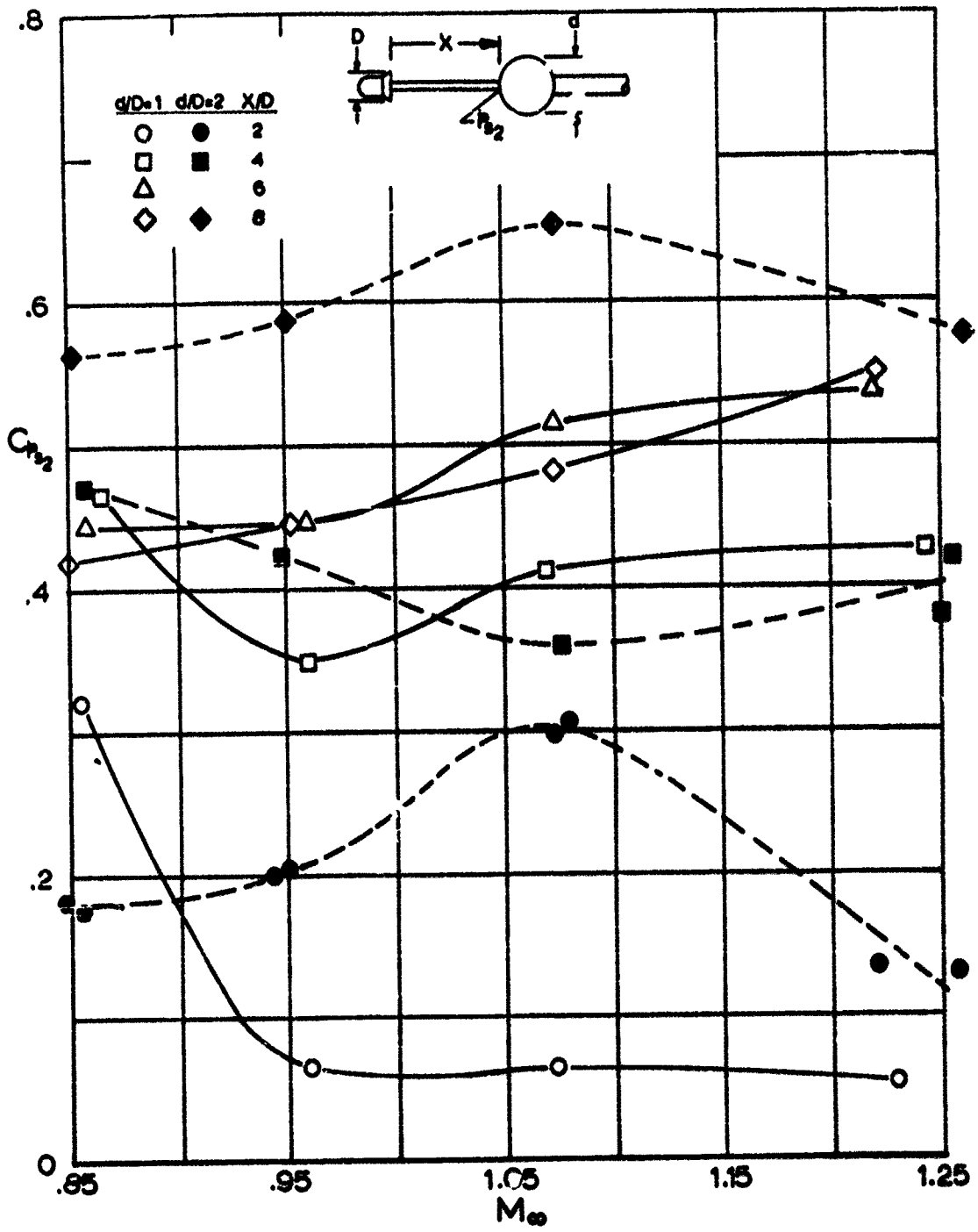

FIG 41. STAGNATION PRESSURE COEFFICIENT OF SPHERE IN WAKE OF SKIRTED HEMISPHERE AT TRANSONIC SPEEDS.

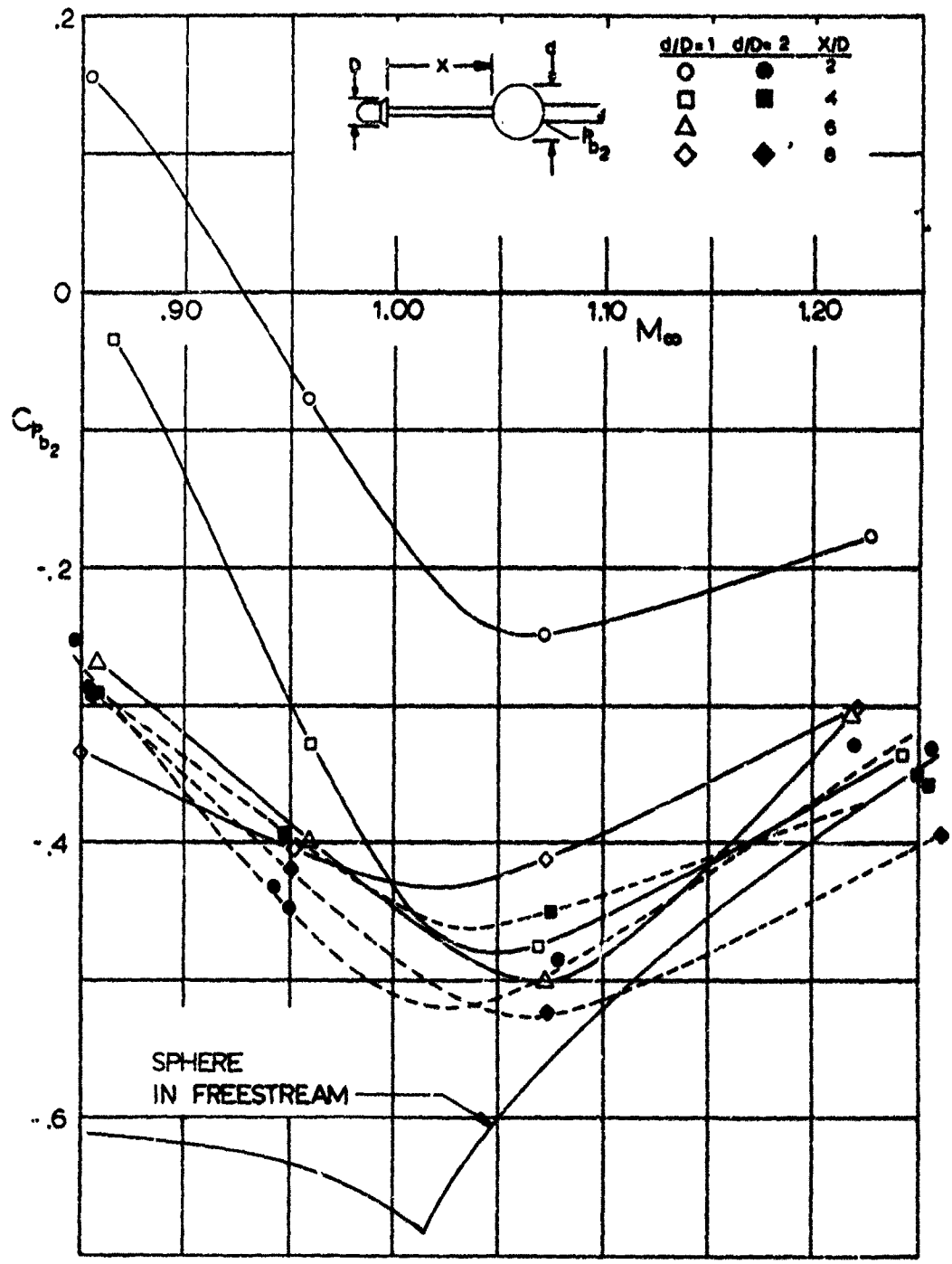

FIG 42. BASE PRESSURE COEFFICIENT OF SPHERE IN WAKE OF SKIRTED HEMISPHERE AT TRANSONIC SPEEDS.

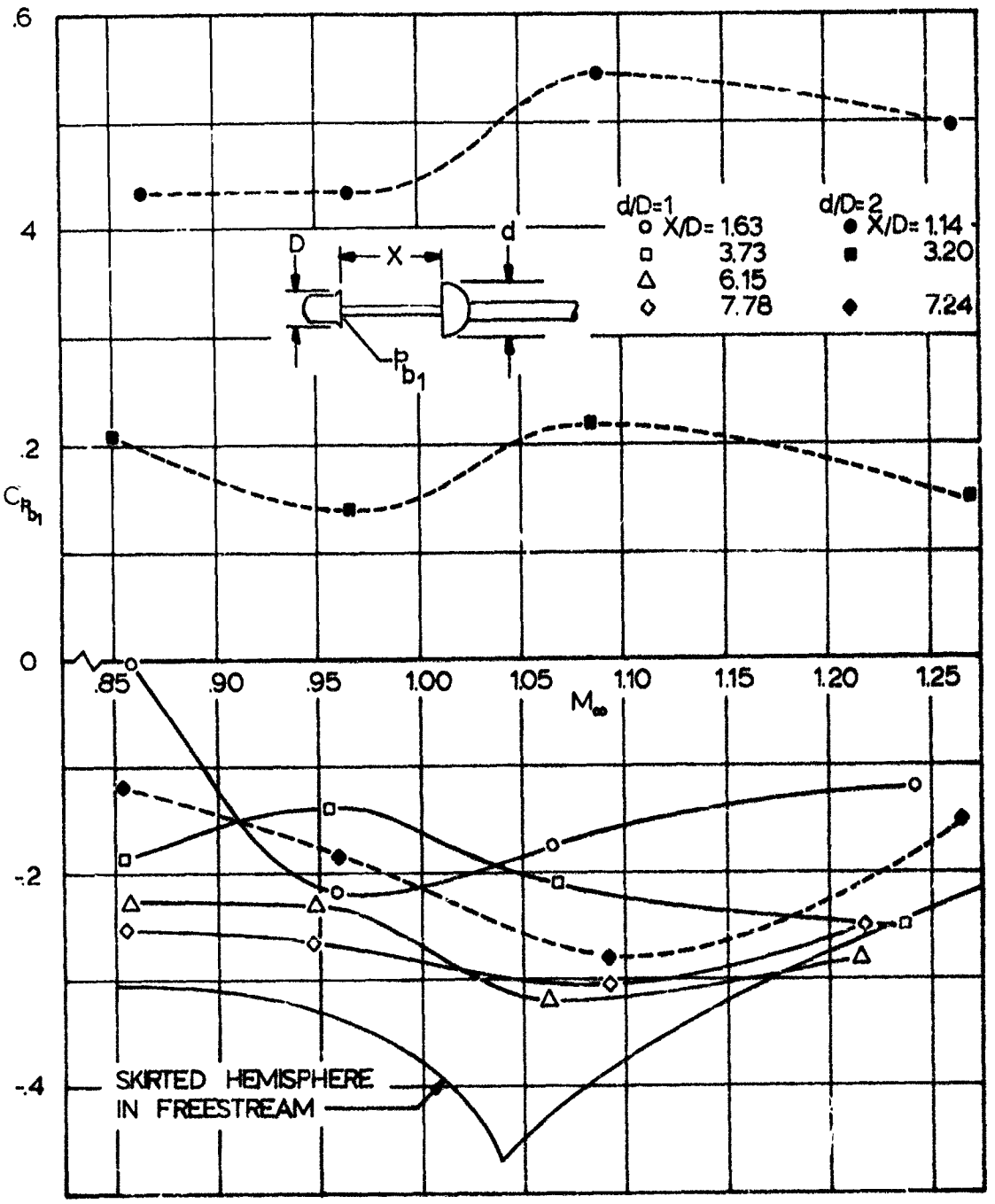

FIG 43. BASE PRESSURE COEFFICIENT OF SKIRTED HEMISPHERE WITH HOLLOW HEMISPHERE IN WAKE AT TRANSONIC SPEEDS.

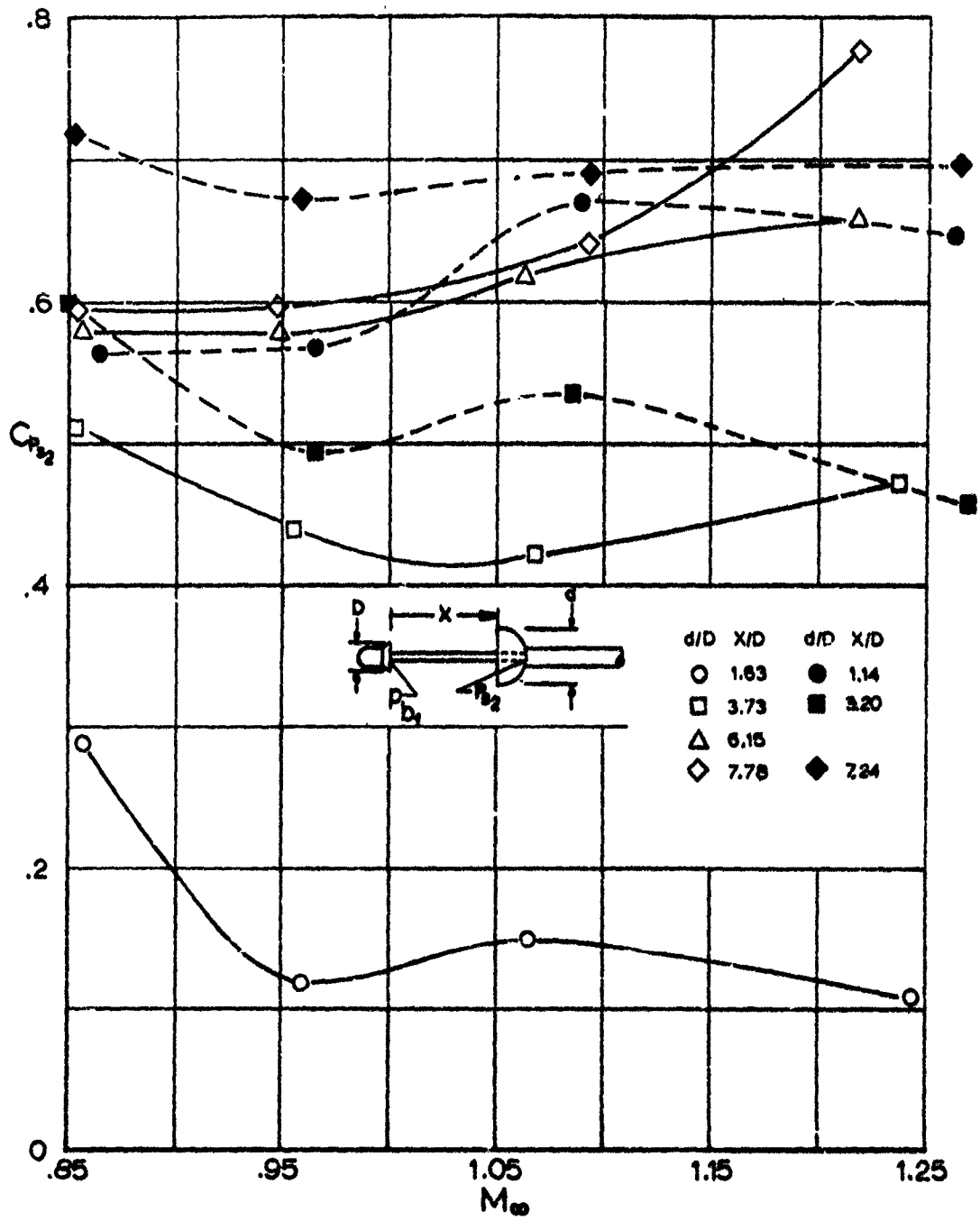

FIG 44. STAGNATION PRESSURE COEFFICIENT OF HOLLOW HEMISPHERE IN WAKE OF SKIRTED HEMISPHERE AT TRANSONIC SPEEDS.

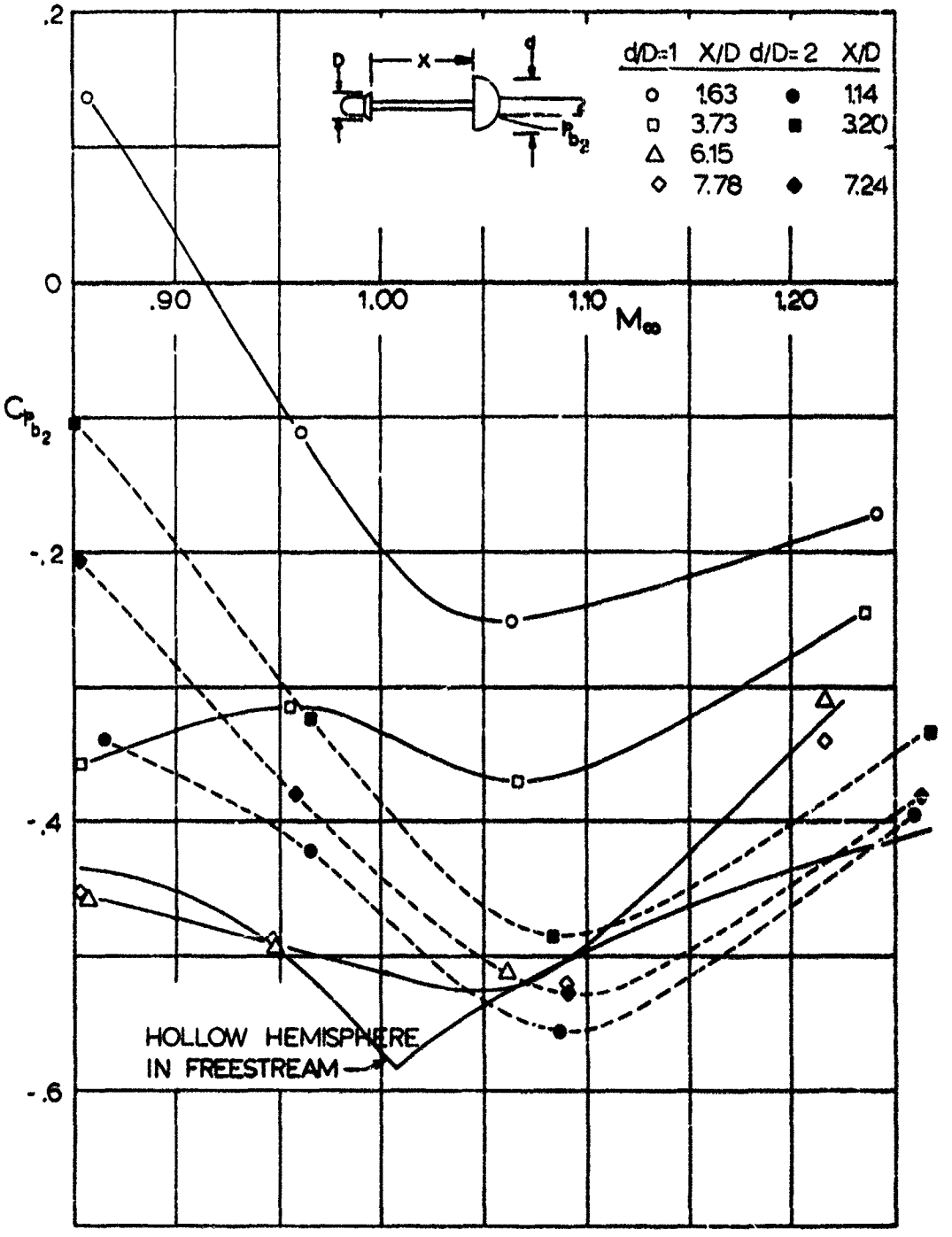

FIG 45. BASE PRESSURE COEFFICIENT OF HOLLOW HEMISPHERE IN WAKE OF SKIRTED HEMISPHERE AT TRANSONIC SPEEDS.

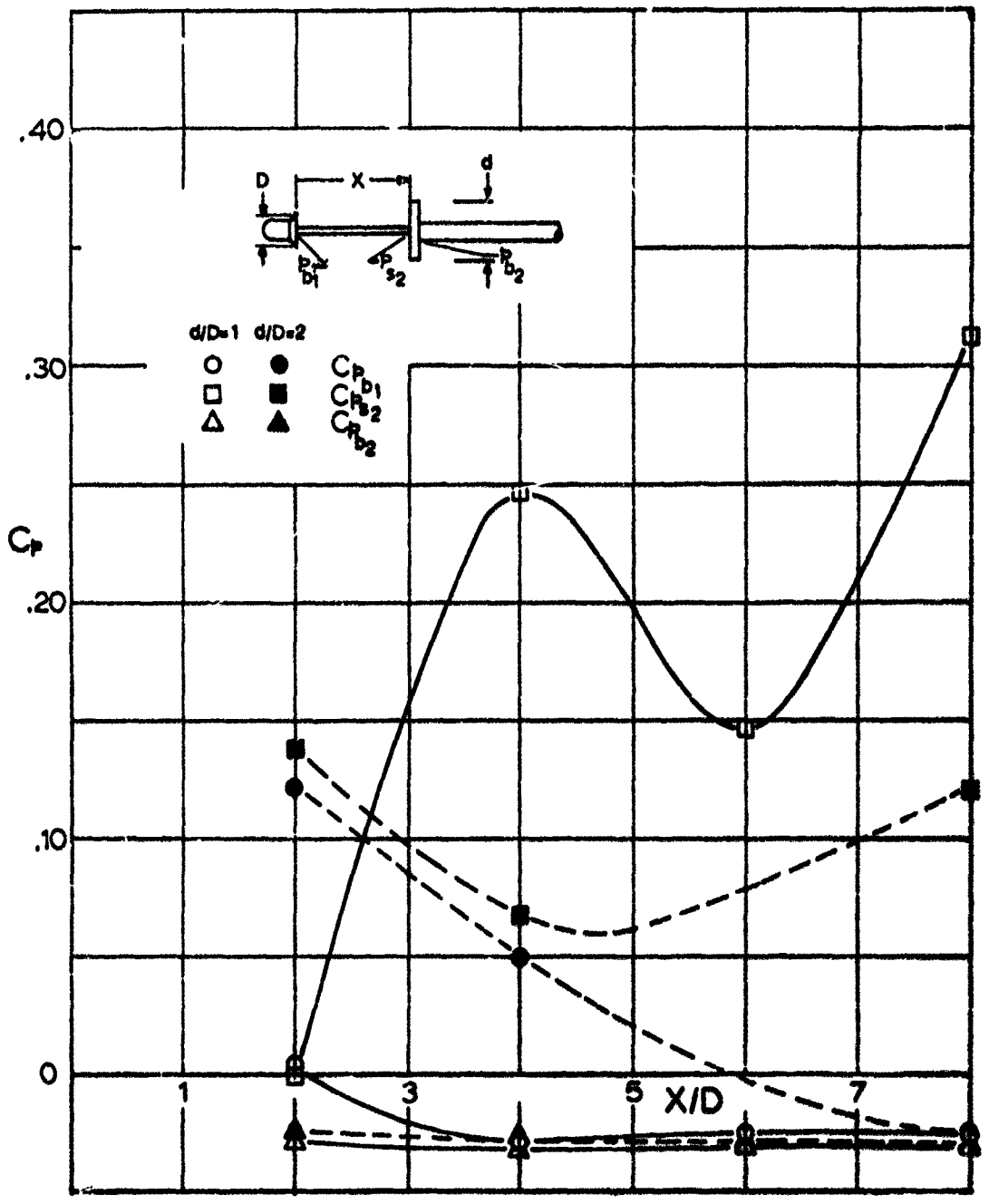

FIG 46. PRESSURE COEFFICIENTS FOR SKIRTED HEMISPHERE AND FLAT PLATE AT $M_\infty = 4.35$.

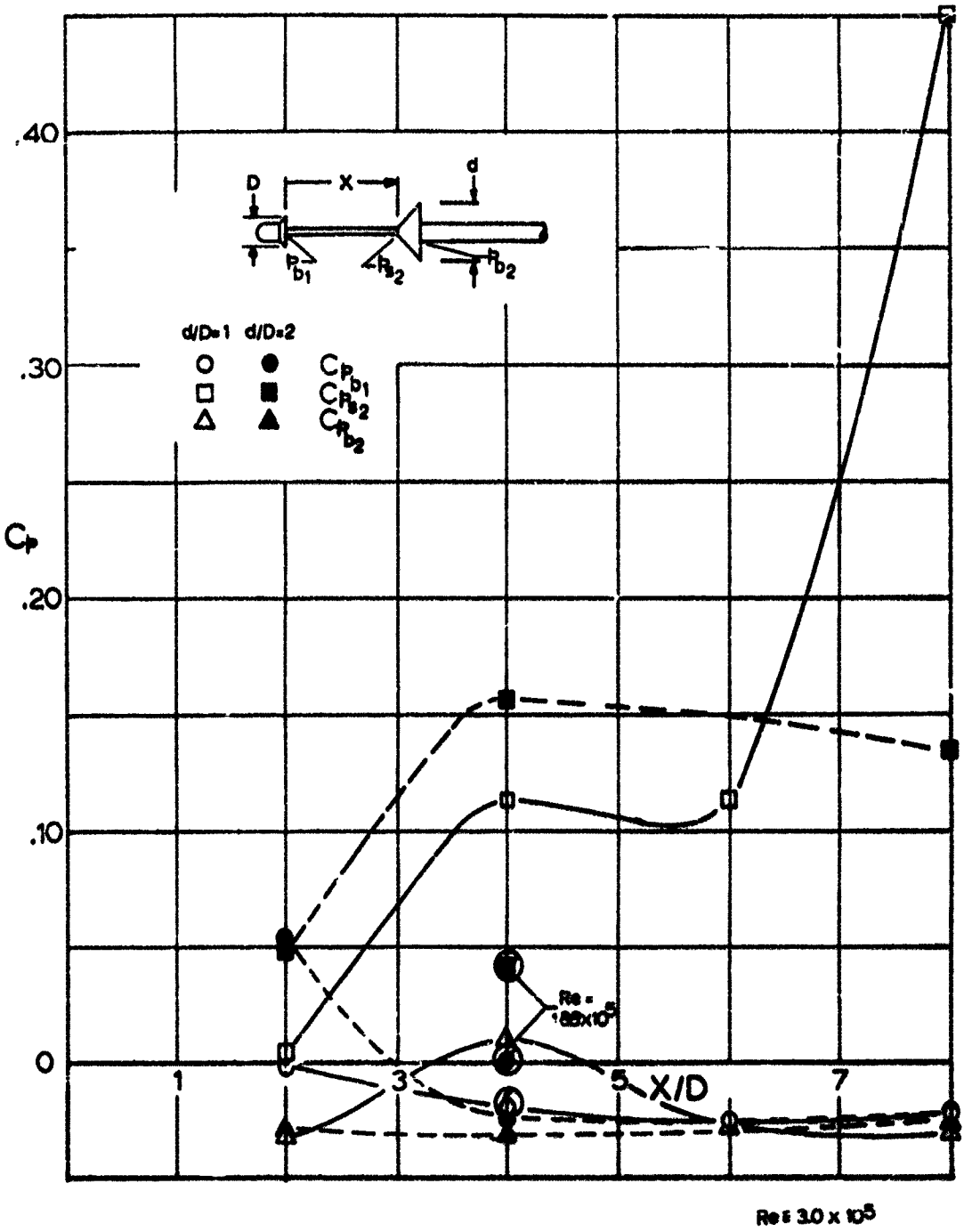

FIG 47. PRESSURE COEFFICIENTS FOR SKIRTED HEMISPHERE AND 45° HALF-ANGLE CONE AT $M_\infty = 4.35$.

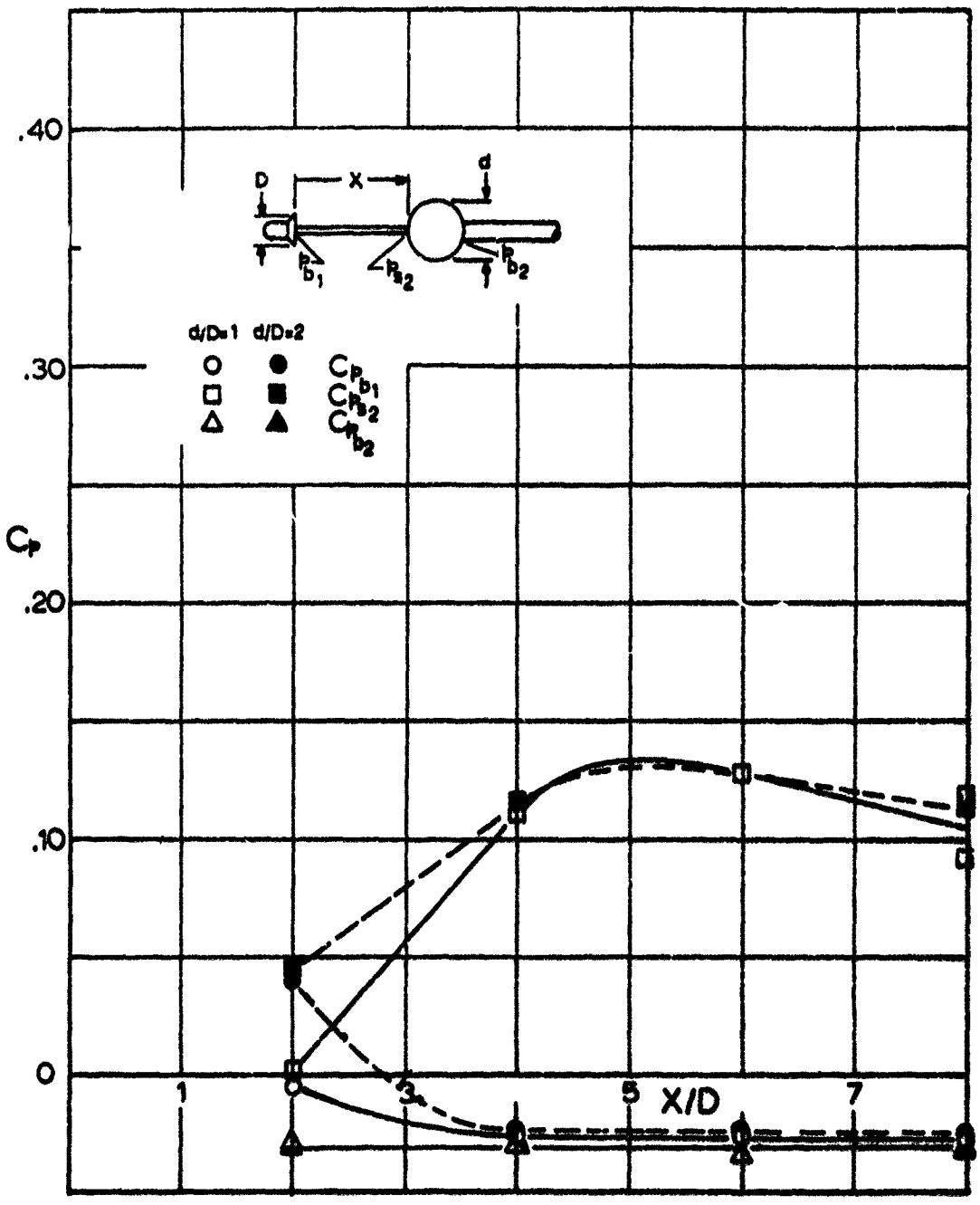

FIG 48. PRESSURE COEFFICIENTS FOR SKIRTED HEMISPHERE AND SPHERE AT M_∞ = 4.35.

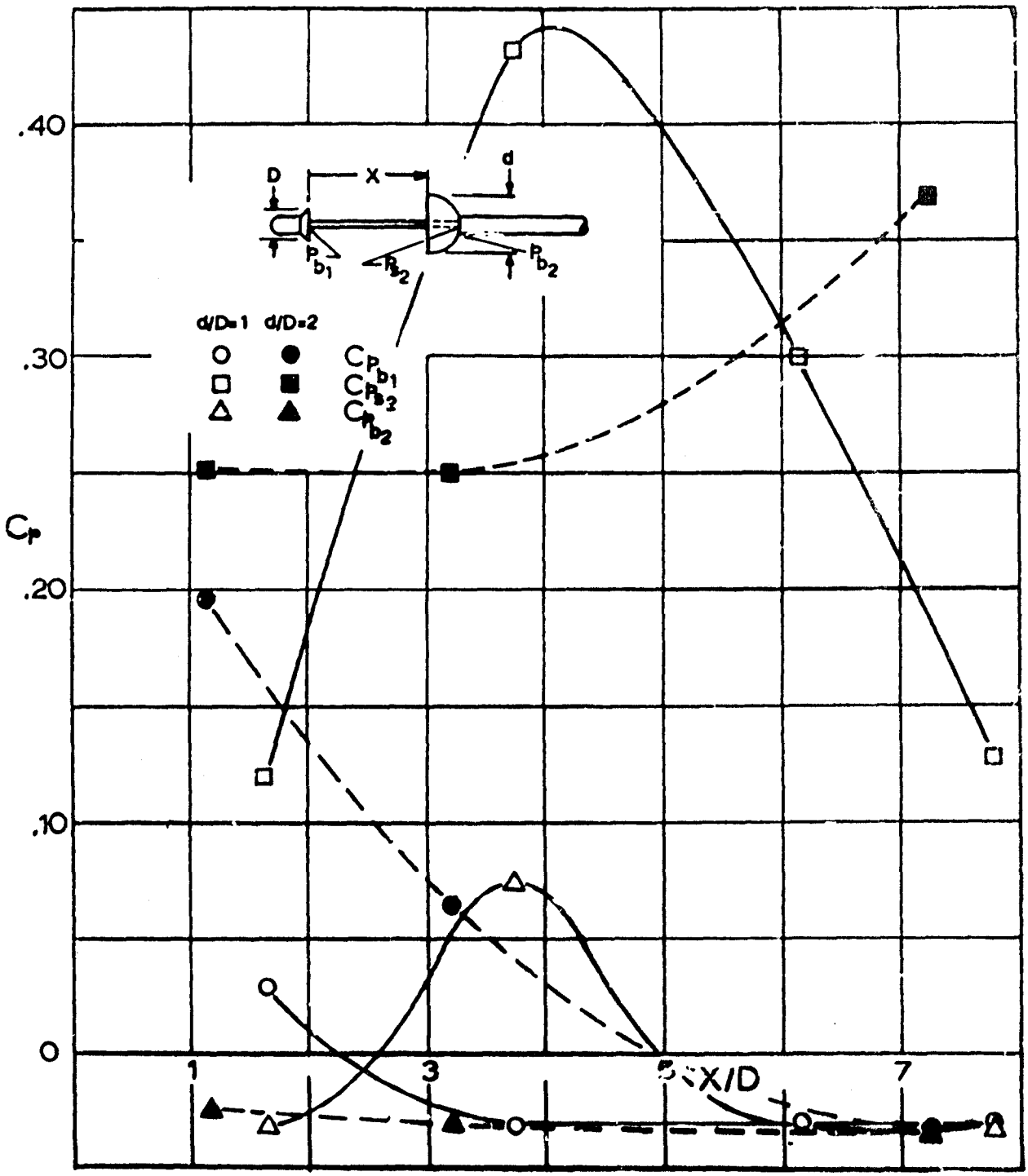

FIG 49. PRESSURE COEFFICIENTS FOR SKIRTED HEMISPHERE AND HOLLOW HEMISPHERE AT $M_\infty = 4.35$.

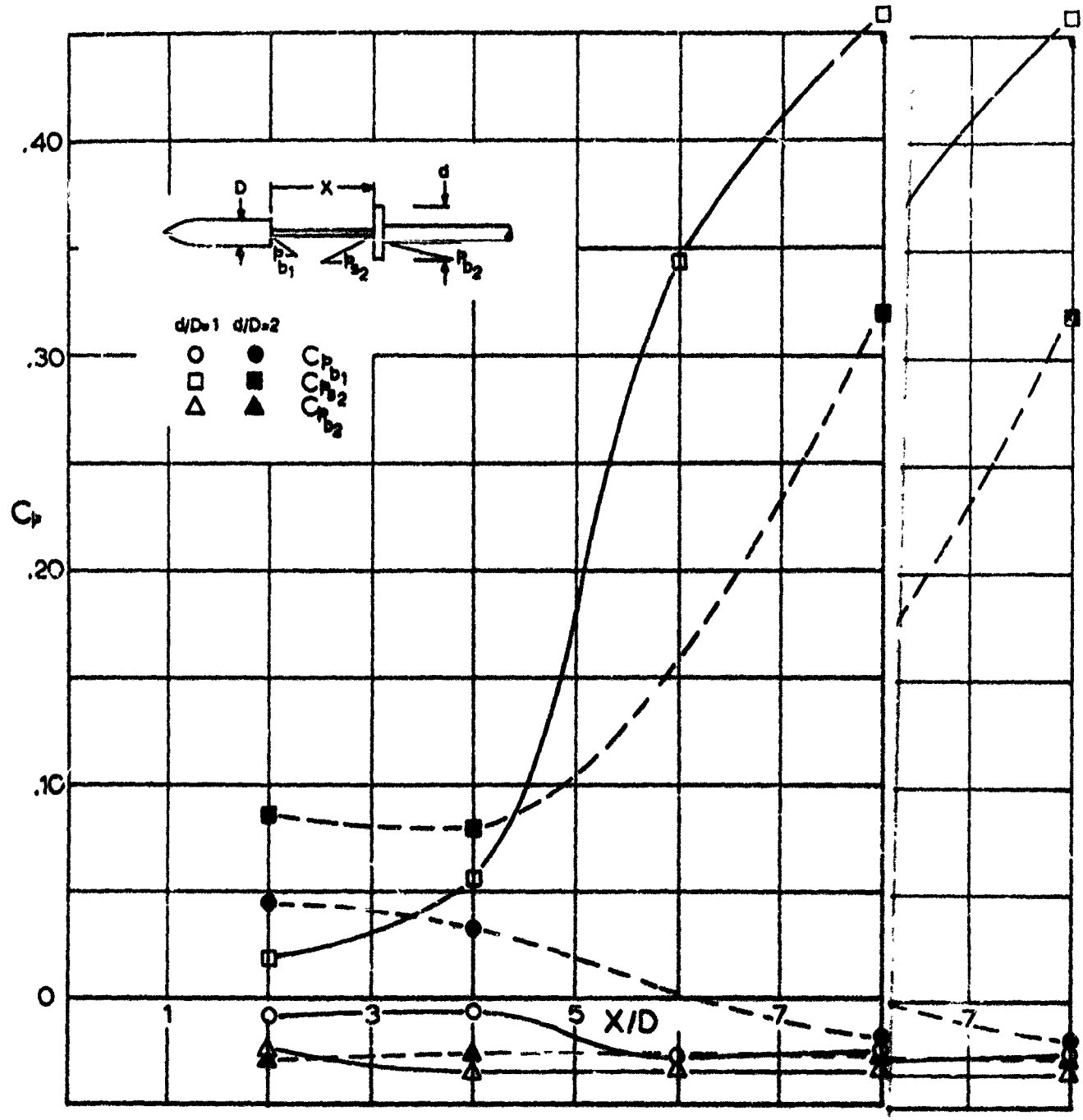

FIG 5C. PRESSURE COEFFICIENTS FOR OGIVE R OGIVE CYLINDER AND FLAT PLATE AT $M_\infty = 4.35$. $_\infty = 4.35$.

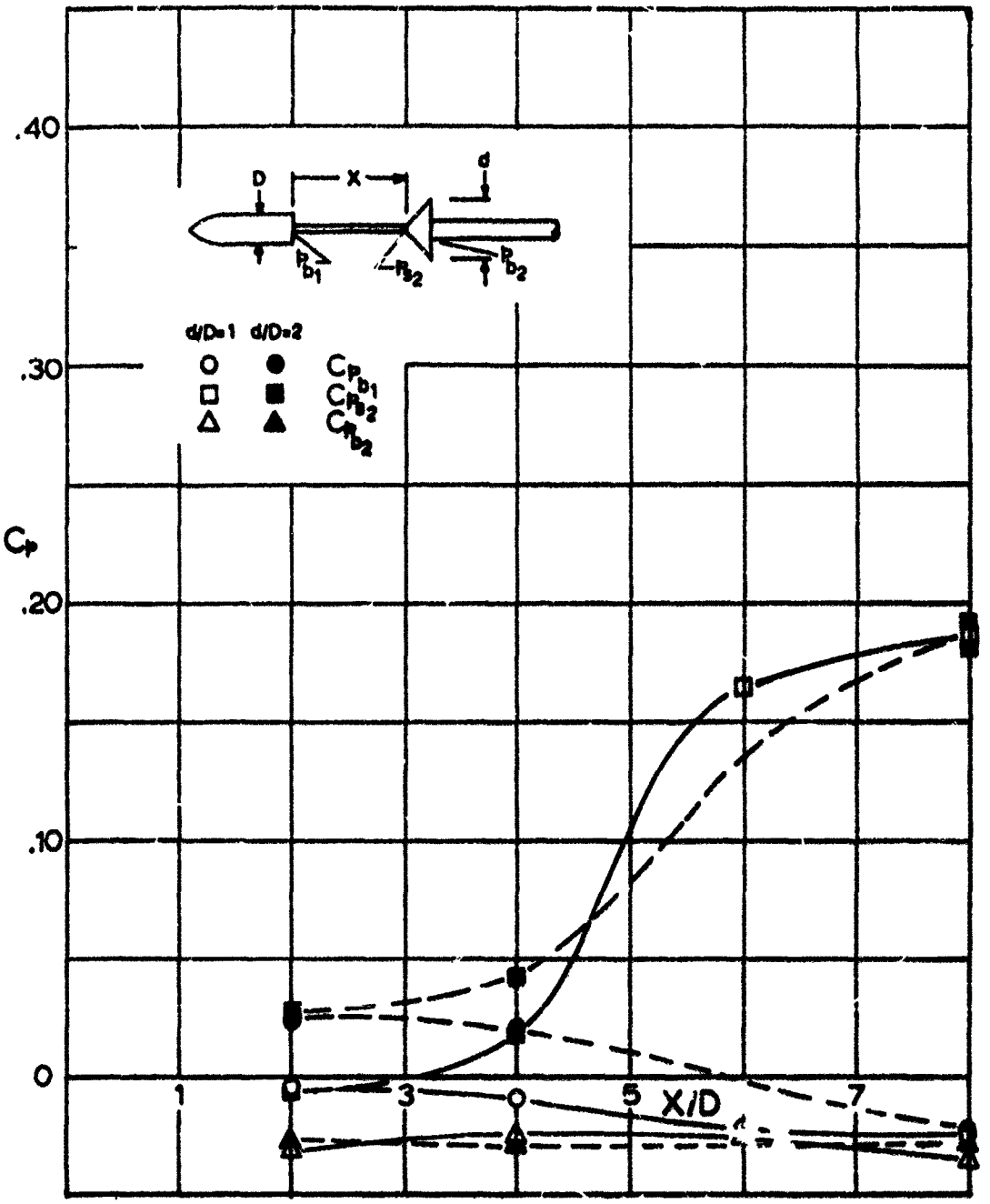

FIG 51. PRESSURE COEFFICIENTS FOR OGIVE CYLINDER AND 45° HALF-ANGLE CONE AT M_∞ = 4.35.

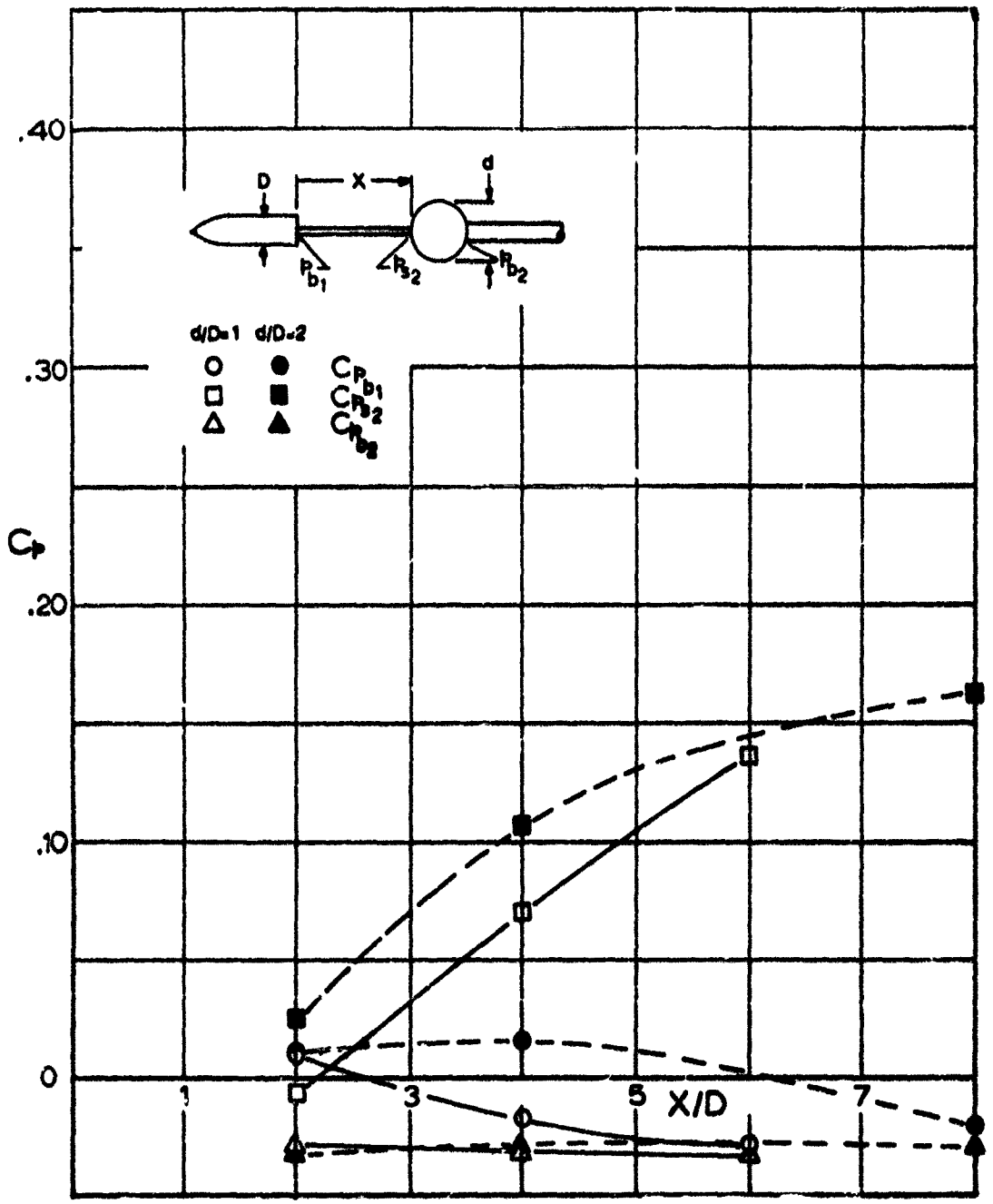

FIG 52. PRESSURE COEFFICIENTS FOR OGIVE CYLINDER AND SPHERE AT $M_\infty = 4.35$.

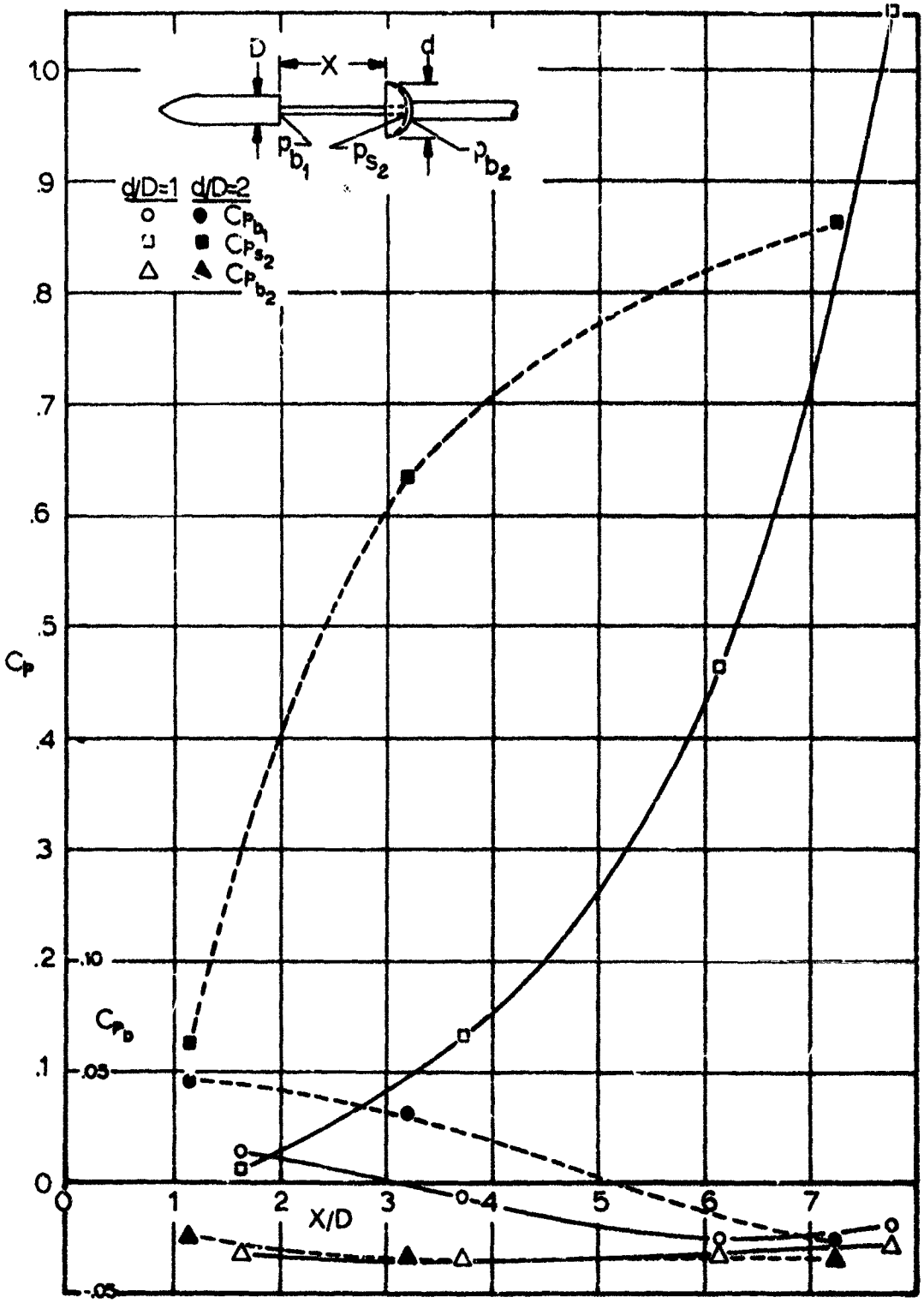

FIG 53. PRESSURE COEFFICIENTS FOR OGIVE CYLINDER AND HOLLOW HEMISPHERE AT M_∞=4.35

APPENDIX IV

REPRESENTATIVE FLOW PHOTOGRAPHS

In this appendix a number of flow photographs are presented. Many of them should not be considered to be very significant, but the pictures are included as additional experimental material and as a matter of record.

A) X/D = 2.0, M_∞ = 1.068, R_θ = 3.13 x 10^5

B) X/D = 4.0, M_∞ = 1.072, R_θ = 3.09 x 10^5

C) X/D = 6.0, M_∞ = 1.062, R = 3.12 x 10^5

FIG 54 FLOW SHADOWGRAPHS OF SKIRTED HEMISPHERE AND FLAT PLATE WITH d/D = 1 AT TRANSONIC SPEEDS (CONTINUED)

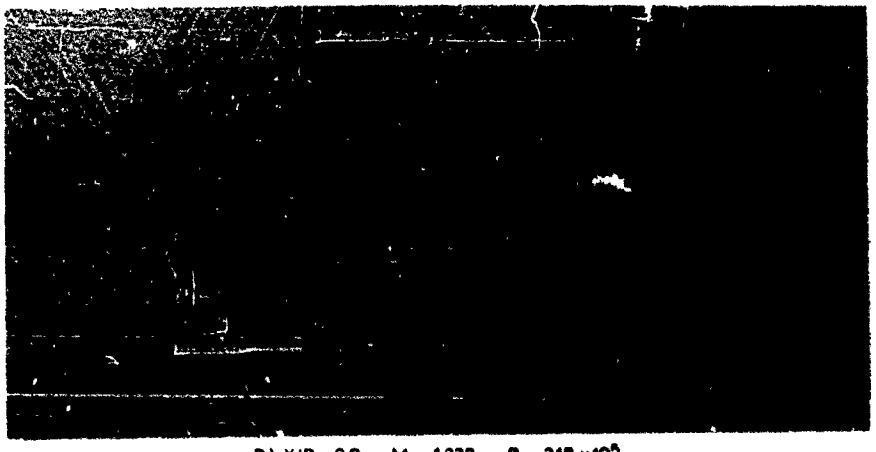

D) X/D = 2.0, $M_\infty = 1.232$, $R_\theta = 3.18 \times 10^5$

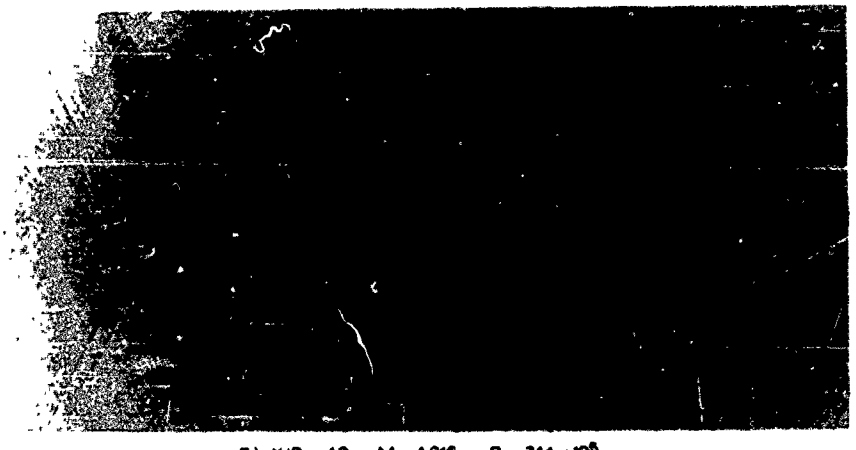

E) X/D = 4.0, $M_\infty = 1.216$, $R_\theta = 3.14 \times 10^5$

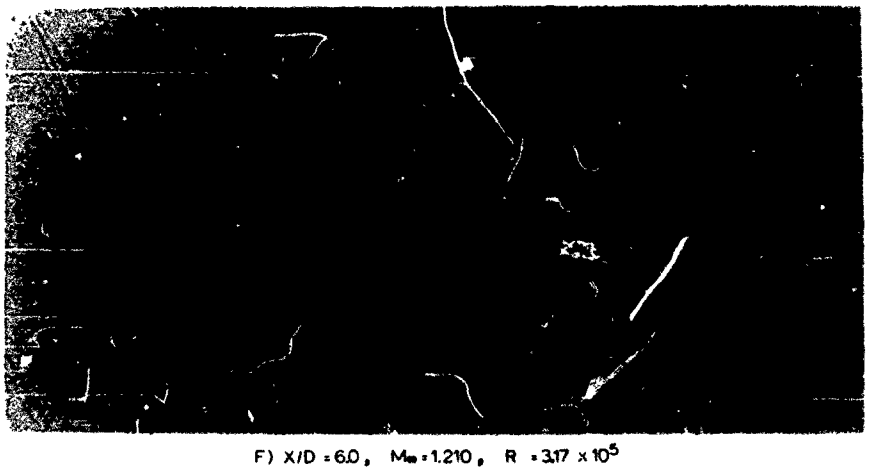

F) X/D = 6.0, $M_\infty = 1.210$, $R = 3.17 \times 10^5$

FIG 54 FLOW SHADOWGRAPHS OF SKIRTED HEMISPHERE AND FLAT PLATE WITH d/D = 1 AT TRANSONIC SPEEDS (CONCLUDED)

A) X/D = 2.0, M_∞ = 1.250, R_θ = 3.20 x 10^3

B) X/D = 4.0, M_∞ = 1.252, R_θ = 3.19 x 10^3

C) X/D = 8.0, M_∞ = 1.255, R_θ = 3.35 x 10^3

FIG 55. FLOW SHADOWGRAPHS OF SKIRTED HEMISPHERE AND FLAT PLATE WITH d/D = 2 AT M_∞ = 1.25

A) X/D = 2.0, M_∞ = 1.065, R_θ = 3.10 x 10^5

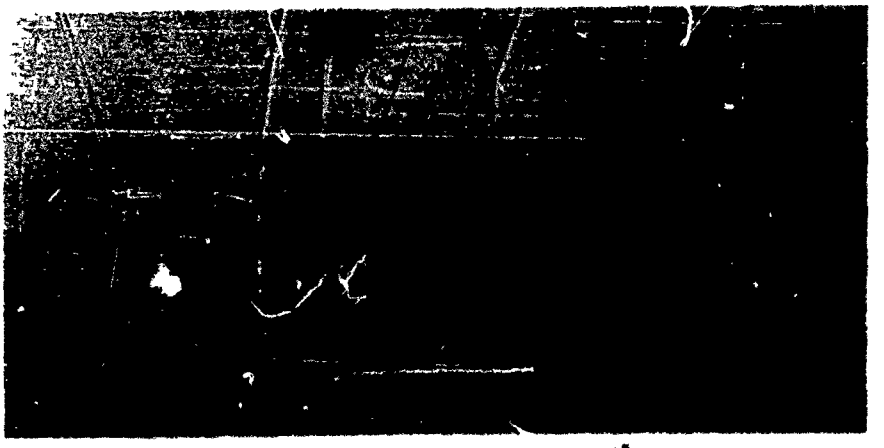

B) X/D = 4.0, M_∞ = 1.065, R_θ = 3.17 x 10^5

C) X/D = 8.0, M_∞ = 1.065, R_θ = 3.09 x 10^5

FIG 56 FLOW SHADOWGRAPHS OF SKIRTED HEMISPHERE AND 45° HALF-ANGLE CONE WITH d/D = 1 AT TRANSONIC SPEEDS (CONTINUED)

D) X/D = 2.0, $M_\infty = 1.25$, $R_\theta = 3.2 \times 10^5$

E) X/D = 4.0, $M_\infty = 1.248$, $R_\theta = 3.20 \times 10^5$

F) X/D = 8.0, $M_\infty = 1.219$, $R_\theta = 3.17 \times 10^5$

FIG 56. FLOW SHADOWGRAPHS OF SKIRTED HEMISPHERE AND 45° HALF-ANGLE CONE WITH d/D = 1 AT TRANSONIC SPEEDS (CONCLUDED)

A) X/D = 2.0, M_∞ = 1.253, R_e = 3.34 x 10^5

B) X/D = 4.0, M_∞ = 1.25, R_e = 3.3 x 10^5

C) X/D = 8.0, M_∞ = 1.206, R_e = 3.34 x 10^5

FIG 57 FLOW SHADOWGRAPHS OF SKIRTED HEMISPHERE AND 45° HALF-ANGLE CONE WITH d/D = 2 AT M_∞ = 1.25

A) X/D = 2.0, M_∞ = 1.072, R_θ = 3.14 x 10^5

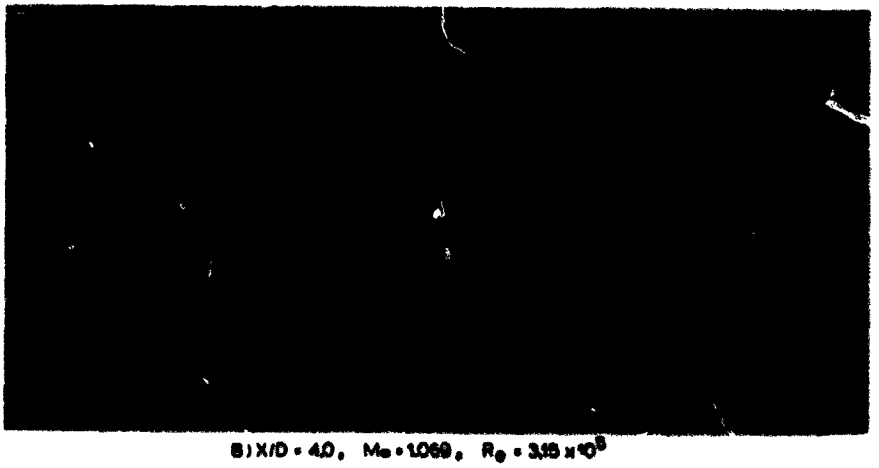

B) X/D = 4.0, M_∞ = 1.069, R_θ = 3.18 x 10^5

C) X/D = 6.0 M_∞ = 1.073 R_θ = 3.18 x 10^5

FIG 58 FLOW SHADOWGRAPHS OF SKIRTED HEMISPHERE AND SPHERE WITH d/D = 1 AT TRANSONIC SPEEDS (CONTINUED)

D) X/D = 2.0, M_∞ = 1.228, R_θ = 3.20 x 10^3

E) X/D = 6.0, M_∞ = 1.219, R_θ = 3.24 x 10^3

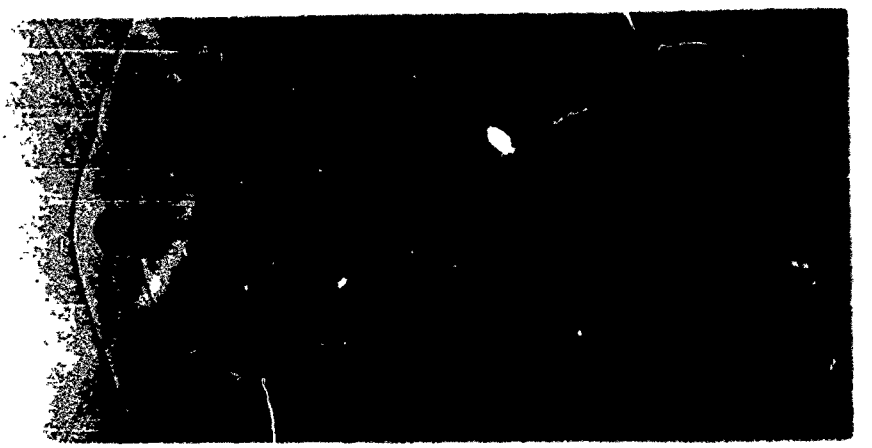

F) X/D = 8.0, M_∞ = 1.221, R_θ = 3.15 x 10^3

FIG 58 FLOW SHADOWGRAPHS OF SKIRTED HEMISPHERE AND SPHERE WITH d/D = 1 AT TRANSONIC SPEEDS (CONCLUDED)

A) X/D = 2.0, M_∞ = 1.079, R_θ = 3.13 x 10^5

B) X/D = 4.0, M_∞ = 1.078, R_θ = 3.15 x 10^5

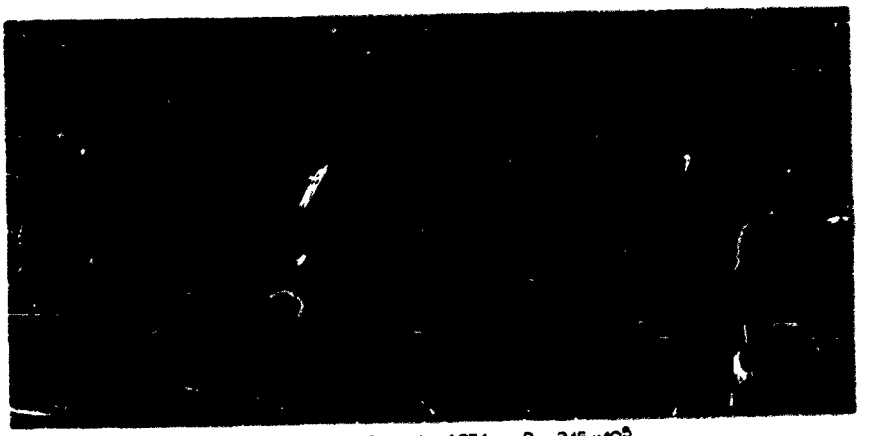

C) X/D = 8.0, M_∞ = 1.074, R_θ = 3.15 x 10^5

FIG 59 FLOW SHADOWGRAPHS OF SKIRTED HEMISPHERE AND SPHERE WITH d/D = 2 AT TRANSONIC SPEEDS (CONTINUED)

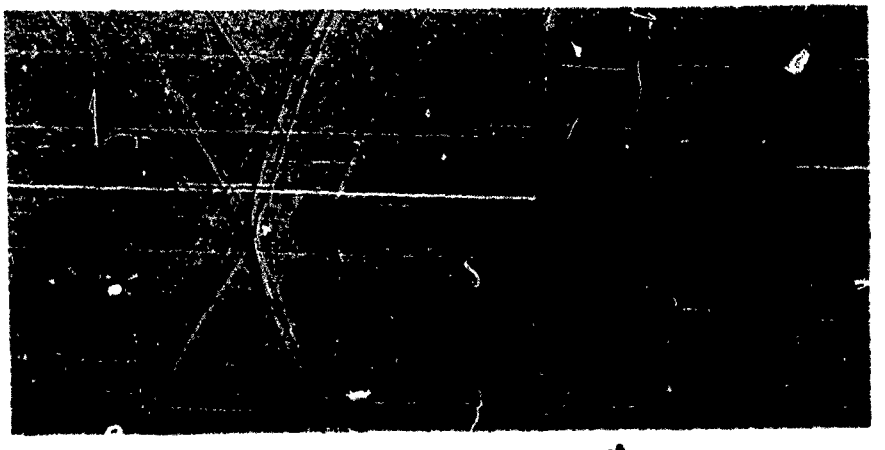

D) X/D = 4.0, M_∞ = 1.250, R_ℓ = 3.19 x 10^6

E) X/D = 8.0, M_∞ = 1.262, R_ℓ = 3.10 x 10^6

FIG 59. FLOW SHADOWGRAPHS OF SKIRTED HEMISPHERE AND SPHERE WITH d/D = 2 AT TRANSONIC SPEEDS (CONCLUDED)

A) d/D = 1, X/D = 3.73, M_∞ = 1.038, R_θ = 3.10x10^5

B) d/D = 1, X/D = 6.15, M_∞ = 1.063, R = 3.11 x10^5

FIG 60. FLOW SHADOWGRAPHS OF SKIRTED HEMISPHERE AND HOLLOW HEMISPHERE AT TRANSONIC SPEEDS (CONTINUED)

C) d/D = 1, X/D = 3.73, M_∞ = 1.237, R_θ = 3.17 x 10^3

D) d/D = 1, X/D = 6.15, M_∞ = 1.217, R_θ = 3.17 x 10^3

E) d/D = 2, X/D = 7.24, M_∞ = 1.265, R_θ = 3.21 x 10^3

FIG 60 FLOW SHADOWGRAPHS OF SKIRTED HEMISPHERE AND HOLLOW HEMISPHERE AT TRANSONIC SPEEDS (CONCLUDED)

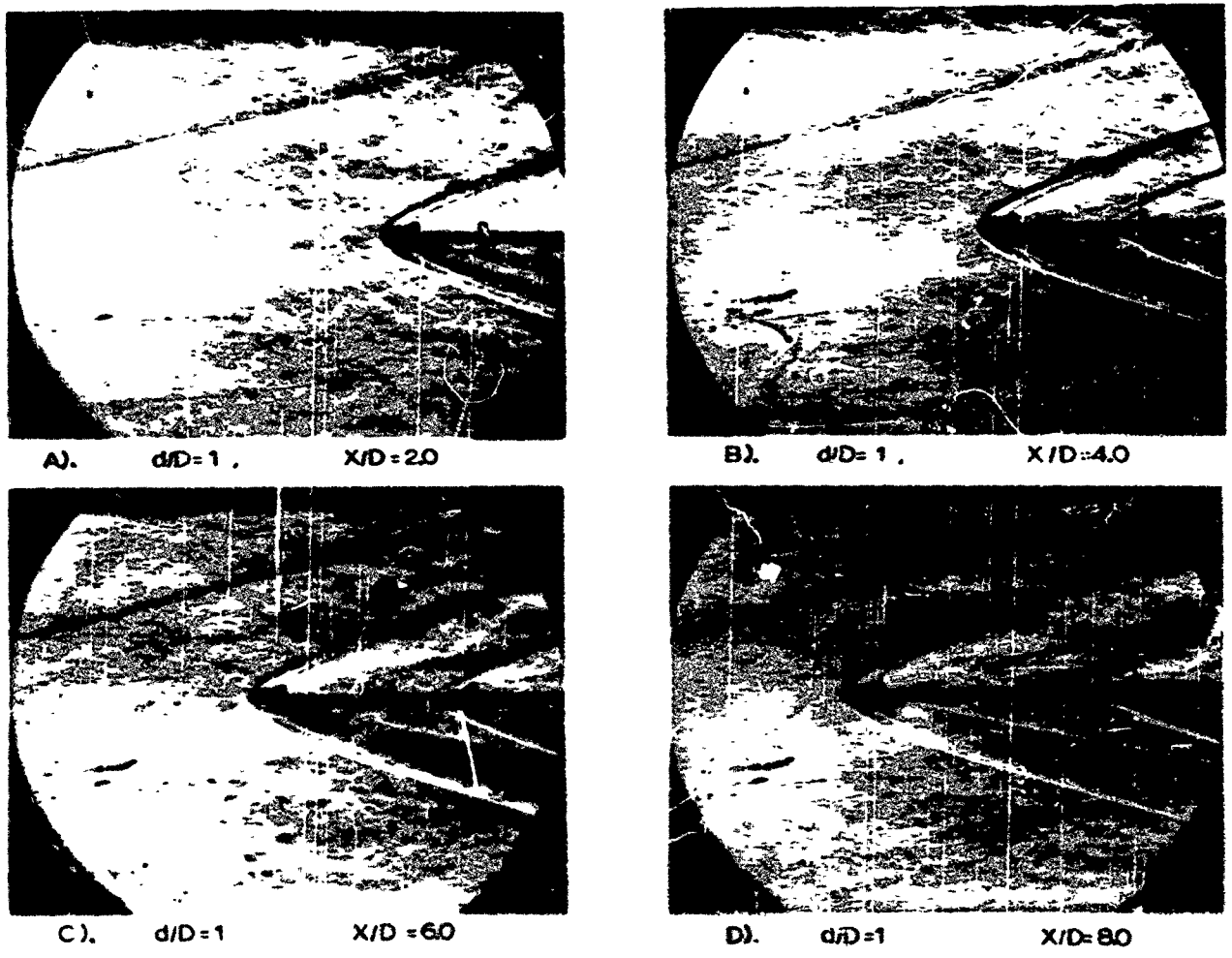

FIG 61. SCHLIEREN PHOTOGRAPHS OF SKIRTED HEMISPHERE AND FLAT PLATE AT $M_\infty = 4.35$, $Re = 3.0 \times 10^5$ (CONTINUED)

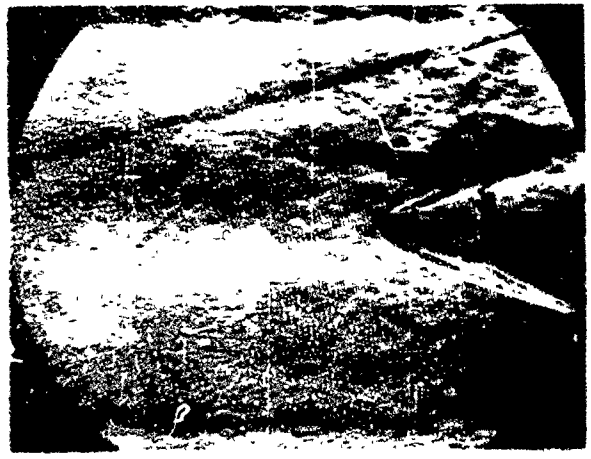

E). d/D=2 , X/D=2.0

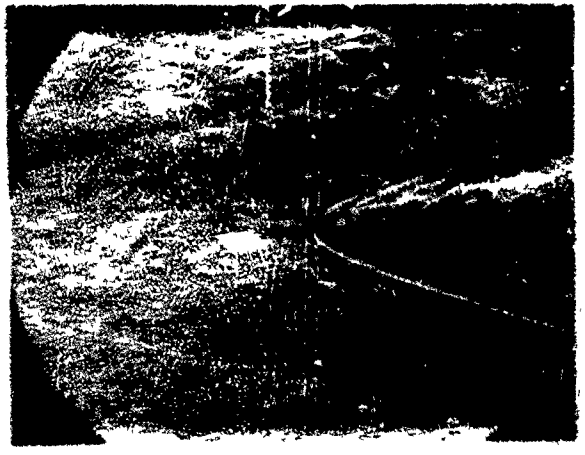

F). d/D=2 , X/D=4.0

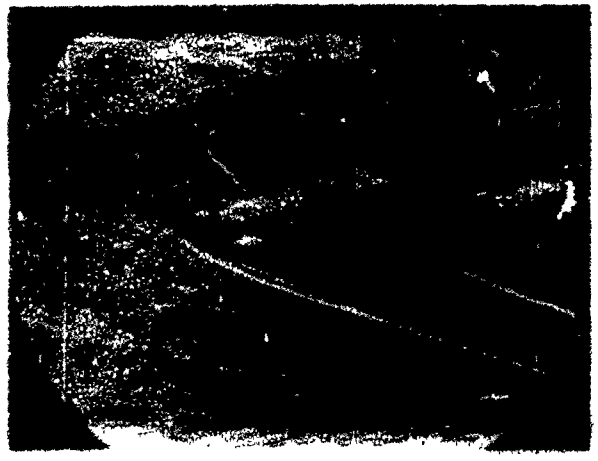

G). d/D=2, X/D=8.0

FIG 61. SCHLIEREN PHOTOGRAPHS OF SKIRTED HEMISPHERE AND FLAT PLATE AT $M_\infty = 4.35$, $Re = 30 \times 10^5$ (CONCLUDED)

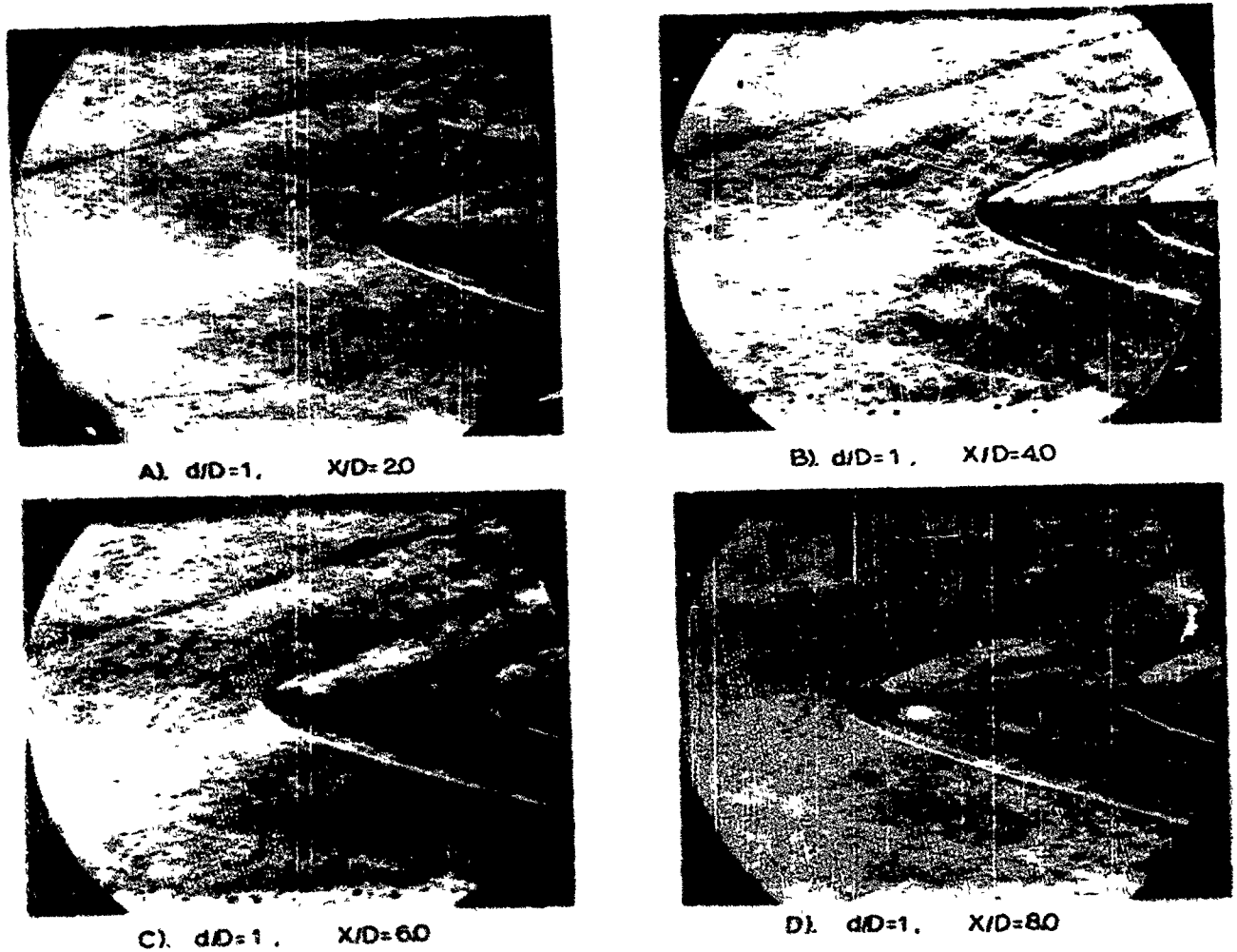

FIG 62. SCHLIEREN PHOTOGRAPHS OF SKIRTED HEMISPHERE AND 45° HALF-ANGLE CONE AT $M_\infty = 4.35$, $Re = 30 \times 10^6$. (CONTINUED)

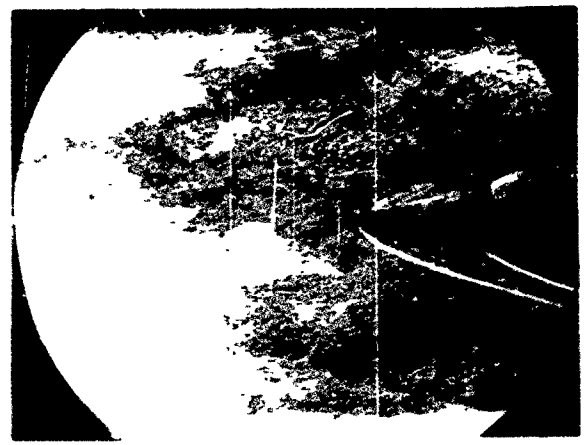

E). d/D=2, X/D=2.0

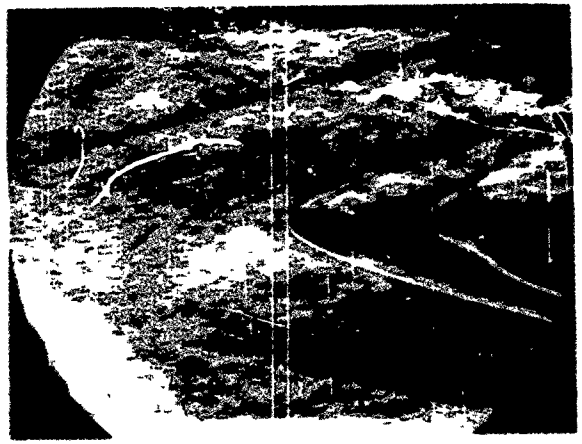

F). d/D=2, X/D=4.0

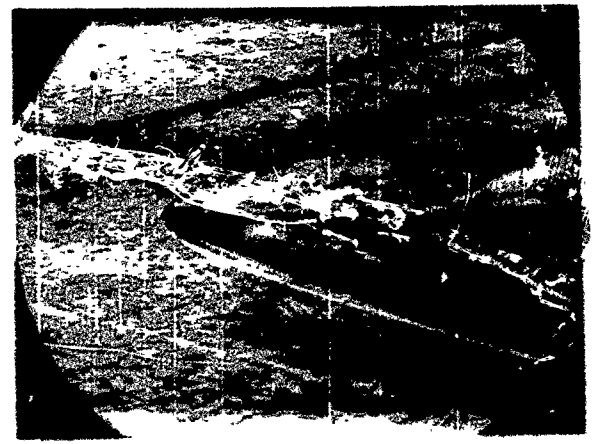

G). d/D=2, X/D=8.0

FIG 62. SCHLIEREN PHOTOGRAPHS OF SKIRTED HEMISPHERE AND 45° HALF-ANGLE CONE AT $M_\infty = 4.35$, $Re \doteq 3.0 \times 10^5$ (CONCLUDED)

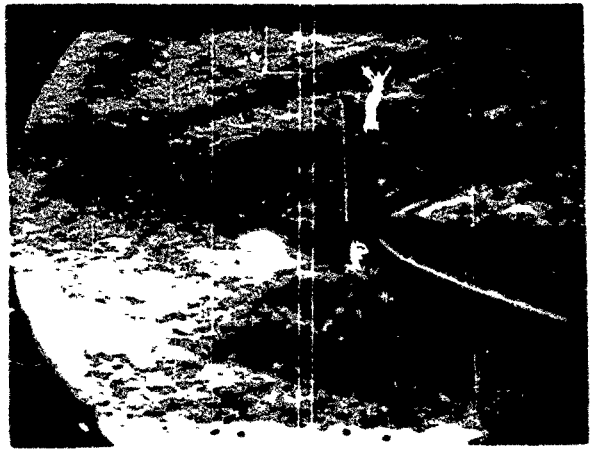

A). d/D = 1 , X/D=2.0

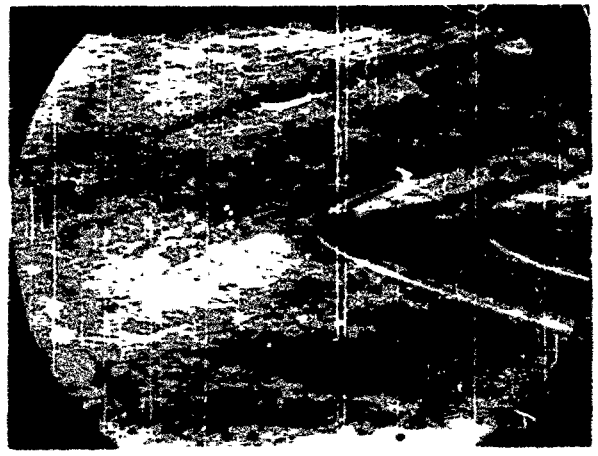

B). d/D= 1 , X/D=4.0

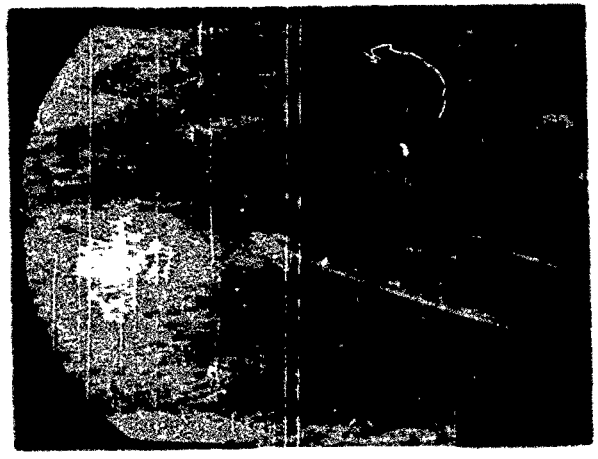

C). d/D = 1, X/D = 6.0

D). d/D=1, X/D = 8.0

FIG 63 .SCHLIEREN PHOTOGRAPHS OF SKIRTED HEMISPHERE AND SPHERE AT $M_\infty = 4.35$, $Re \approx 3.0 \times 10^5$ (CONTINUED)

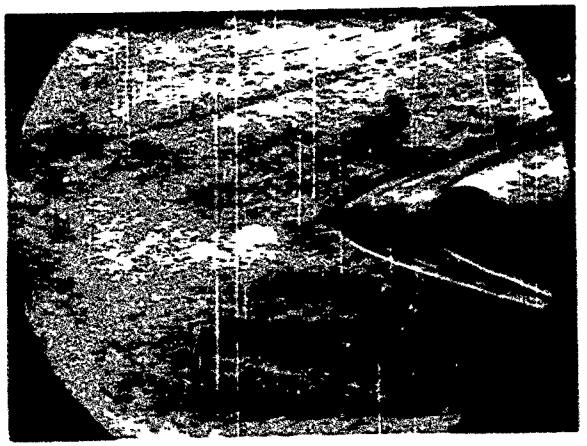

E). d/D= 2, X/D=2.0

F). d/D=2, X/D=4.0

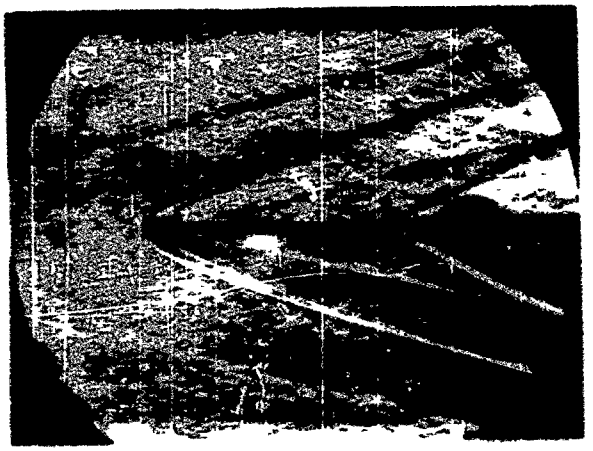

G). d/D=2, X/D=8.0

FIG 63. SCHLIEREN PHOTOGRAPHS OF SKIRTED HEMISPHERE AND SPHERE AT $M_\infty = 4.35$, $Re = 3.0 \times 10^5$ (CONCLUDED)

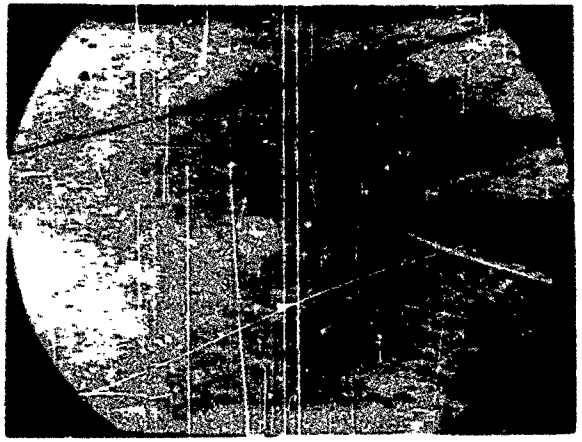

A). d/D=1, X/D=1.63

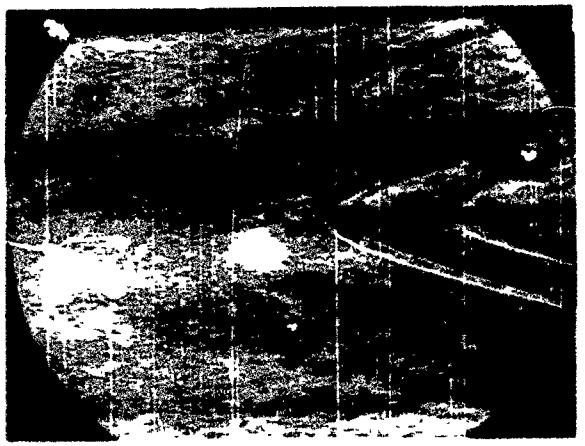

B) d/D=1 X/D = 3.73

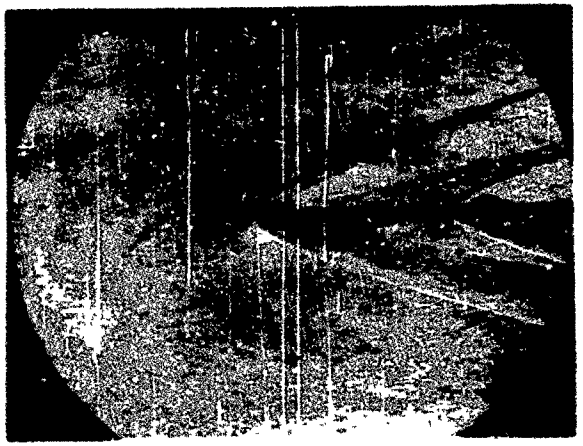

C). d/D=1, X/D =6.15

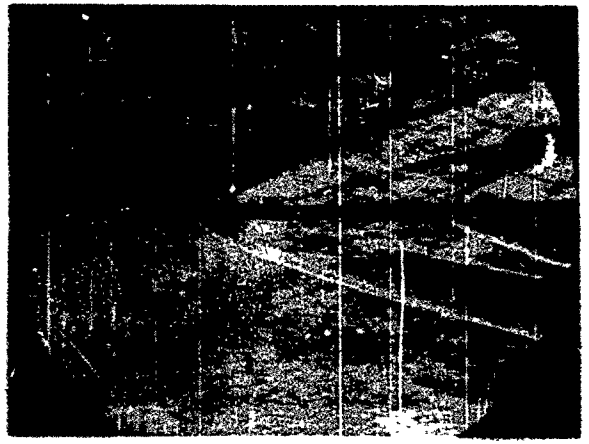

D). d/D=1, X/D=7.78

FIG64. SCHLIEREN PHOTOGRAPHS OF SKIRTED HEMISPHERE AND HOLLOW HEMISPHERE AT M_∞=4.35, Re = 3.0×10^5 (CONTINUED)

E). d/D=2, X/D=1.14

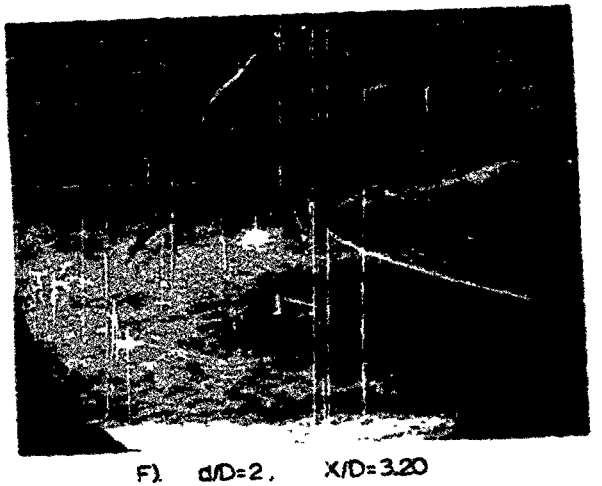

F). d/D=2, X/D=3.20

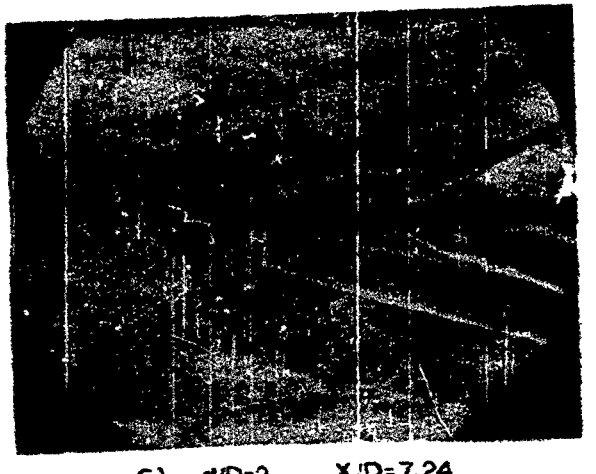

G). d/D=2, X/D=7.24

FIG 64. SCHLIEREN PHOTOGRAPHS OF SKIRTED HEMISPHERE AND HOLLOW HEMISPHERE AT $M_\infty = 4.35$, $Re = 3.0 \times 10^5$ (CONCLUDED)

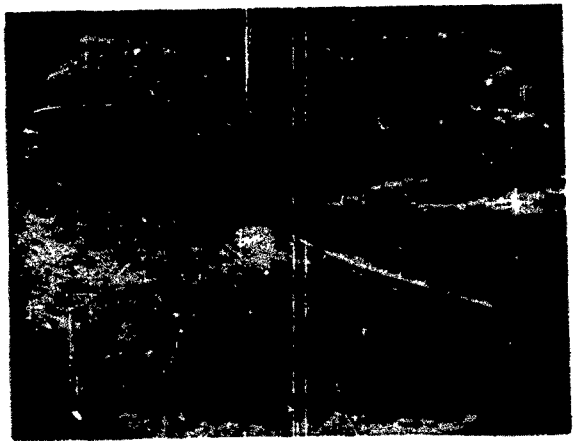

A). d/D=1 , X/D=2.0

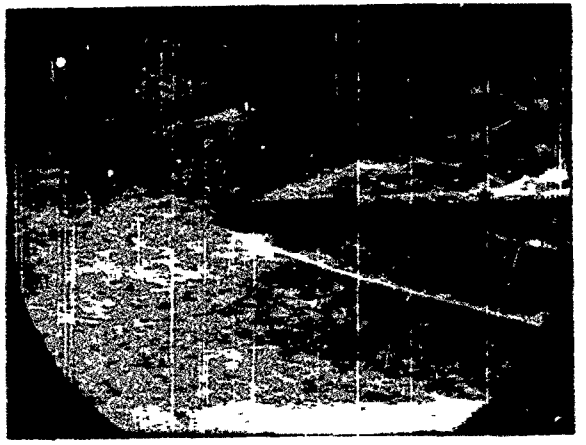

B). d/D=1 , X/D=4.0

C). d/D=1 , X/D=6.0

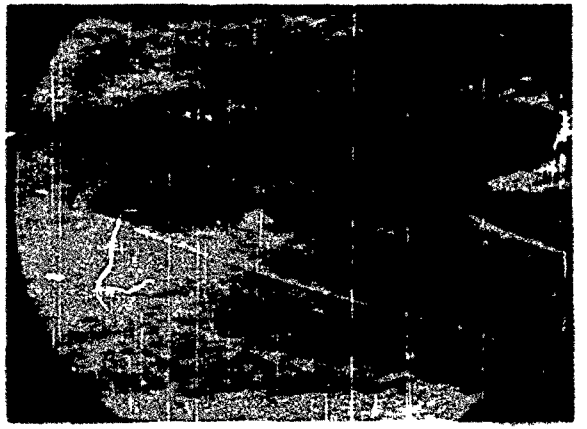

D). d/D=1 , X/D=8.0

FIG 65. SCHLIEREN PHOTOGRAPHS OF OGIVE CYLINDER AND FLAT PLATE AT M_∞=4.35, $Re = 3.0 \times 10^6$ (CONTINUED)

E). d/D=2, X/D=2.0

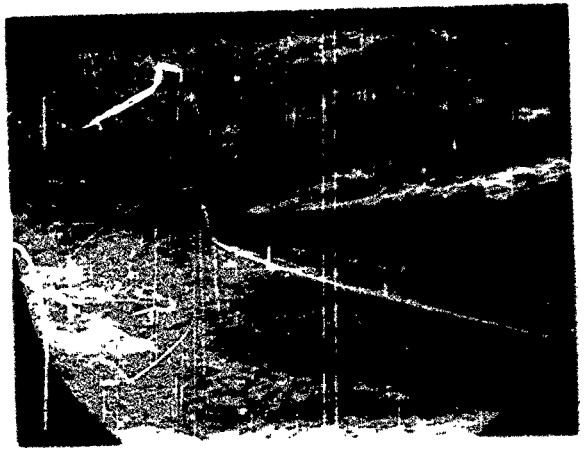

F). d/D=2, X/D=4.0

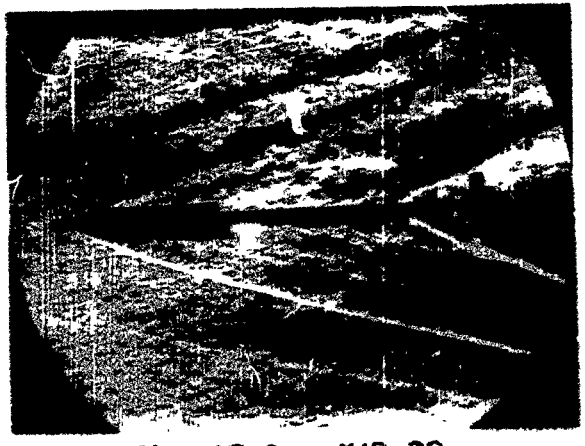

G). d/D=2, X/D=8.0

FIG 65. SCHLIEREN PHOTOGRAPHS OF OGIVE CYLINDER AND FLAT PLATE AT $M_\infty = 4.35$, $Re = 3.0 \times 10^5$ (CONCLUDED)

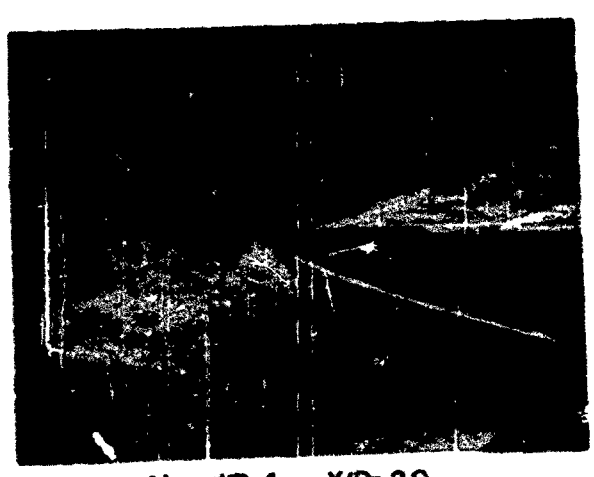

A) d/D=1, X/D=2.0

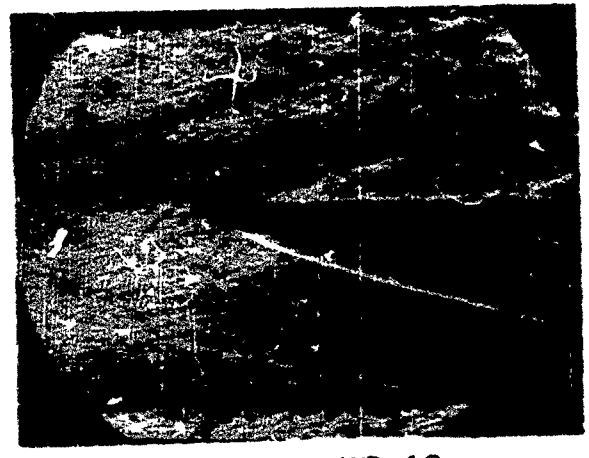

B) d/D=1, X/D=4.0

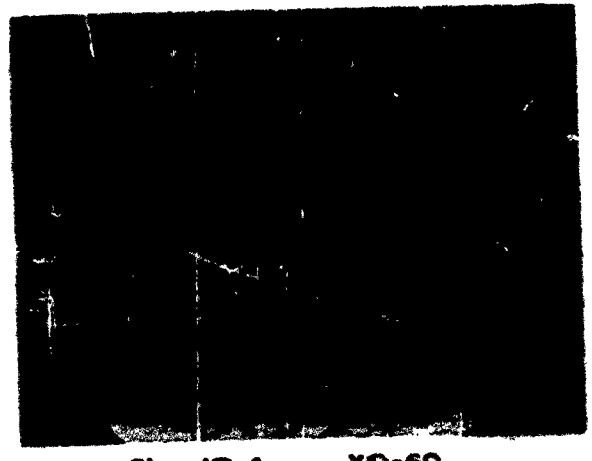

C) d/D=1, X/D=6.0

D) d/D=1, X/D=8.0

FIG 66. SCHLIEREN PHOTOGRAPHS OF OGIVE CYLINDER AND 45° HALF-ANGLE CONE AT M_∞=4.35, Re=3.0 x 10^5 (CONTINUED)

E). d/D= 2. X/D= 2.0

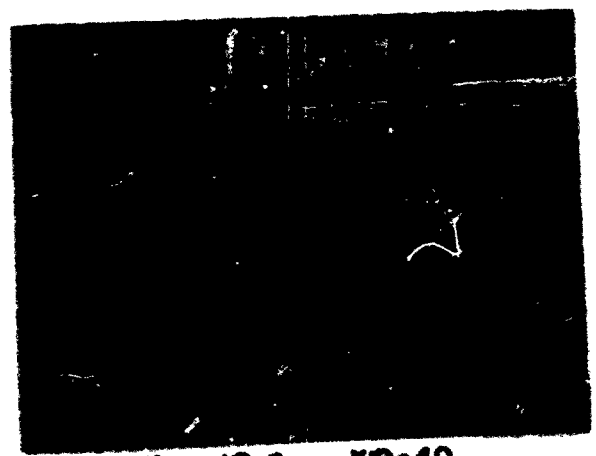

F). d/D=2. X/D=4.0

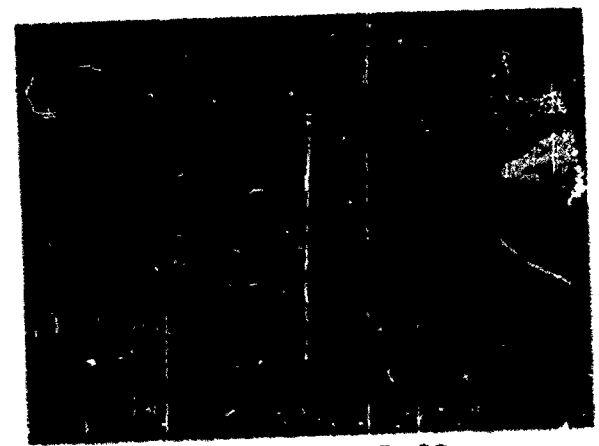

G). d/D=2. X/D=8.0

FIG 66. SCHLIEREN PHOTOGRAPHS OF OGIVE CYLINDER AND 45° HALF-ANGLE CONE AT M_∞=4.35, $Re = 3.0 \times 10^6$ (CONCLUDED)

A). d/D=1 , X/D=2.0

B). d/D=1, X/D=4.0

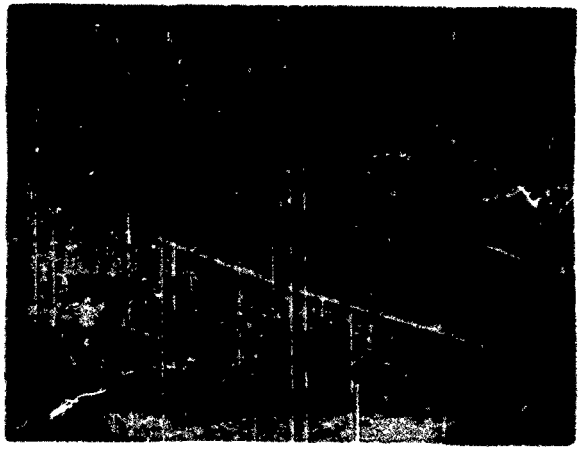

C). d/D=1, X/D=6.0

D). d/D=1, X/D=8.0

FIG 67 SCHLIEREN PHOTOGRAPHS OF OGIVE CYLINDER AND SPHERE AT $M_\infty = 4.35$, $Re = 30 \times 10^6$ (CONTINUED)

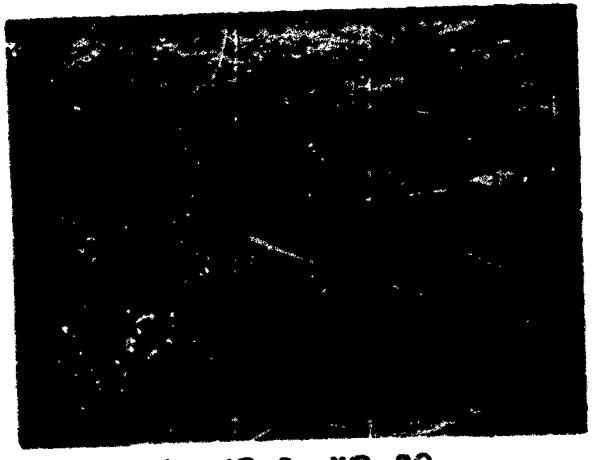

E). d/D= 2, X/D= 2.0

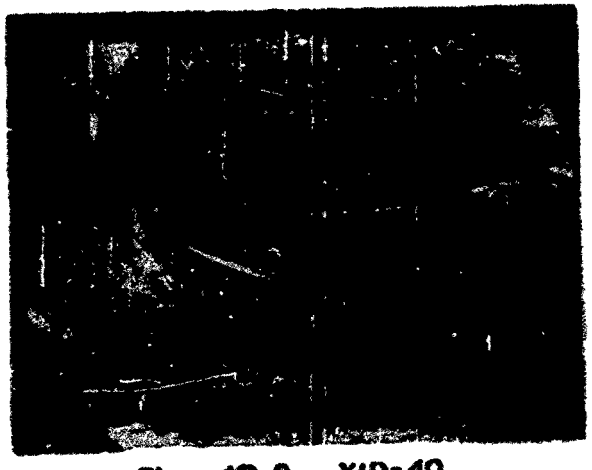

F). d/D= 2, X/D= 4.0

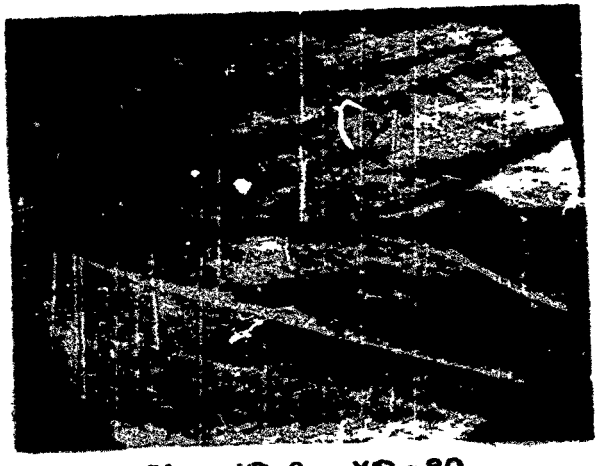

G). d/D= 2, X/D = 8.0

FIG 67. SCHLIEREN PHOTOGRAPHS OF OGIVE CYLINDER AND SPHERE AT M_∞=4.35, Re = 3.0×10^5 (CONCLUDED)

A). d/D=1, X/D = 1.63

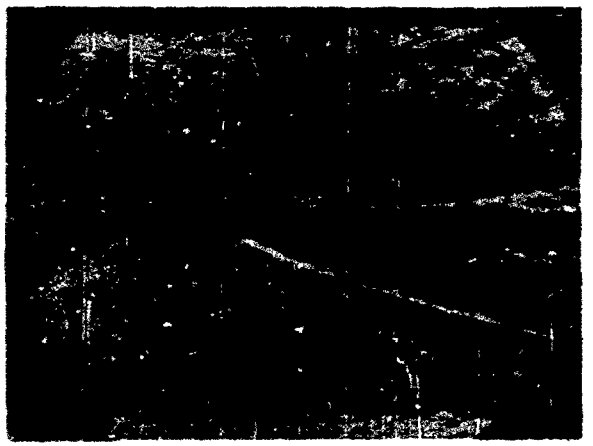

B). d/D=1, X/D= 3.73

C). d/D=1, X/D=6.15

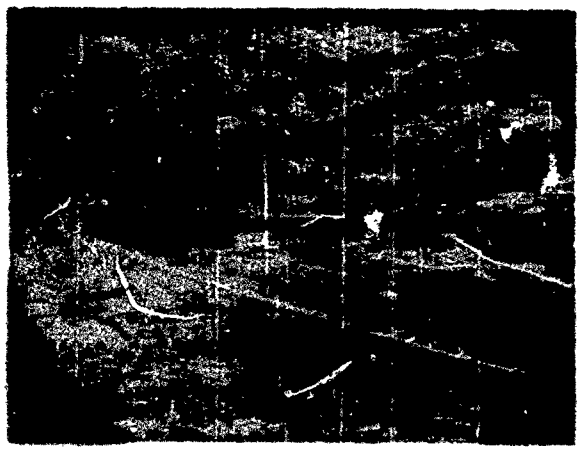

D). d/D= 1, X/D = 7.73

FIG 68. SCHLIEREN PHOTOGRAPHS OF OGIVE CYLINDER AND HOLLOW HEMISPHERE AT M_∞=4.35, Re_∞ 3.0 x 10^5 (CONTINUED)

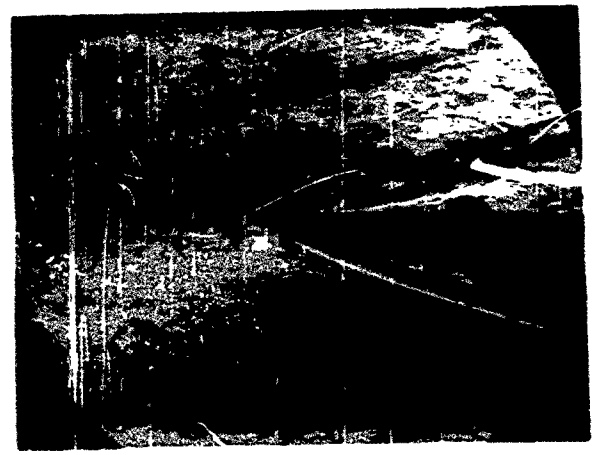

E). d/D= 2, X/D =1.14

F). d/D=2, X/D=3 20

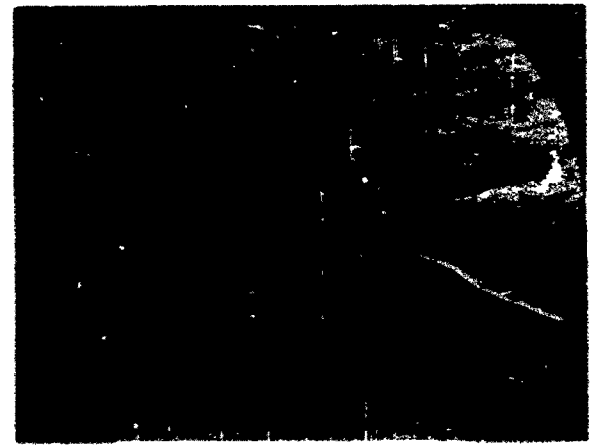

G). d/D=2, X/D =7.24

FIG 68. SCHLIEREN PHOTOGRAPHS OF OGIVE CYLINDER AND HOLLOW HEMISPHERE AT M_∞=4.35, Re= 3.0×10^5 (CONCLUDED)

APPENDIX III

DRAG BALANCE SYSTEM

The drag balance system includes the balance (the mechanical portion of the system) and the associated electronic instrumentation. The balance, an exploded view of which is shown in Fig 69, is composed of two primary parts, the main body and the drag sensing capsule. The electronic instrumentation consists of the drag sensing and calibration transformers, a signal generator, a control unit and a recording unit.

The main body of the balance, which is 2.05 inches long and 1.554 inches in diameter, forms the fixed component of the balance and is rigidly attached to the balance support sting. It houses the drag sensing transformer on a positioner and also an internal pressure tap and thermocouple. The Schaevitz Linear Variable Differential Transformer (Type 010M-L) is attached to the upstream end of a positioning rod. The other end of the rid is spring loaded against a cam, which provides axial positioning of the transformer.

The drag sensing capsule, which is 3.102 inches long and 1.554 inches in diameter, is composed of a fixed inner shell and a floating outer shell. The two shells are coaxially arranged and are connected by two ring type steel diaphragms which provide the spring force for drag sensing. The inner shell slides onto the inner tube of the main body and is rigidly attached to the main body by an adjustment rod which provides adjustment of the width of the slot between the main body and outer shell of the drag sensing capsule.

The outer shell, which is thus free to deflect the diaphragms, forms the drag sensing element. The transformer core is attached to its downstream end and the test model sting is rigidly attached by means of an adapter to the upstream end.

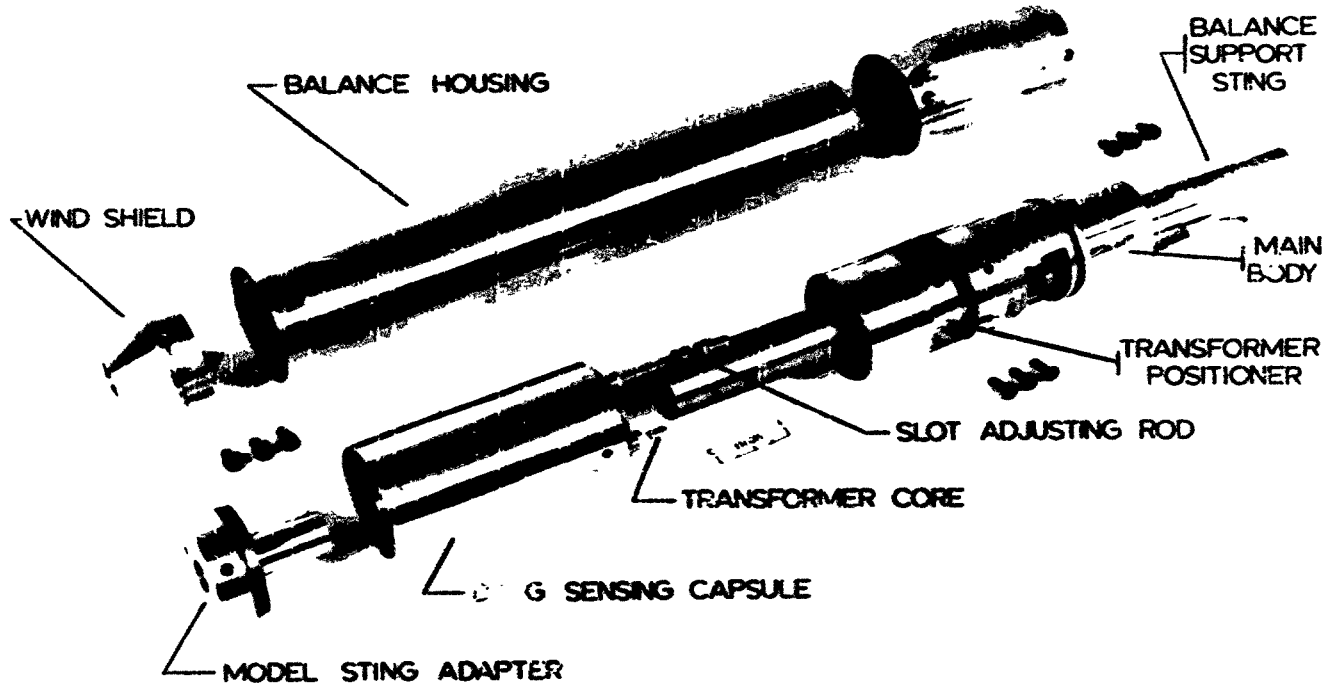

FIG 69 DRAG BALANCE.

A drag force on the test model causes an axial displacement of the outer shell of the drag sensing capsule relative to the fixed main body. This displacement, which is proportional to the drag on the model, is sensed by the Schaevitz LVDT. The LVDT is energized by a 10KC signal generator and its output is transmitted to a Brown Variable Span Recorder through the control unit. Since the output of the signal generator to the LVDT must be constant, the generator is voltage regulated and is located in a sound-proofed room to isolate it from tunnel noise.

As a displacement of the outer shell of the drag sensing capsule causes an equal displacement of the transformer core within the transformer, the transformer gives an output which is proportional to the drag. The control unit converts this output into useful recorder information and also extends the recorder range, permitting measurement of drag over a wide range without loss of sensitivity. Two other LVDTs, a "Hi" and a "Lo" at different points on the scale, are used as calibration transformers, to provide a continual check on the accuracy of the system and minimize errors due to temperature fluctuations.

A linear variation of transformer output with drag, good sensitivity and excellent zero return are obtained.

REFERENCES

1. Aeronautical Research Facilities, University of Minnesota, Institute of Technology, Department of Aeronautical Engineering, Rosemount Aeronautical Laboratories, Research Report No. 132, 1956.

2. Heinrich, H. G.; Hess, R. S., and Stumbris, G.: Drag Characteristics of Plates, Cones and Spheres in the Wake of a Cylindrical Body at Transonic Speeds, RTD-TDR-63-4023.

3. Heinrich, H. G.; Hess, R. S., and Stumbris, G.: Drag Coefficients of Several Bodies of Revolution at Transonic and Supersonic Velocity, ASD-TDR-63-663.

4. Heinrich, H. G. and Hess, R. S.: Pressure Distribution in the Wake of Two Bodies of Revolution at Transonic and Supersonic Speeds, ASD-TDR-62-1104, February, 1963.

5. Heinrich, H. G.: The Drag of Plates, Cones and Spheres in the Wake of Forebodies and the Drag of Two-Body Systems, (Presented at the Symposium on Parachute Technology and Evaluation, April, 1964, at El Centro, California).

Unclassified
Security Classification

DOCUMENT CONTROL DATA - R&D

(Security classification of title, body of abstract and indexing annotation must be entered when the overall report is classified)

1 ORIGINATING ACTIVITY *(Corporate author)*
University of Minnesota
Dept. of Aeronautics & Engineering Mechanics
Minneapolis, Minn.

2a REPORT SECURITY CLASSIFICATION
Unclassified

2b GROUP

3 REPORT TITLE
Drag Characteristics of Several Two-Body Systems at Transonic and Supersonic Speeds

4 DESCRIPTIVE NOTES *(Type of report and inclusive dates)*
Final Report Jan 62 - Dec 63

5 AUTHOR(S) *(Last name, first name, initial)*
Heinrich, Helmut G.
Hess, R. Sheldon

6 REPORT DATE	7a TOTAL NO. OF PAGES	7b NO. OF REFS
December 1964	96	5

8a CONTRACT OR GRANT NO.	9a ORIGINATOR'S REPORT NUMBER(S)
AF33(657)-11184	RTD-TDR-63-4226
b. PROJECT NO. 6065	
c	9b. OTHER REPORT NO(S) *(Any other numbers that may be assigned this report)*
d	n/a

10 AVAILABILITY/LIMITATION NOTICES
Qualified requesters may obtain copies of this report from DDC. Foreign announcement and dissemination of this report is not authorized. DDC release to OTS is not authorized.

11 SUPPLEMENTARY NOTES

12. SPONSORING MILITARY ACTIVITY
Air Force Flight Dynamics Laboratory
Research and Technology Division
Air Force Systems Command
Wright-Patterson AFB, Ohio

13 ABSTRACT

The drag coefficients as well as the stagnation and base pressures of systems using an ogive cylinder or skirted hemisphere as primary body and a flat plate, 45° half-angle cone, sphere, and hollow hemisphere as secondary body have been measured at transonic and supersonic speeds.

The Mach number range was from 0.85 to 1.25 and 4.35. Secondary body size and body separation distance were selected parameters. This is the fourth report in a series of studies dealing with the free stream drag and wake phenomena of bodies of revolution (see Refs 2, 3, and 4).

With a few exceptions in the transonic range, the system drag was less then the sum of the free stream drag of the fore and aft bodies.

DD FORM 1 JAN 64 1473

Unclassified
Security Classification

Unclassified

Security Classification

KEY WORDS	LINK A		LINK B		LINK C	
	ROLE	WT	ROLE	WT	ROLE	WT
Drag Coefficient Transonic Speed Supersonic Speed Stagnation Pressure Base Pressure Primary-Secondary Body Combination Wake						

INSTRUCTIONS

1. ORIGINATING ACTIVITY: Enter the name and address of the contractor, subcontractor, grantee, Department of Defense activity or other organization *(corporate author)* issuing the report.

2a. REPORT SECURITY CLASSIFICATION: Enter the overall security classification of the report. Indicate whether "Restricted Data" is included. Marking is to be in accordance with appropriate security regulations.

2b. GROUP: Automatic downgrading is specified in DoD Directive 5200.10 and Armed Forces Industrial Manual. Enter the group number. Also, when applicable, show that optional markings have been used for Group 3 and Group 4 as authorized.

3. REPORT TITLE: Enter the complete report title in all capital letters. Titles in all cases should be unclassified. If a meaningful title cannot be selected without classification, show title classification in all capitals in parenthesis immediately following the title.

4. DESCRIPTIVE NOTES: If appropriate, enter the type of report, e.g., interim, progress, summary, annual, or final. Give the inclusive dates when a specific reporting period is covered.

5. AUTHOR(S): Enter the name(s) of author(s) as shown on or in the report. Enter last name, first name, middle initial. If military, show rank and branch of service. The name of the principal author is an absolute minimum requirement.

6. REPORT DATE: Enter the date of the report as day, month, year, or month, year. If more than one date appears on the report, use date of publication.

7a. TOTAL NUMBER OF PAGES: The total page count should follow normal pagination procedures, i.e., enter the number of pages containing information.

7b. NUMBER OF REFERENCES: Enter the total number of references cited in the report.

8a. CONTRACT OR GRANT NUMBER: If appropriate, enter the applicable number of the contract or grant under which the report was written.

8b, 8c, & 8d. PROJECT NUMBER: Enter the appropriate military department identification, such as project number, subproject number, system numbers, task number, etc.

9a. ORIGINATOR'S REPORT NUMBER(S): Enter the official report number by which the document will be identified and controlled by the originating activity. This number must be unique to this report.

9b. OTHER REPORT NUMBER(S): If the report has been assigned any other report numbers (either by the originator or by the sponsor), also enter this number(s).

10. AVAILABILITY/LIMITATION NOTICES: Enter any limitations on further dissemination of the report, other than those imposed by security classification, using standard statements such as:

(1) "Qualified requesters may obtain copies of this report from DDC."

(2) "Foreign announcement and dissemination of this report by DDC is not authorized."

(3) "U. S. Government agencies may obtain copies of this report directly from DDC. Other qualified DDC users shall request through _____."

(4) "U. S. military agencies may obtain copies of this report directly from DDC. Other qualified users shall request through _____."

(5) "All distribution of this report is controlled. Qualified DDC users shall request through _____."

If the report has been furnished to the Office of Technical Services, Department of Commerce, for sale to the public, indicate this fact and enter the price, if known.

11. SUPPLEMENTARY NOTES: Use for additional explanatory notes.

12. SPONSORING MILITARY ACTIVITY: Enter the name of the departmental project office or laboratory sponsoring *(paying for)* the research and development. Include address.

13. ABSTRACT: Enter an abstract giving a brief and factual summary of the document indicative of the report, even though it may also appear elsewhere in the body of the technical report. If additional space is required, a continuation sheet shall be attached.

It is highly desirable that the abstract of classified reports be unclassified. Each paragraph of the abstract shall end with an indication of the military security classification of the information in the paragraph, represented as *(TS)*, *(S)*, *(C)*, or *(U)*.

There is no limitation on the length of the abstract. However, the suggested length is from 150 to 225 words.

14. KEY WORDS: Key words are technically meaningful terms or short phrases that characterize a report and may be used as index entries for cataloging the report. Key words must be selected so that no security classification is required. Identifiers, such as equipment model designation, trade name, military project code name, geographic location, may be used as key words but will be followed by an indication of technical context. The assignment of links, rules, and weights is optional.

Unclassified

Security Classification